UCLA
UCLA Electronic Theses and Dissertations

Title
Development of the Computational Unit for an Artificial Axon Network

Permalink
https://escholarship.org/uc/item/31c6z2w9

Author
Vasquez, Hector Garcia

Publication Date
2018

Peer reviewed|Thesis/dissertation

eScholarship.org Powered by the California Digital Library
University of California

UNIVERSITY OF CALIFORNIA
Los Angeles

Development of the Computational Unit for an Artificial Axon Network

A dissertation submitted in partial satisfaction
of the requirements for the degree
Doctor of Philosophy in Physics

by

Hector Garcia Vasquez

2018

© Copyright by
Hector Garcia Vasquez
2018

ABSTRACT OF THE DISSERTATION

Development of the Computational Unit for an Artificial Axon Network

by

Hector Garcia Vasquez
Doctor of Philosophy in Physics
University of California, Los Angeles, 2018
Professor Giovanni Zocchi, Chair

The subject of consciousness is a debated and open question on all levels of inquiry. There is no general consensus for its definition, nor is there agreement in the minimum number of computational units required to produce a conscious experience or to perform the simplest stimulus-response tasks. The unknowns persists down to the interaction between two neurons. When one neuron fires, competing theories exist for how a downstream neuron uses this signal.

A novel, experimental system was developed in the Zocchi lab [AZ16] to explore these questions with a constructivist approach. We call this system the Artificial Axon (AA), and it is the first artificial system to produce an action potential with a voltage-gated ion channel outside of the cell. The long-term direction for the Artificial Axon in our lab is toward a large network of Axons to probe the surface of consciousness with a "brain-like" system. There are many challenges to overcome before such a network is realized. However, we are approaching the end of early development for this system.

My experimental work with the Artificial Axon is in the development of the computational unit for this future network. Because the microscopics of the Artificial Axon and the neuron are the same both are driven by the voltage-gated ion channel we expect overlap between the neuron and the computational unit of the AA in response to input and communication of output. I show that this is certainly the case. I demonstrate that the Artificial Axon is a logic gate, capable of performing simple Boolean logic. I produce a firing rate in the

Artificial Axon, a crucial property in neuron communication and computation. I develop an electronic connection between Axons, and describe its immediate potential for information storage in a larger network. I end the thesis with a demonstration of two Axons performing a simple task. Namely, I use two Axons to steer an RC car toward a light source.

The dissertation of Hector Garcia Vasquez is approved.

Dolores Bozovic

Stuart Brown

William M. Gelbart

Giovanni Zocchi, Committee Chair

University of California, Los Angeles

2018

To my husband, family and friends.

TABLE OF CONTENTS

1 Introduction **1**

1.1 Present approaches and techniques 2

1.1.1 Approaches to measuring neural activity 2

1.1.2 Constructivist approaches 2

1.2 The Artificial Axon 3

2 KvAP and the Artificial Axon **4**

2.1 Nernst and Action potentials in the neuron 4

2.2 Properties of the KvAP 6

2.2.1 KvAP structure 7

2.2.2 The voltage-sensing domain 7

2.2.3 The Kv selectivity filter 9

2.2.4 Inactivation 10

2.3 KvAP Preparation 11

2.3.1 KvAp Expression in *E. coli* 11

2.3.2 KvAP Purification protocol 16

2.4 KvAP Reconstitution into lipid vesicles 18

2.5 Electrophysiological measurement with KvAP 22

2.5.1 Electrophysiological setup 22

2.5.2 Measurement with a voltage clamp 23

2.6 The Artificial Axon 25

2.6.1 The Nernst potential in the Artificial Axon 25

2.6.2 The current-limited voltage clamp 26

2.6.3 Action potential in the Artificial Axon 26
2.7 Hodgkin Huxley model in the Artificial Axon 28
2.8 Future work 31

3 Summation in the Artificial Axon 33
3.1 Summation phenomena in networks of living organisms 33
3.2 Artificial Axon summation components 34
3.3 Channel contribution in the membrane equation 34
3.4 One-pulse input 36
3.4.1 CLVC overwhelms channel current 36
3.4.2 Channel current overwhelms CLVC 38
3.5 Two-pulse input 38
3.5.1 Channels open after first pulse 40
3.5.2 Channels closed after first pulse 41
3.6 Discussion 41
3.6.1 Model 41
3.6.2 Future Work 44

4 Propagation of the action potential 46
4.1 The cable equation 46
4.2 Propagation in the Artificial Axon 49
4.2.1 The experimental setup 49
4.2.2 Results: Propagation across two Artificial Axons 51
4.3 Discussion 54
4.3.1 The CLVC protocol 54
4.3.2 Model 57

4.3.3 Future work 60

5 Firing Rate 62

5.1 Firing rate in the neuron 62

5.2 Recovery from inactivation and spike regeneration 63

5.3 The current clamp 65

5.3.1 Electronic design 66

5.3.2 No trigger 67

5.3.3 Trigger 68

5.3.4 Changing firing rate 71

5.4 Discussion 75

5.4.1 Model 75

5.4.2 Future work 77

6 Synapse 78

6.1 Synapse in the neuron 78

6.2 Electronic synapse for the Artificial Axon 79

6.3 Measurements with the electronic synapse 82

6.3.1 Un-tuned synapse 82

6.3.2 Tuned synapse 84

6.4 Adding electronic synapse connections 86

6.5 Discussion 87

6.5.1 Model 87

6.5.2 Future work 96

7 Navigation 100

7.1 Overview of the electronic system 100
7.2 Electronic system components 102
7.2.1 Photodiode eyes of the car 102
7.2.2 The light source 108
7.2.3 Heating and background 108
7.2.4 The voltage-to-frequency converter 108
7.2.5 Transmitter and receiver 110
7.2.6 Frequency-to-voltage conversion 110
7.2.7 The vehicle 111
7.3 Navigation with two Artificial Axons 112
7.3.1 The electrophysiological parameters 112
7.3.2 A Navigation result 113
7.4 Discussion 117
7.4.1 Model 117
7.5 Concluding remarks 121

References **125**

LIST OF FIGURES

2.1 Subunit and complete structure of the Kv channel from multiple views. The upper figures show a single KvAP subunit and the bottom figures show a complete Kv channel with all 4 subunits from the top and the side views. One subunit contains six amino acid helices that comprise a voltage-sensing domain, a pore domain, and a selectivity filter subunit. In the assembled ion channel, the voltage-sensing domains are positioned on the perimeter of the pore, and the selectivity filter is on the intracellular side of the neuron. These figures are from the thesis of Andrew Wang in Giovanni Zocchi's lab (Manipulation of Molecular Processes with DNA Molecular Springs). The figures were generated in PyMol using the Kv structure solved by the MacKinnon lab [LTC07, ZMK01]. For the subunit in the upper-right corner – Structure PDB ID: 2R9R. 8

2.2 Electrophysiology setup for the Artificial Axon. A $\sim 100-200\mu m$ aperture at the bottom of the cup supports a lipid bilayer and KvAP ion channels. The bilayer separates the solutions on the inner and outer chamber, thus allowing for a Nernst potential to be manually created with the solutions in the cis and trans chambers. The DAQ records the membrane voltage, and the headstage amplifier is a voltage clamp when the switch S is oriented as shown in the figure. When switch S is connected to R_C, the electronics are the current-limited voltage clamp (CLVC), and function as the second ion-channel species in imposing a resting potential in the neuron. 21

2.3 Voltage clamp current on a membrane with ion channels. In this measurement, the switch S in Fig. 2.2 is connected as shown in the figure, shorting R_C, so the Headstage amplifier is a voltage clamp. (a) shows the entire step and (b) shows a frame when the channels are open. At $t = 200\,ms$, the clamp voltage is stepped from $Vc = -120\,mV$ to $-60\,mV$. The channels open, fully inactivate, and the voltage clamp current moves to equilibrium at $2\,nA$. This nonzero current when channels are closed comes from an ohmic leak in either the channels, membrane, or the aperture contact with the lipid-decane mixture. 24

2.4 Measurement of an action potential in the Artificial Axon. The blue trace is the membrane potential, and the yellow trace is a fit using the Hodgkin and Huxley model for an action potential in a neuron. The rest value, imposed by the CLVC is stepped from $-92\,mV$ to $-28\,mV$ and the Axon "fires." The channels open at threshold, between $-30\,mV$ and $-20\,mV$, and K^+ ions flow into the cis chamber, toward the Nernst potential ($40\,mV$), peaking at $25\,mV$. The channels move to complete inactivation, and the membrane potential rests at $-28\,mV$. After 1 second, the rest potential is stepped back down to $-92\,mV$. 27

2.5 Scheme for KvAP gating and measured parameter values [SCM09]. (a) Represents the scheme between the different states of the KvAP channel, and (b) is a table of values for the rate constants in the transition rates between states. In this minimal scheme, the subunits of the ion channel are assigned two Closed states: C_α and C_β. When all four subunits are in the C_α state, Open and Inactive states become accessible. All other combinations of C_α and C_β are inaccessible to Open and Inactive states. α, β and k_i are transition rates between the different states of the scheme, all of which have the form $k_0\, e^{-z\,V}$, where k_0 and z are the rate constants. 29

3.1 Membrane voltage response to one CLVC pulse. The dotted line represents the input (the CLVC voltage protocol), the blue trace is the measured Axon voltage V(t), and the yellow trace is the current through the CLVC. In both (a) and (b) the CLVC protocol is a square pulse from $-109\,mV$ to $54\,mV$, but the pulse width is $30\,ms$ in (a) and $40\,ms$ in (b), the latter being sufficient to open some channels. The CLVC resistance is $R_C = 100M\Omega$. 37

3.2 Response of the Artificial Axon to a sub threshold (a) and above threshold (b) stimulus. In both (a) and (b) the CLVC protocol is a square pulse from $-125\,mV$ to $-25\,mV$, but the pulse width is $50\,ms$ in (a) and $100\,ms$ in (b). The CLVC resistance is $R_C = 100\,M\Omega$, and from the sub threshold $V(t)$ trace, fitting with the membrane equation with closed channels ($p_O = 0$), the Axon values are $C = 192\,pF$ for the membrane capacitance and $R_l = 1.2\,G\Omega$ for the leak resistance. 39

3.3 Coincidence detection with the Artificial Axon. Two sub threshold pulses (dotted line) in close proximity cause the Axon to fire. The first pulse induces opening of some channels, but the channel current cannot overwhelm the clamp (which has the role of the Na^+ gradient in the real neuron) absent the second pulse. The CLVC protocol is two identical pulses from $-123\,mV$ to $-23\,mV$, of width $86\,ms$ and $80\,ms$ apart. The CLVC resistance is$R_C = 100\,M\Omega$, $C = 210\,pF$ and $R_\ell = 0.7\,G\Omega$. 40

3.4 Multiple pulses to open channels. An individual pulse is insufficient to open channels. Two of these pulses must be close in time to open channels. One pulse is from $-109\,mV$ to $727\,mV$, of width $20\,ms$. The CLVC protocol is two such pulses at different separations. In (a), the pulses are $60\,ms$ apart and channels do not open. In (b) the pulses are $40\,ms$ apart, and some channels open, but not enough to overwhelm the CLVC. In (c) the pulses are $20\,ms$ apart and the Axon fires. 42

3.5 Simulation of two-pulse input. The rate constant values in this simulation are based on a fit for channel measurements not presented in this thesis. The coral-colored line represents the fraction of open channels, and the green line represents the fraction of inactive channels. The resemblance in shape across voltage and time of this simulation to the measurement in Fig. 3.3 suggests that the probability traces demonstrate how channels contribute to the membrane potential in measured data. The CLVC protocol is two identical pulses from $-91\,mV$ to $-10\,mV$, $81\,ms$ wide and $70\,ms$ apart. The Axon values are $V_N = 40\,mV$, $V_r = -92\,mV$, $R_C = 100\,M\Omega$, $C = 210\,pF$, and $\chi_\ell = 0$. 43

4.1 Membrane patch of an neuron axon and an equivalent circuit. dR_r is the resistance of the ion-channel, dC is the membrane capacitance, dR_z is the resistance of the solution inside the axon, and V_N is the Nernst potential created by the K^+ concentration gradient across the membrane. The axon is modeled by a series of dz components connected along the axon's axis. 47

4.2 Connection diagram for propagation of an action potential between to Artificial Axons. The capacitor C_{in} function is analogous to empty axon membrane between two patches of ion channels in a neuron, and the resistor R_{in} function is analogous to the resistance of the bulk solution inside the axon. The switch S connects the two AAs, and the component A is a high-impedance op-amp. 50

4.3 Measurement for action potential propagation across two Artificial Axons. The solid blue trace is the membrane potential for Axons 1, and yellow is for Axon 2. The dashed lines are the CLVC protocol for each Axon (described in the text). Membrane potential is measured on the left y-axis and CLVC is measured on the right. In (a) the Axons are connected (see Fig. 4.2) and Axon 2 fires when Axon 1 fires. In (b), the Axons are disconnected and Axon 2 does not fire. 52

4.4 Second measurement for action potential propagation across two Artificial Axons. These measurements are for the same Axon preparations in Fig. 4.3. The CLVC protocols are also the same. The only difference in protocol is the *stimulus* step. In Fig 4.3, the CLVC is stepped to $91\,mV$ for $250\,ms$. In the measurement above, the *stimulus* step is $18\,mV$ for $500\,ms$. 55

4.5 The equivalent circuit of three Artificial Axons connected by RC components for propagation of an action potential. R_{ch} is the resistance from the ion channels, C is the membrane capacitance, V_N is the Nernst potential. V_C and R_C are the CLVC voltage and resistance. An action potential is propagated from left to right. In this circuit, R_{in} and C_{in} order are switched compared to the measurements in Fig. 4.3 and Fig. 4.4. 57

4.6 Two simulations of propagation across nine Artificial Axons. Each column corresponds to one simulation. The simulations use different channel and electrophysiological parameters; the parameters for the Axons in the left column are from the simulation in chapter 3 section 3.6.1, and those for the right-column Axon are from a fit for an AA action potential measurement. The green traces are the membrane potentials, the blue traces are open probability, and the yellow traces are inactivation. In (a) and (d) all Axons are connected, and in (c) and (f), the first Axon is disconnected from the downstream Axons. Two simulations are presented here to demonstrate the behavior of inactivation (yellow traces) at *high-rest* ($-50\,mV$). While there is $\sim 20\,\%$ inactivation in the left-column Axon at $-50\,mV$, inactivation does not prevent Axon firing from a $-50\,mV$ start point. These simulations suggest that the CLVC protocols in section 4.2.2 may be simplified to the CLVC protocol used in these simulations. 59

5.1 A sequence of action potentials from a CLVC protocol. Multiple spikes are shown in (a), and a single spike (blue trace) with the imposed CLVC protocol (gray steps) is shown in (b). The protocol is as follows. The CLVC value is moved from *low-rest* at $-209\,mV$ to at *high-pulse* step at $455\,mV$ for $40\,ms$ to bring the membrane potential to near-threshold for firing. Next is the *stimulus* step, protocol $(-9\,mV,\ 250\,ms)$, where the Axon fires toward the Nernst potential. CLVC is then brought down to $-182\,mV$ for $40\,ms$ (*low-pulse*), and then back to *low-rest* at $-209\,mV$ for $600\,ms$ so that channels may recover from inactivation and fire again. The protocol then repeats. 64

5.2 Schematic of the current clamp. All op-amps used are the low-noise FET precision op-amp AD795. The green dots represent the positions of the stated voltage values, also in green. The current clamp has three components: a summation amplifier circuit, a voltage inverter, and a high-impedance voltage follower. These components work together as follows. The potential difference between the voltage inverter and follower determines the current injected into the AA as $I_{CC} = V_{CC}/R_{CC}$ [VZ18]. 66

5.3 Figure 5.3 shows a measurement of an action potential induced in an Axon by a current clamp. $V_C = -227\,mV$ holds the potential at rest (-110 mV). At $t = 360\,ms$, the current clamp is switched on and injects a constant $100\,pA$ into the Axon, and then is switched off at $t = 10.8\,s$ after the channels have inactivated. $N_0\,\chi_\ell = (1.87\,G\Omega)^{-1}$, and $C = 250\,pF$. 67

5.4 Membrane potential measurement with a CLVC, a CC and a trigger. A sequence of spikes is shown in (a), and two spikes (blue trace) with the imposed CLVC trace (gray steps) is shown in (b). The clamp values are $V_C^{(1)} = -364\,mV$, $V_C^{(2)} = -636\,mV$, $V_{CC} = 10\,mV\,(I_{CC} = 100\,pA)$, $V_T = 0\,mV$, and $\tau_T = 1\,s$. . 69

5.5 Measurement in Fig.5.4 with no trigger. All clamp and electrophysiological values are the same. After the Axon fires, the channels inactivate and the Axon cannot fire again. 70

5.6 A series of spike trains induced by a CLVC, CC and trigger. $I_{CC} = 50\,pA$ in the first train, and I_{CC} increases by $10\,pA$ in the trains that follow. The membrane potential in time is plotted in (a), and the corresponding train frequencies are plotted with their currents in (b). All clamp values are constant. They are: $V_C^{(1)} = -125mV$, $V_T = 14mV$, $V_C^{(2)} = -459\,mV$, and $\tau_T = 500\,ms$. 72

5.7 Several spikes from two different trains in Fig. 5.6. In (a) we see the first spike in a train, which has more open channels than the two action potentials that follow. By the third spike, active and inactive states "stabilize," and the spikes that follow are visually similar in channel contribution, with some variation but no visible trend toward inactivation. (b) is an example of spikes that have become stable in the channel contribution to firing. 73

5.8 One simulated Artificial Axon with two different CC inputs. (a) is a spike train from CC input $100\,pA$, and (b) illustrates the channel open probability (blue trace) and inactivation (yellow trace). Not shown is a trace for the closed-active state, which makes the sum of probabilities equal to 1 at all points in time. (c) and (d) are corresponding simulations for CC input $80\,pA$. Electrophysiological parameters and clamp values are identical to those in Fig. 5.4. The rate constants in the simulation are not a perfect fit, but the fit is sufficient to describe the membrane and channel behavior. 76

6.1 An electronic synapse switch for the Artificial Axon. A_1 and A_2 are the Low-noise precision FET op-amp AD795, and the relay is the Magnecraft W172DIP-5 Reed Relay. A_1 is a high-impedance op-amp, and A_2 drives the relay switch. When $V_{pre} > 0$, the current clamp injects current $I_s = V_{pre}/R_s$ into the post-synaptic Axon (see Fig.5.2). 80

6.2 This is the same *synapse switch* and current clamp in Fig. 6.1 with one shifted connection. The inputs to the summation amplifier in the CC (see Fig. 5.2) are separated from the rest of the CC by the relay in the synapse. The switch in red is a reed relay that disconnects the two Axons from each other. V_s is an input voltage supplied by a DAQ to amplify the synapse strength by $I_s = (V_{pre} + V_s)/R_s$, where I_s is the current injected into the post-synaptic Axon. All unlabeled resistances are the same resistance $R = 100\,k\Omega$. 81

6.3 Two Axons connected by a synapse. The blue trace is the membrane potential for the pre-synaptic Axon, the dark-yellow line over the trace is a fit for the pre-synaptic Axon, and the lighter yellow trace is the membrane potential for the post-synaptic Axon. There are no triggers in this experiment, and $V_s = 0$. The CLVCs hold their respective Axons at rest. Shortly after $t = 0$, CC_{pre} is switched on, inducing a spike in the pre-synaptic Axon. When $V_{pre} > 0$ at $t \approx 0.5\,s$, the synapse injects current into the post-synaptic Axon until $V_{pre} < 0$ at $t \approx 1.5\,s$. The post-synaptic Axon fires, and V_2 remains high until the channels fully inactivate. At $t \approx 3.3\,s$, CC_{pre} is switched off and V_{pre} returns to rest. The electrophysiological parameters found in the fit are $N_0 = 461$, $C = 175\,pF$, $\chi_\ell = (68\,G\Omega)^{-}1/N_0$, and $V_N = 56\,mV$. The clamp values are provided in the text. 83

6.4 A synapse measurement at two different strengths. The top and bottom figures are for pre and post-synaptic Axons, respectively. V_s is too small in the blue traces to induce firing in the post-synaptic Axon. When V_s is made $\sim 2\times$ larger (yellow trace), the post-synaptic Axon fires. There is a negligible offset in the V_{pre} switching value; the synapse switches on at $\sim -0.5\,mV$ and switches off at $\sim -1.5\,mV$. The clamp values are listed in the text. 85

6.5 Two Axons connected by two synapses. Two synapses connect two Artificial Axons such that each Axon receives input from – and provides input to – the other Axon. The bottom synapse takes input from Axon 1 and outputs to Axon 2, and the top synapse takes input from Axon 2 and outputs to Axon 1. The DAQs change the synapse strengths, so that the output current from the CC is $I_{ij} = \left(R_s^{(ij)}\right)^{-1} \alpha_{ij} \left(V_i + V_s^{(ij)}\right) \Theta(V_i)$, where index i refers to the pre-synaptic Axon, j is for the post-synaptic Axon, and Θ is the Heaviside step function. . . 86

6.6 Simulation of two Axons connected by a synapse. The pre-synaptic Axon is the blue trace, and the post-synaptic Axon is the yellow trace; firing in the pre-synaptic Axon induces firing in the post-synaptic Axon. The Axons are held at rest with CLVCs. A stimulating current $ICCpre =$ from $< t <$ brings the pre-synaptic Axon to firing. While $V_{pre} > 0, /mV$, the synapse injects current I into the post-synaptic Axon. The channel parameters are taken from the simulations in section 5.4.1. In this simulation, V_N is raised to $60\,mV$ and $N_0 = 10^3$. 88

6.7 Two Axons connected by two synapses in a candidate network-node. The Axon in (a) excites the Axon in (b) with positive synapse current, and the Axon in (b) polarizes the Axon in (a) with negative synapse current. The outcome is an Axon (a) action potential with rising and falling edges from the ion channels and not from a trigger. Figure (c) plots p_O and inactivation in time for both Axons. The blue and light-blue traces are p_O and inactivation in Axon (a), respectively. The yellow traces in (c) are for the Axon in (b). 90

6.8 Simulation for one node's response to constant CC inputs. This is the same node from Fig. 6.7. (a)-(c) show the response to a constant $50\,pA$ input to AA_{full}, and (d)-(f) show the response to $60\,pA$ input. This node's key features as a computational unit are (i) the firing rate changes with changing input, and (ii) the firing rates are maintained with no trend toward inactivation. 91

6.9 Oscillator with four Axons and 4 excitatory synapses. Axon 1 is the blue trace, Axon 2 is yellow, Axon 3 is green and Axon 4 is orange. The Axons are connected (pre-synapse $\rightarrow$ post-synapse) in a loop as $1 \rightarrow 2 \rightarrow 3 \rightarrow 4 \rightarrow 1$. A $70\,pA$, $500\,ms$ pulse is applied to Axon 1. Consequently, all Axons fire consecutively and indefinitely. When an Axon fires, a trigger pulls the potential down to a large negative value for channel recovery from inactivation. (d) displays only the first few spikes. In (e), a dark-colored trace corresponds to p_o for an Axon of the same color, and the lighter-colored trace is the inactivation for the same Axon. All channel and electrophysiological parameters are identical to Fig. 6.8, with exception to $R_s = 300\,M\Omega$. 94

6.10 Oscillator with six Axons and no triggers. The thick blue trace is Axon 1, and the others in the background are Axons 2 (yellow), 3 (green), 4 (orange), 4 (purple) and 5 (brown). The Axon connection loop goes $1 \rightarrow 2 \rightarrow 3 \rightarrow 4 \rightarrow 5 \rightarrow 6 \rightarrow 1$. Axon 1 is stimulated to fire with a $100\,pA$, $500\,ms$ pulse, and the Axons fire sequentially and indefinitely. The channel and electrophysiological constants are identical to each other at to Fig. 6.9, but the synapse resistor value here is $R_s = 400\,M\Omega$. 97

6.11 Four Axons connected by inhibitory and excitatory input to produce an oscillator. The connection scheme is shown above (a), where (+) corresponds to excitatory input and (-) corresponds to inhibitory input. In this connection scheme, the Axons fire indefinitely with no trigger. A small pulse is applied to the first Axon, after which there is no intervention in the circuit. The Axon color scheme and excitatory pulse in this figure are identical to Fig. 6.11, and the parameters for this figure are identical to Fig. 6.10 (with exception in the inhibitory synapses). 98

7.1 System block diagram. The complete system consists of two such circuits, one for the right (R) photodiodes and AA and one for the left (L) components. VFC: voltage to frequency converter; FVC: frequency to voltage converter. 101

7.2 Measured photodiode output $V(r, 0)$ with fit. Equations 7.1 and 7.6 fit the output behavior and saturation distance r_0 very well. $V_S = 10\,V$, $V_b = 1.2\,V$, $P = 728\,mW$, $\phi = 0$, $R_F = 1\,M\Omega$, $R_\lambda = 0.52\,A/W$, and $A = 2.29 \times 2.29\,mm$. . . . 104

7.3 Photodiode and amplifier circuits. There are two OPT301 photodiodes in this diagram. The output of the first photodiode is equal to $V_0 = i_1 R_F$, where R_F is external to the photodiode and i_1 is the photodiode current. The output pin of the first photodiode is connected to the ground pin of the next. The output of the second photodiode is the sum of the individual outputs, equal to $V_0 = i_1 R_F + i_2 R_F$. More photodiodes can be added by continuing to connect in this way, from output pin to ground. The final output to be sent to the Artificial Axon is the sum $V_o = \Sigma_n i_n R_F$. In the navigation circuitry specifically, $V\pm = \pm 12\,V$ and $R_F = 44\,M\Omega$. 105

7.4 Top-view schematic of the photodiode arrangement for right-turns. 106

7.5 Photodiode relative responsivity for turning in one direction. The photodiodes are oriented at 90° from each other, facing forward, backward and outward. The sum of individual outputs combine to produce one input to the artificial axon. This sum is represented by the blue trace, while the yellow, orange and green traces represent individual photodiode outputs. The x-axis angles are referenced from the outward-facing photodiode's incidence angle $\phi = 0°$. 107

7.6 Connection diagram for the Burr-Brown VFC32. V_{in} is the photodiode output to be converted to frequency, and f_{out} is the output converted to frequency. An external resistor value $R_1 = 48\,k\Omega$ is chosen to make the VFC frequency linearly proportional to the photodiode output, and an external capacitor value $C_1 = 8\,nF$, is chosen to cap the frequency maximum at $4\,kHz$. The pull-up resistor $R_{pu} = 10k\Omega$, integrating capacitor $C_2 = 22\,nF$, and $\pm V_{CC} = \pm 12\,V$. The pin connection diagram is taken directly from the datasheet for the VFC32, and the external connections in the figure are added manually. 109

7.7 Whole time series of action potentials corresponding to the navigation run. Time $t = 0\,s$ corresponds to the start of the video. The data recording begins 1.75 seconds later. (a) Left axon; (b) right axon. 114

7.8 Still of the room of the room of the demo, seen from the ceiling. The car and light source are at diametrically opposite corners. Visible on the right is the optical table with the artificial axons and the electronics, as well as H.G.V. 115

7.9 Car trajectory corresponding to the navigation run. The light source is at the origin; the scales on the axes are in m, and the car starts at $(x, y) = (3.4, 3.0)$. . 116

7.10 (a) Membrane potential in the Left artificial axon (blue trace) and the Right AA (yellow trace) for part of the navigation run. (b) The signal at the output of the voltage to frequency converter (VFC), for the R and L circuits, and the same time interval as in (a). The currents injected by the synapses into the respective AAs are proportional to these signals. 118

7.11 Illustration of the model vectors. There are two photodiodes for turns on each side of the car, represented by the normal vectors $\hat{\mathbf{n}}_{ij}$. The vectors r_L and r_R point form the light source at the origin to the left and right turn photodiodes, respectively. ϕ_{R2} is the incident angle for light on one photodiode. 120

7.12 Car trajectory obtained from a simulation where the right AA has a firing rate 1.9 times higher than the left AA, for the same light seen. The car still "finds" the light source, which is at the origin. 122

LIST OF TABLES

2.1 Buffers used in the Purification protocol. The acronym *PIC* expanded is *Protease Inhibitor Cocktail*. 16

ACKNOWLEDGMENTS

I would not be here, submitting this thesis today, were it not for the support I received from selfless and wonderful people. First, my heartfelt gratitude goes to Giovanni Zocchi. You are a great scientist, advisor and mentor. From you and your brilliant intuition I have learned how to be a more critical thinker, and how to approach and solve problems, among many other lessons that have made me a more well-rounded person. I am forever grateful for the opportunity to work with such a great advisor.

I thank my colleagues in the lab, Yilin Wong and Zahra Alavi, for your help with equipment and experimental protocols. Thank you for your company and conversation, which made the day-to-day in the basement more enjoyable. Thank you Amila Ariyarante for imparting on me your experimental knowledge of ion channel expression and reconstitution, and all the electrophysiology that followed. Furthermore, I thank you for your patience in *all* my questions, especially for the extra-small, high-volume questions on all topics. I would also like to express my gratitude to Diego Quiroga for your help in troubleshooting me out of a problem I could not crack on my own; in the process I learned how to make more informed guesses and test steps in troubleshooting.

I would like to express my gratitude to *all* my friends. I wish I could list *everyone* individually. Your friendship is fuel.

I would like to express my gratitude to a few individuals I have met during my time at UCLA. Thank you for your friendship, for your help with lab work and homework. Thank you Michael Ip, Kim Phifer, Alex Cahill, Andreea Georgescu, Tom Neiser and Alden Fan. I would also like to thank Jenny Lee, who was in my corner on Day 0; I am grateful for your support, as are all the individuals on this list.

Outside UCLA, I express my deepest gratitude to my husband Patrick Vasquez. Thank you for all your emotional support and patience; I will spend a lifetime repaying you. To David Cerrillo and Margarita Cornejo, I cannot express enough how thankful I am for you both. For two years, you gave me a room in your home so that I could take the needed courses to apply to physics programs. There was always a plate of leftovers for me, when I

would come home at midnight from school, and you asked for nothing in return. From the bottom of my heart, thank you. Candace Wong: I've expressed my gratitude to you many times over these last few years, and you can expect that I will continue to do so. Thank you.

Finally, I would like to thank my parents, my brothers and my sister Brandi Miller, and my in-laws for your support.

VITA

2003–2006 B.S., Psychobiology, UCLA, Los Angeles, California

2009–2011 B.S., Physics, UC Riverside, Riverside, California

2012–2018 Teaching Assistant / Teaching Fellow, Department of Physics and Astronomy, UCLA, Los Angeles, California

PUBLICATIONS

Hector Garcia Vasquez and Giovanni Zocchi. "Coincidences with the Artificial Axon." *EPL*, **119**:48003, 2017

Hector Garcia Vasquez and Giovanni Zocchi. "Analog control with two Artificial Axons." *arXiv:1806.08001*, 2018

CHAPTER 1

Introduction

The language of consciousness eludes us [Koc18, Kot05]. There are major competing theories [DKC98, TBK16] and fierce debates that revolve around the question, "what is consciousness?" There are 10^{11} neurons in the human brain. Searches for the minimum number of neurons required in a conscious experience have yielded estimates as low as $\sim 10^3$ [CK98]. Estimates for major computations, such as identifying human faces, are as low as 10 neurons [Koc04]. And one single neuron has been reported to respond to only one individual human face [QRK05]. The language of consciousness begins with the ion channel. Its behavior, its response to voltage dictates how a neuron responds to stimulus, how a neuron communicates a stimulus to another neuron, to clusters, all the way up to the level of how we perceive a stimulus and respond.

We take a constructivist approach to this question in a novel system developed by the Zocchi lab [AZ16], called the Artificial Axon (AA). To our knowledge, this is the first system that supports an action potential outside of the cell. My work with the Artificial Axon is in the development of the computational unit for a future "brain-like" network of Artificial Axons. The long-term goal of this work is to study complex network behavior that arises from the ion channel microscopics; a constructivist approach to ultimately asking the questions related to the origins of consciousness.

1.1 Present approaches and techniques

1.1.1 Approaches to measuring neural activity

Existing electrophysiological techniques probe both neuron activity at single and multi-cell levels. Some techniques measure the activity of individual neurons, and others measure the activity in the extracellular region outside of many cells; this latter, extracellular measurement is called a local field potential (LFP) recording. In brain slice electrophysiology, a slice of brain tissue is isolated and prepared for single-neuron or LFP measurements [SSD99]. In cultured-cell techniques, neurons are grown in the lab on micro-electrode arrays for extracellular recording [ODB15]. Live animal recordings are performed with implanted electrodes (called tetrodes) that record from up to dozens of neurons [FKN08].

These techniques have limitations in common. While these techniques are able to measure activity from many neurons, the individual connections are often difficult to discern. These techniques take advantage of the placement of many electrodes to triangulate the origin of a neuron signal. These techniques probe the behavior of tuned, mature neurons and networks. Channel leaks, densities, population conductance, and neuron connection strengths are all tuned, to name a few examples. What is lost is the ability to probe for the elements that are important in producing a viable computational unit and network. The tuned elements just now described, for example, are elements we contend with in our synthetic system; these elements and discussions arise in the chapters of this thesis. Furthermore, the mechanisms and tissue in neurons responsible for maintaining homeostasis and non-signal processes bring with them uncontrolled variables that cannot be decoupled from desired signals in a measurement.

1.1.2 Constructivist approaches

Existing constructive approaches are computational [AES09], electronic [al11, al13], or based on real neurons, directing their pattern of connection [al02, FSM05, FM06, CBW06, FRM08, al12], and re-programming stem cells in 3D cultures [al15].

The first two have a long history, and, crucially, they are based on electronics. Specifically, neuromorphic chips (NMCs) are currently competitive with traditional von Neumann architecture neural networks in solving complex problems in pattern recognition [al17]. However, NMCs are simulators of spiking nerves, based on a fundamentally different microscopic process, namely electronics. Although the higher level architecture may be designed similar to a real network of neurons, the microscopics is different. Cultured neurons have been used by the Moses group to construct logic functions such as AND, also demonstrating a remarkable reliability achieved through a redundancy of connections [FRM08].

1.2 The Artificial Axon

The setup chambers and support structure we use for the Artificial Axon was developed for single and multi-channel electrophysiological recording [HLK99, WFF90]. However, as was mentioned above, an action potential has never been measured outside of the cell before the work of the Zocchi lab [AZ16]. In the absence of a second ion channel species, we use electronics to impose a resting potential on the membrane – what we call the current-limited voltage clamp (CLVC).

My work in the Zocchi lab is toward the development of a computational unit for a future "brain-like" network of Artificial Axons, much like the neuron is the computational unit for the brain. Because the neuron and Artificial Axon share the same microscopics, the properties of the computational unit in the Artificial Axon are also shared with the neuron. In this thesis, I demonstrate that the Artificial Axon is a threshold detector and a logic gate like the neuron. I develop the Artificial Axon to sustain input-dependent firing rates, and I develop an electronic synapse connection between Axons. I end with a demonstration of the Artificial Axon's potential in a network of only two Axons; I use two Axons to steer an RC car toward a light source.

CHAPTER 2

KvAP and the Artificial Axon

In our system, we use the voltage-gated potassium ion channel, KvAP. This channel is selectively permeable to K^+ ions, and its open/close states are voltage-dependent. The KvAP protein is composed of four trans-membrane subunits, each with an identical pore domain, selectivity filter and voltage-sensing domain (VSD). The channels open when the membrane is depolarized, and slowly inactivate after prolonged membrane inactivation. The channel recovers from inactivation after a long period of membrane polarization from $\sim 1\,s$ to $\sim 10\,s$. We use the KvAP channel in a novel system developed by the Zocchi lab [AZ16], called the Artificial Axon (AA). To our knowledge, this is the first system that supports an action potential outside of the cell.

In this chapter, I discuss the Artificial Axon and the $KvAP$ ion channel we use in the system. I begin with a brief introduction to the Nernst and rest potentials of a neuron, which are important potentials in the Artificial Axon. I describe the properties of the KvAP ion channel and the laboratory protocols we use to produce the protein in the lab for experiment. I then introduce the electrophysiological setup of the Artificial Axon, and discuss the model we use to simulate experiments and fit action potential measurements. I end with a discussion of a few immediate directions we may take in the development of the Artificial Axon.

2.1 Nernst and Action potentials in the neuron

The Nernst potential phenomena is what drives the action potential in the neuron. I briefly describe the Nernst potential here, then describe the action potential spike in terms of Nernst potentials.

The neuron lipid membrane separates the inside of the cell from the extracellular space. This membrane (i) suspends protein pores in its bilayer and (ii) keeps separate the different ion concentrations inside and outside the cell.

Protein pores sit in the membrane of the neuron, these pores open and close in response to voltage across the membrane, and a protein pore species will only allow one ion species through its pore. These proteins are called *voltage-gated ion channels*. One ionic species will have different concentrations inside and outside of the cell. All ion charges are balanced, so there is no net charge across the membrane. But when (for example) a potassium ion channel is open, K^+ ions will flow through the channel in the direction of the gradient. Flowing K^+ ions leave behind Cl^- ions, producing a charge separation and thus a potential that counters the flow of ions in the concentration gradient direction. This charge separation will continue until some potential is achieved that fully counters the concentration gradient, and the flow of ions stops. This potential, where ion flow stops, is called the *Nernst potential*.

The two main ion species in the neuron – K^+ and Na^+ – have concentration gradients in opposite directions: there is more K^+ inside the neuron with respect to the outside, and there is more Na^+ outside compared to inside. When the membrane is depolarized, the Na^+ channel species opens first because it is faster than the K^+ channel. Na^+ ions move toward the sodium Nernst potential, and inactivate. The slower K^+ channels open and K^+ ions flow in the opposite direction toward the potassium Nernst potential, also ending in inactivation. The result is a spike in the membrane potential, where the rising edge is caused by Na^+ ions moving toward their Nernst potential and the falling edge is caused by K^+ ions moving toward their Nernst potential. Without further depolarizing stimulus, the membrane returns to its resting potential.

The expression for the Nernst potential of an ion species is given by

$$V_N = \frac{kT}{|e|} ln \frac{c_{in}}{c_{out}} \tag{2.1}$$

where k is the Boltzmann constant, T is temperature, e is electronic charge, and c_{in} and c_{out} are the concentrations of the ion species inside and outside the cell, respectively.

The resting potential of the membrane is also a result of the Nernst potential phenomena. There is a small, nonzero leak in closed channels that establishes a resting potential away from the Nernst potentials of both sodium and potassium. The expression for rest is

$$V_r = \frac{\chi_K V_N^K + \chi_{Na} V_N^{Na}}{\chi_K + \chi_{Na}} \tag{2.2}$$

V_r and V_N are reproduced in the Zocchi lab with the system we call the Artificial Axon. We use one ion channel species and electronics to reproduce an action potential outside of the cell, the details of which are described in this chapter. First I begin with a description of the ion channel we use in the Artificial Axon – the voltage-gated potassium ion channel, *KvAP*.

2.2 Properties of the KvAP

Voltage-gated K^+ ion channels (Kv channels) are trans-membrane proteins in the neuron that almost exclusively allow only potassium ions to pass through the membrane by way of a pore in the structure of the protein channel. Pore open/close states – gating – are voltage-dependent. When the potential inside the neuron is positive with respect to the outside, the pore is open and K^+ ions travel into the neuron through the pore. When the potential inside the neuron is negative with respect to the outside, the pore is closed.

We use the Kv channel KvAP in the Artificial Axon. The KvAP is named after the Archaea extremophile *Aeropyrum Pernix*, the bacteria in which it was first discovered. *Aeropyrum Pernix* is a thermophile, first discovered in a deep-sea vent off the coast of Kodakara-Jima Island, Japan [SNU96]. It's optimal temperature range is $32° - 35° C$. In the lab, all experiments with the channel are at 20°.

The KvAP channel crystallographic structure was first solved in 2003 in the Roderick MacKinnon lab, and was the first time a Kv channel structure was solved [RJL03]. The MacKinnon lab is also where our lab acquired the KvAP channel.

2.2.1 KvAP structure

Figure 2.1 shows the subunit and complete structure of the Kv channel from multiple views. These figures are from the thesis of Andrew Wang in Giovanni Zocchi's lab (Manipulation of Molecular Processes with DNA Molecular Springs). The figures were generated in PyMol using the Kv structure solved by the MacKinnon lab [LTC07, ZMK01]. For the subunit in the upper-right corner – Structure PDB ID: 2R9R.

The KvAP channel is made up of four subunits in the membrane, and each subunit is one connected polymer chain with six major helices. The representation in the upper-left corner shows the major helices and their function in the channel. The first three cyan helices (S1-S3) provide structure to the voltage-sensing domain, and the yellow S4 helix is the voltage sensor helix in this domain. The four charges on S4 are from Arginine amino acids on the helix, the actual voltage sensor. The S4-S5 linker in orange provides separation of the domains and allows for large swings of S4 across the membrane during open/close transitions [JRC03, JLC03] and potentially rotations on the membrane plane; only the open structure is known and much about the motion of the domains during open/close transitions is unknown. Different models for open/close transitions are proposed [YBC06, PYA07]. S5-S6 in blue constitute the cavity and filter in the pore. The helix between S5 and S6 is the selectivity filter, responsible for the KvAP's permeability to (almost exclusively) K^+ ions.

The representation in the upper-right corner is a side-view of a KvAP subunit. The pink spheres represent K^+ ions along the S5-S6 selectivity filter. The bottom figures are complete representations of the Kv ion channel from the top and side views. These views elucidate (i) how S5 and S6 helices produce the pore, and (ii) the position of the S4 helix and the rest of the voltage-sensing domain with respect to the pore.

2.2.2 The voltage-sensing domain

Like the amino acid structure in the selectivity filter, four Arginine amino acids in the S4 helix (the paddle) of the voltage-sensing domain are highly conserved across Kv channels [JLC03, Sig94, Bez00]. Each Arginine carries a positive charge, and these four positive

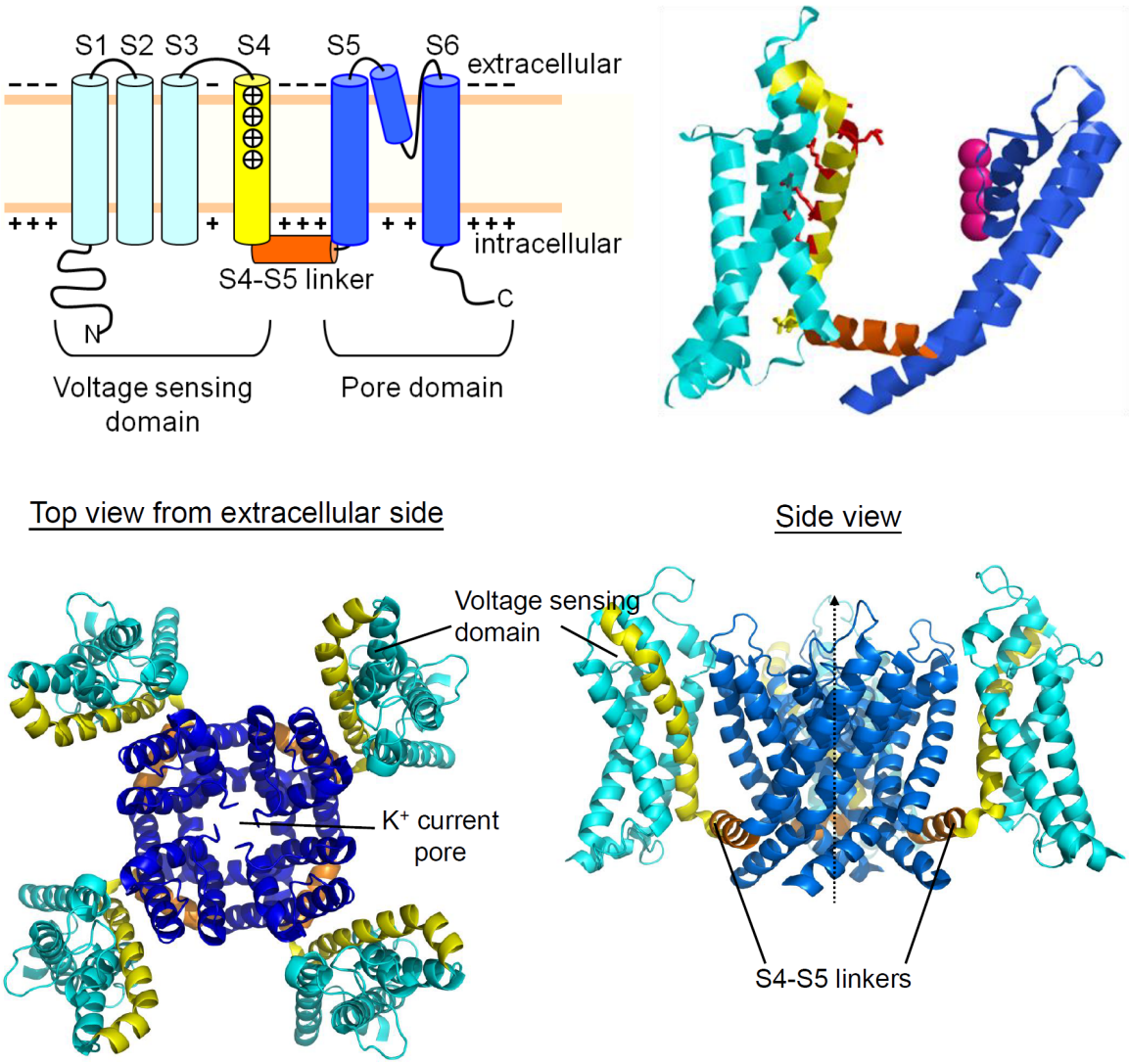

Figure 2.1: Subunit and complete structure of the Kv channel from multiple views. The upper figures show a single KvAP subunit and the bottom figures show a complete Kv channel with all 4 subunits from the top and the side views. One subunit contains six amino acid helices that comprise a voltage-sensing domain, a pore domain, and a selectivity filter subunit. In the assembled ion channel, the voltage-sensing domains are positioned on the perimeter of the pore, and the selectivity filter is on the intracellular side of the neuron. These figures are from the thesis of Andrew Wang in Giovanni Zocchi's lab (Manipulation of Molecular Processes with DNA Molecular Springs). The figures were generated in PyMol using the Kv structure solved by the MacKinnon lab [LTC07, ZMK01]. For the subunit in the upper-right corner – Structure PDB ID: 2R9R.

charges are the voltage sensor in a subunit of the channel. These charges physically move the paddle across the membrane as they follow the membrane potential. When the intracellular side of the neuron is positive with respect to the extracellular side, the paddles move toward the extracellular side and the pore opens. When the extracellular side is positive, the paddles move toward the intracellular side and the pore closes [JRC03]. The movement of these paddles produces a current – called the gating current – that is detectable and has been measured in Kv channels [AB73, SSP96, AM96].

For the pore to open to allow K^+ across the membrane, all four paddles must be oriented toward the extracellular side. I refer to one paddle on the extracellular side as "subunit in the *open* state," and a paddle on the intracellular side as "subunit in the *closed* state." These paddles move independently from each other, and only follow the voltage. At any given time, the paddles may randomly be in any combination of open-closed states. Only when all 4 paddles are in the open state is the channel open. In all other combinations, the channel is closed.

As was stated above in subsection 2.2.1, only the open structure for the KvAP ion channel is known. Therefore, the gating mechanism is unknown. There are multiple proposed models for the motion of the channel domains in open/close transitions [YBC06, PYA07, JRC03], most of which involve large swings of the S4-S5 linker (see Fig. 2.1).

2.2.3 The Kv selectivity filter

The selectivity filter is highly invariant across all Kv species in the five amino acids TVGYG [HLA94]. This filter is responsible for the high selectivity of Kv channels to K^+ ions over others. Against Na^+, for example, Kv channels are a reportedly 150 times more permeable to K^+ over Na^+ [LHM01]. The key to this permeability is the energy cost to strip the water molecules from an ion's hydration shell as it passes through the pore. As potassium ions pass through the selectivity filter in the pore of the ion channel, they are stripped of their water molecules. The potassium ion interactions with water are replaced by interactions with oxygen atoms in the carbonyl groups of the polypeptide backbone [ZMK01, JLC03].

The filter structure is optimized for minimal energy cost to dehydrate K^+ over Na^+, Ca^+ and Cl^-, the other ions in the neuron.

Ions are believed to travel through the pore single-file, with a fixed number of K^+ occupation sites inside the pore. It is astounding that through this seemingly rate-limiting structure, K^+ ions can travel through an open pore at 10^8 ions s^{-1}. While this problem is unresolved at the atomic level, simulations and theoretical work suggest solutions to this rate-limiting problem[BR01].

2.2.4 Inactivation

Most Kv channels do not stay open indefinitely, but rather undergo inactivation after prolonged periods of membrane depolarization. Inactivation is a slow process in the KvAP channel; pore opening occurs at $\sim 10\,ms$, and inactivation occurs over $\sim 100\,ms$ and more. When channels close and become inactive, they may recover and become active and able to open once again, but only after a period of prolonged negative membrane potential (extracellular potential with respect to intracellular region of the neuron). Inactivation in the KvAP is a significant consideration in the experiments we perform.

The mechanism for inactivation in Kv channels is still unknown, but evidence points to the selectivity filter as the culprit [YSC94, LJY96, KLK99]. The leading theory for the mechanism was proposed in a 2007 paper with experiments in selectivity filter mutations and simulations [CJL07]. In the interpretation of their findings, the open-closed states of a subunit are a property of VSD position in the membrane, and active-inactive states are assumed to be a property of selectivity filter conformation. Therefore, there are (at minimum) four subunit states: open-active, closed-active, open-inactive, and closed-inactive. When a subunit is in the open state, the selectivity filter in the open-activated state is unstable and "collapses" (changes conformation, which is responsible for inactivation); in the open state, the open-inactivated state is the stable state. In the closed state, the closed-active state is stable (selectivity filter prefers the un-collapsed state) and the closed-inactive state is unstable.

The rate of inactivation in Kv channels may be changed by manipulating external parameters. Higher salt concentrations will decrease the channel inactivation rate [KK98]. Lipid composition is known to change the inactivation rate as well [SCM09].

2.3 KvAP Preparation

In this section I present the protocols for production the KvAP protein in our lab. The three major processes in the protocols are Expression – production of a large amount of protein by *E. coli*, Purification – isolation of the protein from lysed cells and other organic matter, and Reconstitution – fusing channel protein into the membranes of vesicles. These vesicles are the final product, and are aliquoted then flash-frozen for later use.

Individual vesicle aliquots are later thawed for experiment and vesicles are pipetted over lipid membranes in our experimental setup. The vesicles fuse with the lipid membrane, thus putting ion channels on the bilayer.

2.3.1 KvAp Expression in *E. coli*

The wild type KvAP gene in the pQE-60 vector was given to our lab by the Roderick MacKinnon group.

There is a singular cysteine in the sequence at site 247 that is replaced with a serine by site-directed mutagenesis; a single thymine is replaced with an adenine, replacing the code for cysteine (TGC) with serine (AGC). This cysteine is problematic, as it forms disulfide bonds with other subunits and channels, resulting in protein aggregation that renders the sample unusable. The wild type KvAP may be purified and reconstituted successfully by addition of TCEP to the buffers for the sample in the protocol steps, but the yield of viable protein is low in comparison with mutated KvAP protein.

The protein Expression protocol below yields $\sim 10\,g$ of *E. coli* cells with KvAP protein. The final product is $\sim 2-3\,mg$ of KvAP protien. All steps in the protocol are performed at room temperature unless otherwise specified. The protocol for KvAP Expression below

is adapted from [RJL03].

Day 1 of Expression:

1. Pre-chill a $1.5\,mL$ microcentrifuge tube in ice.
2. Preheat SOC medium (stored at $-20°C$) to $42°C$ in a water bath.
3. Perform the following steps with sterilized pipette tips.
4. Thaw an aliquot of KvAP plasmid on ice (stored at $-20°C$).
5. Thaw XL1-Blue Competent Cells (stored at $-80°C$) cells on ice. When the cells have thawed, aliquot $100\,\mu L$ of cells into the pre-chilled tube. Return the XL1-Blue cells to storage at $-80°C$.
6. Add $1.7\,\mu L$ of β-mercaptoethanol to the aliquot. Gently swirl the mixture.
7. Incubate the cells on ice for 10 minutes. Gently swirl the tube every 2 minutes.
8. Add $\sim 8\,ng$ of KvAP plasmid to the aliquot of cells. Gently swirl the mixture.
9. Incubate the tube on ice for 30 minutes.
10. Heat-shock the tubes in a 42C water bath for 45 seconds, then incubate the tubes on ice for 2 minutes.
11. Add $0.9\,mL$ of $42°C$ SOC medium to the cells and incubate the tubes at $37°C$ for 1 hour with shaking at 225250 rpm.

Do the following steps under a flame for a sterile environment.

12. Use three separate Ampicillin/LB-agar petri dishes (stored at $4°C$) in the following steps. Note that Ampicillin resistance comes from the pQE-60 vector that contains the KvAP gene. Plate a $180\,\mu L$ pool of SOC medium (room temperature) into each dish, and add $20\,\mu L$ of $100\,mg/mL$ Ampicillin stock solution (stored at $4°\,C$) to each

pool. Plate $1\,\mu L$, $5\,\mu L$ and $25\,\mu L$ of cells into the pools on separate plates spread the mixtures with a sterile spreader (sterilize spreader between spreads). Label each plate with the plasmid volume added.

13. Store the cells at $4^\circ\,C$ in case plating must be re-done. The cells will remain viable for one week. Bleach and discard the tube afterward.

14. Incubate the plates for at least $16 \sim 20$ hours overnight at $37^\circ C$. Incubate the plates in the inverted position to prevent contamination from falling moisture on the lid to the agar. Note that an incubation time closer to 16 hours is ideal.

Day 2 of Expression:

Do the following steps under a flame. Use sterilized pipette tips for all steps involving Transformed *E. coli*.

1. Use 2 -3 autoclaved culture tubes, or sterilize the culture tubes with a flame.

2. Add $5\,mL$ of LB broth to each culture tube. The broth used is either from storage at $-20^\circ C$ with $100\,\mu L$ Ampicillin stock solution, or it is made from powder before the start of the Day 2 protocol: $25\,g$ LB Broth, Miller, powder for $1\,mL$ DI water, autoclaved then brought to $100\,\mu L$ Ampicillin stock solution after cooling.

3. If the LB broth does not have a concentration of Ampicillin, then add $5\,\mu L$ Ampicillin stock solution to each tube. This is called the *inoculation* step.

4. Use a $1\,mL$ pipette to pick up one colony on the agar plate. Choose a colony that is away from the edges of the dish and other colonies. Gently pipette this colony into one tube, and pump broth into the pipette several times to wash cells off the pipette tip. Repeat for the remaining culture tubes, with a new colony and new pipette tip.

5. Cover the mouth of the tube with foil sterilized by either autoclave or by flame.

6. Incubate the tubes at $37^\circ C$ for ~ 5 hours with shaking at $225 \sim 250\,rpm$.

7. Store the agar plates at $4°C$ in case the colonies do not grow in any tube; the steps above may be repeated with new colonies. After $\sim$ 2 hours, cloudiness in the tubes indicates successful cell growth. If there is cell growth in the culture tubes, then bleach, parafilm and discard the agar plates.

Perform the following steps during the 5 hours of incubation.

8. Add $25\,g$ of LB broth powder to $1\,L$ of DI water in a $2\,L$ flask. Prepare 6-7 flasks. Cover the mouth flask with foil, and place autoclave tape on the foil.

9. Autoclave the flasks in a liquid cycle.

10. Use autoclave gloves to remove the flasks from the autoclave. Store the flasks on a counter at room temperature to cool down.

At the end of the 5 hours, turn on a flame for the steps that follow.

11. Choose one of the autoclaved flasks, and add $1\,mL$ of Ampicillin stock solution. Confirm that the flask is cool to the touch, as hot broth may destroy cells and/or the Ampicillin. The remaining flasks are used the next day.

12. Choose a random culture tube with cell growth, mix with a pipette, and pour the contents into the cooled $2\,L$ flask with Ampicillin. The unused tubes may be bleached and discarded.

13. Incubate the $2\,L$ flask at $37°C$ with shaking at 220 rpm for $16 \sim 20$ hours overnight. Note that an incubation time closer to 16 hours is ideal.

Day 3 of Expression:

1. After $\sim$ 16 hours of overnight incubation, measure the optical density (OD) in the $2\,L$ flask. Under a flame, take a sample from the $2\,L$ flask for OD measurement, and dilute the sample with unused LB broth (no *E. coli*) n times before measurement; no more than $n = 10$ dilution is necessary. Take unused LB broth as a blank for the spectrometer, and measure the OD at wavelength $600\,nm$.

2. Calculate the volume V_i of *E. coli* in the incubated $2\,L$ flask that is needed to bring the OD in the unused broth V_f to $OD = 0.1$. OD is directly proportional to concentration, so in the equation for mass conservation $C_i \times V_i = C_f \times (V_f + V_i)$, we may use OD in place of C to determine volumes. Note that if C_i is large, the equation reduces to $V_i \times C_i \approx V_f \times C_f$. For example, if the measured OD in the diluted sample is 0.4, and the incubated *E. coli* was $3\times$ diluted ($n = 3$), then the actual OD is $0.4 \times 3 = 1.2$. To bring the OD to 0.1 in $V_f = 1\,L$ of unused broth, the volume added is $V_i = 1\,L\,/(1.2/0.1 - 1) = 91\,mL$.

Do the following under a flame.

3. Add $1\,mL$ of Ampicillin stock solution to each $2\,L$ flask of unused broth.

4. add the calculated volume V_i of incubated *E. coli* broth to each flask of unused broth to bring the OD to 0.1.

5. Incubate the flasks at $37°C$ with shaking at 220 rpm for 4 hours. Bleach and discard what remains of the broth in the original overnight flask.

6. After 4 hours, check the OD every 20 minutes.

7. When the OD reaches 0.8, add $400\,\mu L$ IPTG ($1\,M$) to each flask for a final IPTG concentration of $0.4\,mM$. IPTG induces expression of KvAP protein in *E. coli*.

8. Incubate at $37°C$ with shaking at 220 rpm for 4 more hours.

9. Weigh the empty $1\,L$ Nalgene centrifuge bottles that will be used to centrifuge the *E. coli* at the end of the 4 hours, and label each empty bottle with its weight. The mass of the cells will be needed in the steps below.

10. At the end of 4 hours, centrifuge the cells in the Nalgene bottles for 20 minutes at 4000 rpm. Balance all bottles before centrifugation. At this point, there is no need for sterile environments and surfaces, and mixing bottle contents together is fine.

		Stock Solutions	Amount	Final Concentration
Lysis Buffer	Tris-HCl KCl ddH_2O Lysozyme PIC DNase B-ME	500 mM, pH 8.0 1M 10mg/ml 14 M	5.0 mL 5.0 mL 35.0 mL 10 mg (1 tablet) 10 µL 7.4 µL	50 mM pH 8.0 100 mM 0.2 mg/mL 2 µg/mL 2 mM
add after lysis	Decylmaltoside	500 mM	4.0 mL	40 mM
Wash Buffer	Tris-HCl KCl Imidazole Decylmaltoside ddH_2O	500 mM, pH 8.0 1 M 1 M, pH 8.0 500 mM	2.0 mL 5.0 mL 1.0 mL 0.5 mL 41.5 mL	20 mM, pH 8.0 100 mM 10 mM 5 mM
Elution Buffer	Tris-HCl KCl Imidazole Decylmaltoside ddH_2O	500 mM, pH 8.0 1 M 1 M, pH 8.0 500 mM	2.0 mL 5.0 mL 20.0 mL 0.5 mL 22.5 mL	20 mM, pH 8.0 100 mM 400 mM 5 mM

Table 2.1: Buffers used in the Purification protocol. The acronym *PIC* expanded is *Protease Inhibitor Cocktail*.

11. Remove all but very little supernatant to mix and consolidate all the pellet into as few bottles as possible. Continue centrifugation at 4000 rpm for 20 minutes until bottles are to a minimum, then remove all supernatant.

12. Store the bottles with cells at $-80°C$. Storage at $-20°C$ is acceptable if the cells are to be used within 1 month.

2.3.2 KvAP Purification protocol

All buffers used in the purification process are listed in Table 2.1.

The cells are lysed in the EmulsiFlex -C3 High Pressure Homogenizer; the protocol in this paragraph is specific to the recommendations for this homogenizer. Thaw the expressed

pellet at room temperature. Suspend every $1\,g$ of protein in $3\,mL$ of Lysis Buffer. Dissolve all clumps and solid particles in the pellet-buffer mixture with a magnetic stir bar to avoid clogs in the homogenizer. Lyse the cells at pressures between $15000 - 18000\,psi$. Run the sample through the homogenizer 3-4 times to completely lyse the cells.

After cell lysis, add decylmaltoside (DM) stock solution to the lysed solution to extract the KvAP from *E. coli* cell wall fragments in solution. DM is a detergent with a hydrophilic head and hydrophobic tail that shields the hydrophobic regions of the KvAP subunit from water molecules. Bring the DM concentration to $40\,mM$ and gently rotate the sample for 3 hours. Centrifuge the sample for 30 minutes at 15,000 rpm.

While the sample is in centrifugation, wash $\sim 2\,mL$ of Talon Cobalt beads (Clonetech) in a Talon affinity column. Wash the beads slowly with $30\,mL$ of Wash Buffer, $10\,mL$ at one time.

After centrifugation, collect the supernatant and discard the precipitate. Add the beads to the supernatant and gently rotate the mixture for one hour. The C terminal of a KvAP subunit possesses six genetically added Histidine residues – a His tag. Cobalt ions on the Talon beads for a complex with the His tag [Hen95], effectively attaching KvAP subunits to the Talon beads to separate the KvAP from remnant *E. coli* protein in the sample solution.

After one hour of sample rotation with the beads, separate the beads from solution using a Talon affinity column. Keep enough solution with the beads to keep them submerged at all times. Run the solution through the filter 4 times so that the protein can completely bind to the beads. Wash the beads with $30\,mL$ Wash Buffer to remove *E. coli* protein bound to the beads by non-specific binding. Imidazole at low concentrations competes for binding sites with non-specifically bound protein. Wash the beads slowly, in increments of $10\,mL$.

Elute the protein with $8 - 10\,mL$ of Elution Buffer. The high concentration of imidazole removes the KvAP from beads. Suspend the first $1\,mL$ of Elution Buffer in the column for a few minutes to remove the majority of KvAP protein from the beads. Elute the remaining Elution Buffer slowly, in increments of $1\,mL$.

Finally, add 1.5 units of thrombin per milligram of KvAP protein to remove the His tag

from the subunits. Keep the eluted sample in thrombin overnight at $12°C$.

2.4 KvAP Reconstitution into lipid vesicles

This protocol was adapted from [HLK99]. The KvAP sample is prepared for mixing with lipid vesicles, and both processes are time-sensitive. The sample volume is reduced to 100's of microliters, at which the protein may aggregate and become unusable. The lipid vesicles, once prepared, will begin to merge into larger vesicles and structures that are also unusable. Timing is important, thus vesicle and protein preparation should be performed as concurrently as possible. If one preparation is complete before the other, either lipid vesicles or KvAP should be stored at $4°C$ until the other is ready for mixture.

Preparation of lipid vesicles

First, remove a DPhPC lipid (Avanti) glass vial aliquot from storage at $-80°C$. The DPhPC lipids are stored in chloroform. Gently dry the DPhPC lipids with nitrogen gas for 10 minutes to evaporate the chloroform. After 10 minutes, add $250\,\mu L$ of pentane to wash the lipids, and evaporate the pentane with nitrogen gas for another 10 minutes. Then place the vial in a vacuum for 30 minutes to further remove chrloroform.

Suspend the lipid in Reconstitution (RC) Buffer - $450\,mM$ KCl, $10\,mM$ HEPES, pH 7.4. Bring the lipid concentration to $20\,mg/mL$ in RC Buffer. Vigorously vortex this mixture for 30 minutes. At the end of vortexing, the solution is milky and opaque. This indicates that the lipid merged into large structures and multilamellar vesicles.

Sonicate the vesicles in a bath sonicator until the lipid solution is nearly transparent. A clear solution indicates that small unilamellar vesicles have formed. This process can take anywhere between 30 minutes to one hour or more; increasing the bath temperature to $\sim 40\,C$ improves the small-vesicle production process.

Use a $500\,mM$ DM-in-RC Buffer stock solution to bring the concentration of DM in the lipid solution to $10\,mM$. Allow the mixture to dissolve for 30 minutes with very gentle vor-

texing or, to avoid the induction of re-merging in the lipids, gently mix the solution with a pipette every few minutes for 30 minutes. At the end of this step, store the lipid in $4°C$ if the KvAP sample is not ready for mixture with the lipid.

Preparation of KvAP

Concentrate the KvAP sample to $2\,mL$ by centrifugation. Use the Amicon Ultra-15 to centrifuge at no more than $5000 \times g$; excessive speeds may induce leaks in the filters.

Run the concentrated sample through the size-exclusion Superdex-200 10-300 GL (GE Healthcare) to separate KvAP in the sample from thrombin, His tag, and remaining protein impurities in solution. Flow through the column is controlled by an HPLC (Bio-Rad). The HPLC Buffer: $100\,mM$ KCl, $20\,mM$ Tris-HCl at pH 7.5 and $5\,mM$ Decylmaltoside. The purified sample volume is typically between $2 \sim 4\,mL$.

Centrifuge the collected sample concentration down to $\sim 10\,\mu g/\mu L$ using the Amicon Ultra-4. The final volume is typically between $100 \sim 200\,\mu L$, which depends on the mass of the sample. Centrifuge at speeds no higher than $7500 \times g$; 10 minutes is typically enough time to achieve these concentrations. At the end of this step, store the sample in $4°C$ if the lipid is not ready for mixture with the protein.

When both lipid and protein preparations are complete, mix the solutions together. The lipid:protein mass ratio should be between 3:1 and 5:1; ratios closer to 3 have produced the best multi-channel recording results. Note that for single-channel recordings, lipid:protein ratios are on the order of 1000:1.

After mixing, bring the DM concentration up to $17.5\,mM$ with $500\,mM$ DM-in-RC Buffer. Allow the mixture to sit for 2 hours; this is called an incubation step. Very gently vortex the mixture every 20 minutes or, to avoid re-merging of lipids, gently mix with a pipette.

Detergent is removed from the sample solution in two steps. First the sample is run through desalting columns (Thermo, Zeba-spin desalting column for $2\,mL$). This step re-

moves DM from solution, resulting in protein transition from solution into the vesicle membrane [HKM98]. Second, adsorbent beads (Bio-Rad, Bio-Beads SM-2 Adsobents) slowly remove residual detergent [RLM98] over the course of 48 hours.

The columns and beads must first be washed before use. This washing step is done during the 2-hour incubation period. Three desalting columns are washed 3× each by passing RC Buffer through the column with centrifugation. Spin the columns with RC buffer for 2 minutes at $1000 \times g$, at $4°C$. Next, prepare four 1.5 mL tubes with adsorbent beads for washing. Wash each tube of beads 3× with methanol, 3× with DI water, and 3× with RC Buffer. At the end of the wash, keep the beads suspended in RC Buffer. A note on bead volumes: too much bead volume may remove detergent too quickly and result in re-merging of lipids into larger, unusable structures; bead volumes that are too small will not remove all the detergent. Aim for a bead:sample volume ratio of $\sim 1:1$, leaning toward less beads. For example: typically, the final protein sample volumes are $\sim 300\,\mu L$ and larger. Therefore, start with $400\,\mu L$ of beads in each tube, and remove/add beads when the final sample volume is known. Store the beads at $4°C$.

At the end of the 2 hour incubation period, pass the sample through the three desalting columns. Spin at $1000 \times g$ for 2 minutes at $4°C$ through each column, collecting the sample in a clean tube after every spin. Put the final sample volume in one tube with beads and store the mixture at $4°C$ for 12 hours. Exchange the beads – place the sample in a new bead tube – every 12 hours, for 48 hours total.

At the end of the 48 hours, aliquot the sample into $10 - 20\,\mu L$ volumes in $0.2\,mL$ tubes. Flash freeze the aliquots in a dry ice and ethanol bath, and immediately store the aliquots at $-80°C$.

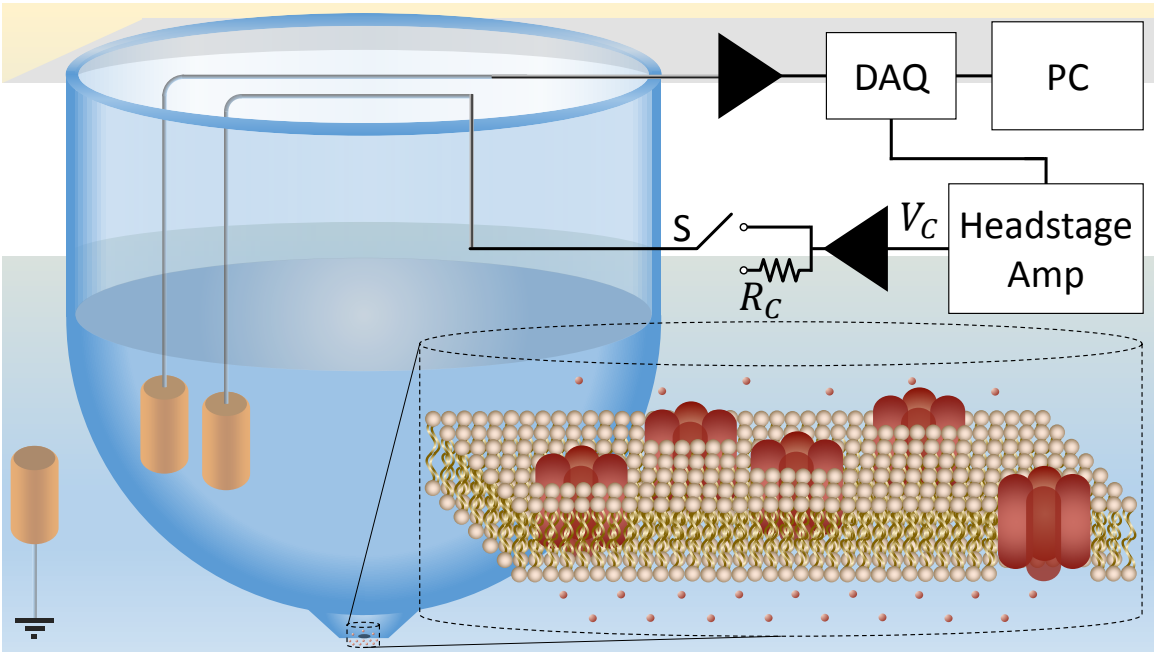

Figure 2.2: Electrophysiology setup for the Artificial Axon. A $\sim 100 - 200\mu m$ aperture at the bottom of the cup supports a lipid bilayer and KvAP ion channels. The bilayer separates the solutions on the inner and outer chamber, thus allowing for a Nernst potential to be manually created with the solutions in the cis and trans chambers. The DAQ records the membrane voltage, and the headstage amplifier is a voltage clamp when the switch S is oriented as shown in the figure. When switch S is connected to R_C, the electronics are the current-limited voltage clamp (CLVC), and function as the second ion-channel species in imposing a resting potential in the neuron.

2.5 Electrophysiological measurement with KvAP

2.5.1 Electrophysiological setup

The setup for electrophysiological measurements is shown in Fig. 2.2. The Headstage Amplifier imposes a voltage across the lipid membrane in the aperture of the support cup, inducing a response in the voltage-gated KvAP channels in the membrane.

The lipid bilayer support structure (cup) and Teflon chamber design in the Zocchi lab are described in [WZ11, AZ13, AZ15, AZ16]. The support structure for the lipid bilayer is a plastic centrifuge tube (Ultra-Clear^{TM}, Beckman-Coulter) with a $100 \sim 200\,\mu m$ aperture sliced into the bottom of the tube. The method for producing the aperture in-lab is adopted from [WFF90].

The lipid preparation for the membrane bilayer is the same as the protocol described in section 2.4 for drying the lipid. But instead of re-suspending the dried lipid in RC Buffer, the lipid is suspended in decane to a concentration of $20\,mg/mL$. The area around the aperture is painted carefully with the decane-lipid mixture. The decane on the cup is then dried with a gentle blow of N_2 gas for 10 minutes of longer. The cup may also be dried in a chamber for 10 minutes. The cup is then put into the chamber, and a pipette is used to paint a lipid bilayer membrane over the aperture with fresh decane-lipid mixture. A magnified section of the lipid bilayer on the aperture is shown in Fig. 2.2. The red structures in the bilayer represent KvAP ion channels, and the red dots are K^+ ions. KvAP Vesicles are pipetted directly above the membrane from the inside of the cup in $\sim 1\,\mu L$ increments. The vesicle lipid fuses with the bilayer, effectively inserting the KvAP into the bilayer.

The cup is held firmly in place by a Teflon chamber. The chamber and cup are filled with a K^+ buffer ($X\,mM$ KCl, $10\,mM$ HEPES, pH 7.4; X varies by experiment); these solutions are kept separate by the lipid membrane. We refer to the inside of the cup as the *cis* chamber, and the Teflon chamber as the *trans* chamber.

The tan cylinders represent AgCl electrodes. The electrode in the *trans* chamber is connected to ground. As such, the *trans* chamber is analogous to the extracellular region

of an axon, and the *cis* chamber is equivalent to the intracellular region. The channels are oriented in the membrane to open when the *cis* potential is positive: when the potential in the *cis* chamber is positive with respect to ground, channels in the active state will open and K^+ ions will flow from the *cis* to the *trans* chamber, ultimately inactivating; when the *cis* chamber is negative with respect to ground, the channels close. The left-most electrode in the *cis* chamber (Fig. 2.2) measures the membrane potential, and the DAQ records the voltage. The right-most electrode in the *cis* chamber injects current into the chamber. The form of the current in time depends on the position of the switch S.

2.5.2 Measurement with a voltage clamp

The Headstage Amplifier, with the switch S position as shown in Fig. 2.2 (shorting the resistor R_C), is a voltage clamp. The voltage V_C is imposed on the membrane by the DAQ. The Headstage Amplifier circuit can source enough current to overwhelm the channel current, thus maintaining the membrane potential at V_C.

Figure 2.3 shows a measurement of the current injected by the voltage clamp onto the membrane in one clamp voltage step from $-120\,mV$ to $60\,mV$. At $t = 300\,ms$, the clamp voltage is stepped from $V = -120\,mV$ to $60\,mV$ and the channels open then inactivate. (a) shows the complete step in voltage, and (b) shows a subset of the measurement, when the channels open. At $t < 0$ the voltage is set to $-120\,mV$. The voltage clamp injects $4\,nA$ onto the membrane to counter an ohmic leak that comes from either the membrane, its interface with the support structure, or from the channels; the source of this leak is unknown. The spike shortly after the step at $t = 300\,ms$ is from the charging of the membrane, which separates charge and behaves like a capacitor. The channels open and move to complete inactivation, the current reaching equilibrium from the ohmic leak at $2\,nA$. Finally, at $3.2\,s$ the clamp voltage is stepped back down to $-120\,mV$, where the channels will recover from inactivation.

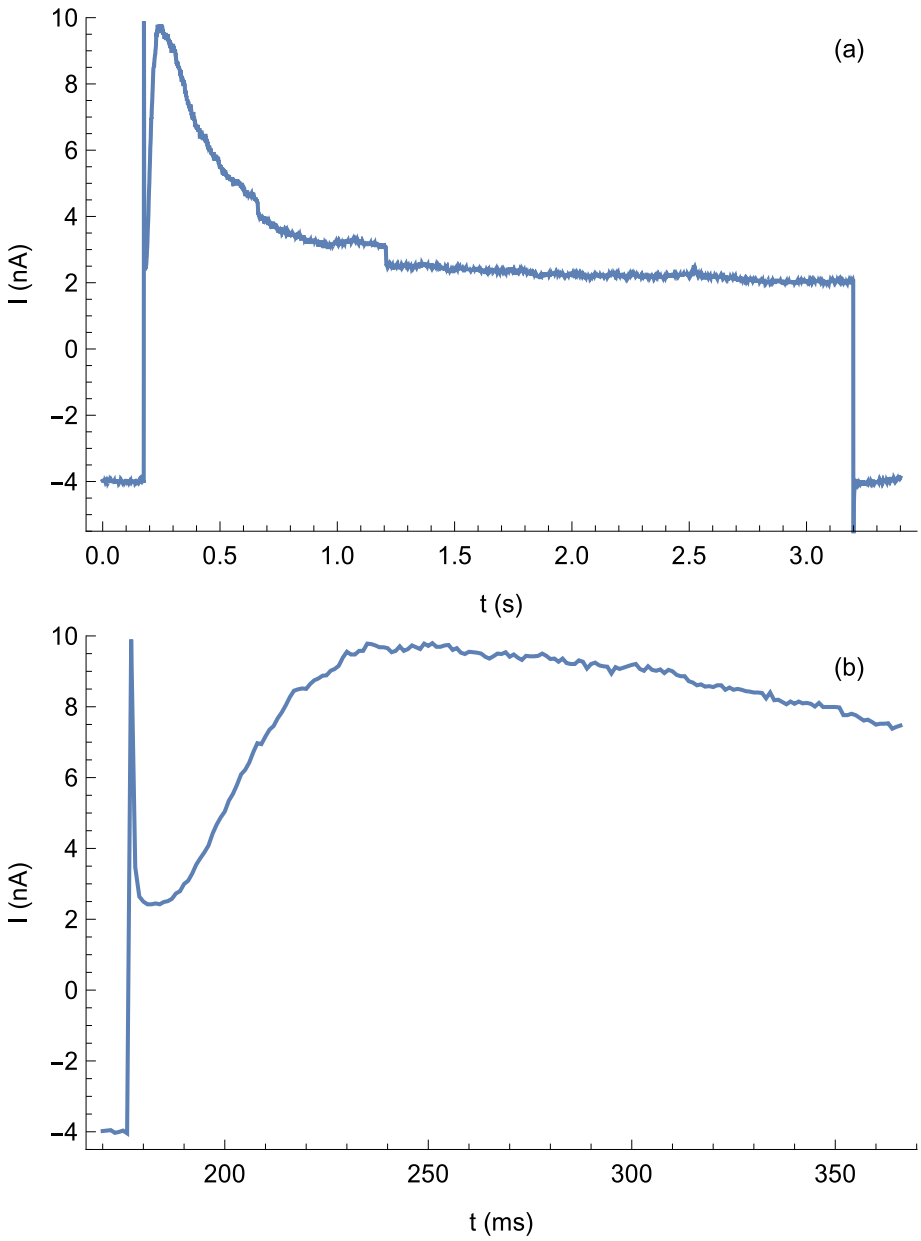

Figure 2.3: Voltage clamp current on a membrane with ion channels. In this measurement, the switch S in Fig. 2.2 is connected as shown in the figure, shorting R_C, so the Headstage amplifier is a voltage clamp. (a) shows the entire step and (b) shows a frame when the channels are open. At $t = 200\,ms$, the clamp voltage is stepped from $Vc = -120\,mV$ to $-60\,mV$. The channels open, fully inactivate, and the voltage clamp current moves to equilibrium at $2\,nA$. This nonzero current when channels are closed comes from an ohmic leak in either the channels, membrane, or the aperture contact with the lipid-decane mixture.

2.6 The Artificial Axon

2.6.1 The Nernst potential in the Artificial Axon

A high KCl concentration buffer in the trans chamber and low concentration in the cis chamber produces the Nernst potential in our system. We are able to manually produce a Nernst potential across the lipid membrane because of the separation of solutions in the cis and trans chambers by the lipid membrane itself. When KvAP channels open in the membrane, K^+ ions will travel toward the Nernst potential into the cis chamber, to spike as the rising edge of an action potential.

A typical trans chamber buffer is $150\,mM$ KCl, $10\,mM$ HEPES, pH 7.4. A cis chamber of $30\,mM$ KCl, $10\,mM$ HEPES, pH 7.4 is balanced with $120\,mM$ sucrose. The sucrose balances the KCl in the cis chamber against osmotic pressures that burst the membrane. To manually establish the Nernst potential, both chambers are initially filled with $150\,mM$ KCl buffer. To exchange the cis buffer with a lower-concentration solution, the aperture is first sealed with a generous volume of decane-lipid mixture; membranes are sensitive to bursting during buffer exchange, but decane-lipid mixture is more robust. The cis solution is exchanged in increments of $\sim 100\,muL$ to avoid bursting or leaks through the decane seal. Exchanges with excessive volumes may result leaks and loss of decane around the aperture. Losing decane around the aperture will make it difficult to paint membranes; the membranes are fragile and sensitive to bursting.

Using eqn.2.1, we find the Nernst potential across the chambers:

$$V_N = \frac{kT}{|e|} ln \frac{[K^+]_{trans}}{[K^+]_{cis}} \approx +40\,mV \tag{2.3}$$

where $[K^+]_{trans}$ and $[K^+]_{cis}$- are the K^+ concentrations in the trans and cis chambers, respectively.

Once the Nernst potential is established across the chambers, the lipid membrane is painted onto the aperture using the decane-lipid seal, and channels are inserted into the membrane. When channels open, K^+ ions will flow through the ion channels toward the

Nernst potential [AZ16], as is the case in the rising edge of an action potential in the neuron. To produce a falling edge requires a second channel species and gradient, as described in section 2.1. At the moment, we have one ion channel species in the system. We use electronics as a substitute for the seconds species, as described in the section below.

2.6.2 The current-limited voltage clamp

When switch S is flipped in Fig. 2.2 to connect the electrode to the resistance R_C, the Headstage amplifier becomes what we call the current-limited voltage clamp (CLVC) [AZ16]. In this orientation, the Headstage amplifier cannot source enough current to "instantly" impose a voltage on the membrane, as is the case in Fig. 2.3. The time to charge the membrane is on an RC timescale $\tau = R_C\, C$, where C is the lipid membrane capacitance.

In a chamber preparation with a Nernst potential across a membrane with channels, the CLVC functions as a second ion channel species in producing a resting potential V_r:

$$V_r = \frac{\chi_K\, V_N^K + R_C^{-1}\, V_C}{\chi_K + R_C^{-1}} \tag{2.4}$$

This equation has the same form as eqn. 2.2 for a rest potential produced by two ion gradients. The difference here is that the second species terms are replaced by the CLVC values R_C and V_C.

2.6.3 Action potential in the Artificial Axon

Figure 2.4 shows one measurement with the CLVC and concentration gradient. The blue trace is the membrane potential, and the yellow trace is a fit of the action potential with the model described in the next section. The rest potential is brought up to the threshold value $-28\,mV$ from $-92\,mV$, and the Axon "fires." For $t < 100\,ms$, the CLVC value $V_C = -116\,mV$, but the rest potential is at $-92\,mV$ because of the ohmic leak across the membrane; the leak conductance in this preparation is $(569\,M\Omega)^{-1}$. At $t = 100\,ms$, the rest value is stepped up to $-28\,mV$ with $V_C = -41\,mV$ for 1 second. For the first $120\,ms$ of this

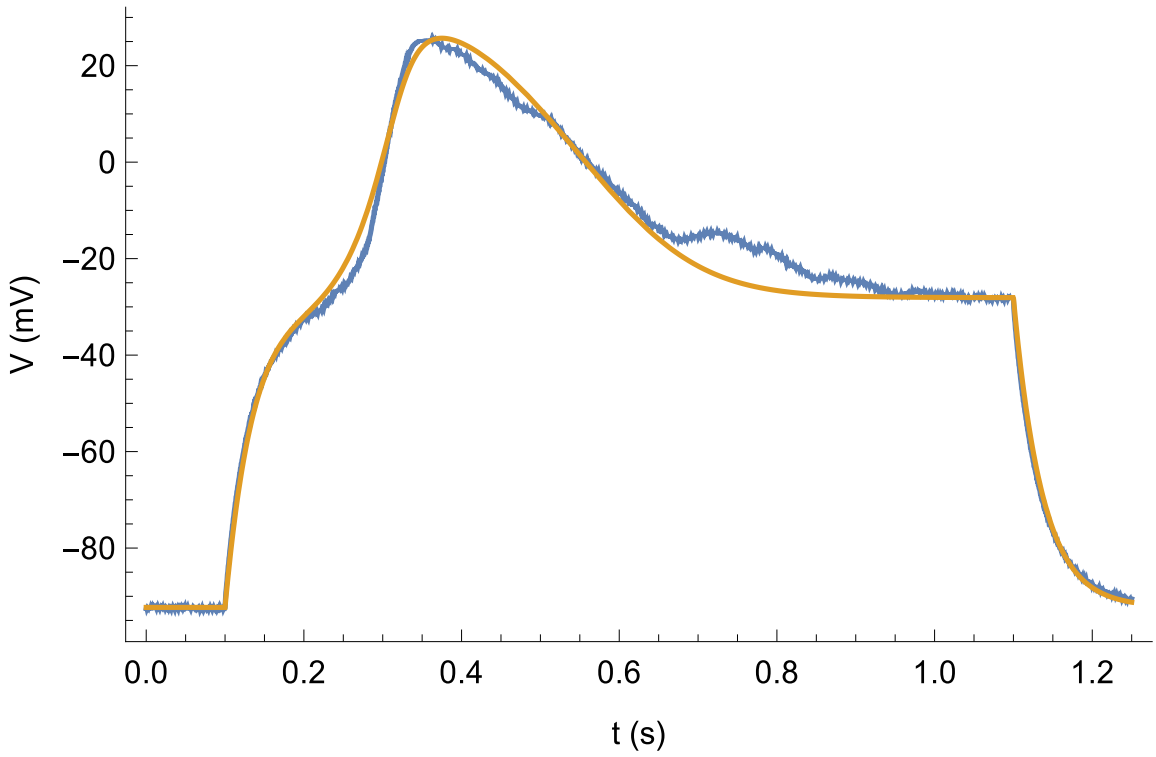

Figure 2.4: Measurement of an action potential in the Artificial Axon. The blue trace is the membrane potential, and the yellow trace is a fit using the Hodgkin and Huxley model for an action potential in a neuron. The rest value, imposed by the CLVC is stepped from $-92\,mV$ to $-28\,mV$ and the Axon "fires." The channels open at threshold, between $-30\,mV$ and $-20\,mV$, and K^+ ions flow into the cis chamber, toward the Nernst potential ($40\,mV$), peaking at $25\,mV$. The channels move to complete inactivation, and the membrane potential rests at $-28\,mV$. After 1 second, the rest potential is stepped back down to $-92\,mV$.

CLVC step, the membrane potential rises to the new rest potential with the RC behavior of charging a capacitor; the membrane capacitance for this measurement is $C = 420\,pF$. The threshold value, where the KvAP channels open and fire an action potential, is roughly between $-30 \sim -20\,mV$. The channels open and the Artificial Axon fires toward the Nernst potential ($\sim 40\,mV$) to a peak of $25\,mV$. The channels then move toward full inactivation and the membrane potential moves to rest at $-28\,mV$. Finally, at $t = 1.1\,s$ the CLVC is stepped back down to its original value $V_C = -116\,mV$. The leak conductance and capacitance are found using the known Nernst potential and clamp values with the two rest potentials. The channel contribution in the fit is found using the model described in the section below.

2.7 Hodgkin Huxley model in the Artificial Axon

The model we use to fit the action potential in the Artificial Axon is the Hodgkin and Huxley model for action potentials in the neuron [HH52]. The model contains (i) an equation for current contributions to charging a capacitor (the membrane), and (ii) a system of ordinary differential equations for the different states of the channel, where the rate constants for the transitions between states are represented by exponential functions of voltage. In this section, I present these components of the model.

Membrane separates charge and thus has a capacitance C. The equation for charging the membrane in the Artificial Axon is

$$\begin{aligned} C\frac{dV}{dt} &= N_0\,(p_O\,\chi + \chi_\ell)[V_N - V(t)] + \frac{1}{R_C}[V_C - V(t)] \\ &= I_{ch} + I_\ell + I_C \end{aligned} \tag{2.5}$$

I_{ch} is the current contribution from the channels, I_ℓ is the current contribution from the ohmic leak, and I_C is the current contribution from the CLVC. V_N is the Nernst potential and V_C is the CLVC voltage value. N_0 is the number of channels in the membrane, χ is the conductance of a single KvAP channel ($10\,pA/60\,mV$), χ_ℓ is the leak conductance, which is

(a)

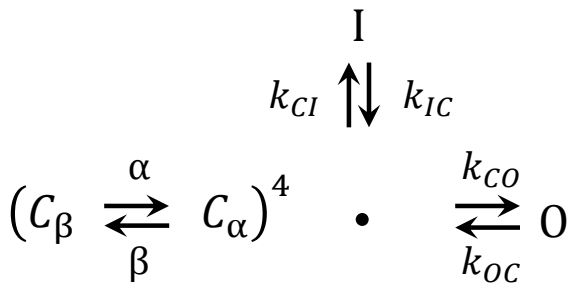

(b)

$k_0 e^{-zV}$	α	β	k_{CO}	k_{OC}	k_{CI}	k_{IC}
$k_0\ (s^{-1})$	54.4	0.011	12.4	9.8	17.7	0.008
z (V^{-1})	-26	67	1	12	-1	30

Figure 2.5: Scheme for KvAP gating and measured parameter values [SCM09]. (a) Represents the scheme between the different states of the KvAP channel, and (b) is a table of values for the rate constants in the transition rates between states. In this minimal scheme, the subunits of the ion channel are assigned two Closed states: C_α and C_β. When all four subunits are in the C_α state, Open and Inactive states become accessible. All other combinations of C_α and C_β are inaccessible to Open and Inactive states. α, β and k_i are transition rates between the different states of the scheme, all of which have the form $k_0\, e^{-z\,V}$, where k_0 and z are the rate constants.

different in every preparation.

The term p_O is the open probability for a single channel. This term describes one state out of many possible states for the KvAP channel, as briefly described in subsection 2.2.4. We use a simplified scheme for the KvAP [SCM09], shown in Figure 2.5(a). This scheme has 3 ion channel states: Open (probability $p_O(t)$), Inactive (probability $p_I(t)$), and Closed; this last Closed state consists of several "internal" states. Each subunit in the channel is assigned two states, C_α and C_β. The closed state that is accessible to the open and inactive states requires all 4 subunits be in the C_α state, associated with probability $p_4(t)$. Probabilities $p_3(t)$, $p_2(t)$, $p_1(t)$ and $p_0(t)$ are associated with states inaccessible to the open and inactive states. These probabilities correspond to 3, 2, 1, and 0 subunits in the C_α state, respectively. The transition rates between states are represented by exponential functions of voltage $k_0 e^{-z\,V}$, where k_0 and z are rate constants. These constants have been measured for KvAP [SCM09], and are presented in Figure 2.5(b).

The channel state probabilities and rate constants are combined in a system of ordinary differential equations that represent the change in states across time. The equations are:

$$\begin{pmatrix} p'_O(t) \\ p'_I(t) \\ p'_4(t) \\ p'_3(t) \\ p'_2(t) \\ p'_1(t) \\ p'_0(t) \end{pmatrix} = \begin{pmatrix} -k_{OC} & 0 & \cdots & 0 & 0 \\ 0 & -k_{IC} & & 0 & 0 \\ k_{CO} & k_{CI} & & 0 & 0 \\ & 0 & \ddots & 0 & 0 \\ 0 & 0 & & 2\beta & 0 \\ 0 & 0 & & -3\alpha\,\beta & \beta \\ 0 & 0 & \cdots & 4\alpha & -4\alpha \end{pmatrix} \begin{pmatrix} p_O(t) \\ p_I(t) \\ p_4(t) \\ p_3(t) \\ p_2(t) \\ p_1(t) \\ p_0(t) \end{pmatrix} \tag{2.6}$$

The full 7×7 matrix is provided separately for space:

$$\begin{pmatrix} -k_{OC} & 0 & k_{OC} & 0 & 0 & 0 & 0 \\ 0 & -k_{IC} & k_{IC} & 0 & 0 & 0 & 0 \\ k_{CO} & k_{CI} & -(k_{CI}+k_{CO}+4\beta) & 4\beta & 0 & 0 & 0 \\ 0 & 0 & \alpha & -(\alpha+3\beta) & 3\beta & 0 & 0 \\ 0 & 0 & 0 & 2\alpha & -(2\alpha+2\beta) & 2\beta & 0 \\ 0 & 0 & 0 & 0 & 3\alpha & -3\alpha\,\beta & \beta \\ 0 & 0 & 0 & 0 & 0 & 4\alpha & -4\alpha \end{pmatrix} \tag{2.7}$$

Equations 2.5 and 2.6 complete the model for the membrane potential and channel states in the Artificial Axon.

Equations 2.6 alone are used as a model for KvAP channel current in a voltage clamp system with constant V_C input and symmetric ion concentration conditions [SCM09]. The typical choice for initial conditions corresponds to membrane potentials below $-120\,mV$, where the closed channel state $p_0 \approx 1$ and all other states ≈ 0. At $t = 0$ the clamp value V_C is stepped to some more-positive value, where channels will open. The channel current is simply $I_{ch} = N_0\,\chi\,p_O(t)\,V$, where V is the membrane potential ($V = V_C$ when there is no leak). Analytical solutions given these initial conditions and step protocol is described in chapter 20 of [SN09].

2.8 Future work

A direction that is not an immediate priority but is a worthwhile direction is in the replacement of KvAP with another ion channel. While the KvAP is a robust channel for experimentation, it is $1000\times$ slower than K^+ channels in the neurons of animal brains. The large negative potentials required for recover from inactivation in the KvAP is also limiting; this issue arises in future chapters.

A second ion channel species may solve the inactivation issue, but such an addition to the system would not be trivial for several reasons. First, the process for producing the KvAP protein described in this chapter is not a small task. Producing *two* such species will add ex-

tra challenges. Compatibility between channel species must also be taken into consideration. To list some examples, these two species must have compatible thresholds, resting potentials for inactivation recovery, opening and inactivation-recovery rates; essentially, issues that are resolved in tuned neurons.

The CLVC, an electronic solution in establishing V_r, may be resolved without a second channel species, instead resolved more simply with Gramicidin pores. Gramicidin is a transmembrane protein that allows both K^+ and Na^+ ions to travel through its pore with a different conductance for each ion. Gramicidin is added to the AA to the cis chamber with a pipette, and control over concentrations may provide tune-ability in the AA's ability to return to rest after an action potential. A test in the Artificial Axon with Gramicidin and two ion concentration gradients (K^+ and Na^+) revealed that $\chi_{Na} = 3\chi_K$, with a resting potential given by eqn. 2.2. In a preparation with two gradients, Gramicidin, and KvAP ion channels, the K^+ concentration gradient would be used to establish the height of an action potential spike, and the Na^+ gradient would be used to establish the resting potential.

The directions mentioned in this section are long-term endeavors. The Artificial Axon, with KvAP and the CLVC, has tremendous potential. I demonstrate the Axon's potential in the chapters that follow.

CHAPTER 3

Summation in the Artificial Axon

3.1 Summation phenomena in networks of living organisms

Neurons communicate their action potentials by depolarizing the membranes of other neurons as either excitatory or inhibitory input. In the neurons of animal brains, one excitatory post-synaptic potential event (EPSP) will not induce an action potential in a downstream neuron. Brain neurons require integration of EPSPs between two and hundreds to induce post-synaptic firing.

Summation events are the key functions of neurons. This integration of inputs into one output is a neural computation [BCP07]. Given the two types of pre-synaptic input excitatory and inhibitory a neural computation is essentially a logic gate, analogous to gates in electronics hardware. These logic gates fundamentally unalike in composition and structure are both capable of performing simple Boolean logic calculations, the basis of computation.

A functional logic gate in a brain-like synthetic system like the Artificial Axon (AA) must fire in response to summation events. In this chapter, it is shown that the integration of input induces firing in the Artificial Axon, much like neurons in the brain. As such, the Artificial Axon can function as the basic unit of a computational network, connected to other units to perform calculations.

3.2 Artificial Axon summation components

Summation events that induce post-synaptic firing only affect one ion-channel species in the axon of a neuron cell. In summation, the target of pre-synaptic input is the post-synaptic axon voltage; all the biological hardware in the synapse and post-synaptic soma is simply a means of EPSP (and IPSP) signal transmission. Depolarization to threshold in the axon only affects the sodium ion-channels, the species responsible for the front end of a spike; once the axon potential spikes toward the Nernst potential of sodium, the neural computation is complete.

The Artificial Axon satisfies this minimum criteria for computation; membrane depolarization induces firing toward the Nernst potential of a single channel species. The AA therefore functions as a logic gate, analogous to a post-synaptic neuron cell.

CLVC pulse protocols simulate pre-synaptic input in the production of summation in the Artificial Axon. In a neuron, the trigger zone does not receive independent EPSPs, but rather the integration of EPSP input. The CLVC is sufficient to mimic this integration. Measurements in this chapter are done with CLVC pulse protocols. Input from one or more Artificial Axons in place of the CLVC is described in later chapters.

3.3 Channel contribution in the membrane equation

To describe the membrane voltage behavior in the measurements of this chapter, the membrane equation is rewritten into a more intuitive form.

In terms of currents:

$$\begin{aligned} C\frac{dV}{dt} &= N_0(p_O\,\chi + \chi_\ell)[V_N - V(t)] + \frac{1}{R_C}[V_C - V(t)] \\ &= I_{ch} + I_\ell + I_C \end{aligned} \tag{3.1}$$

where I_{ch} is the channel current, I_ℓ is the leak current, and I_C is the CLVC current. I_C and I_ℓ have the same form, and will thus behave the same way in time. Merging these currents

in the membrane equation yields the form

$$C\frac{dV}{dt} \;=\; N_0\, p_O\, \chi[V_N - V(t)] + \left(N_0\chi_\ell + {R_C}^{-1}\right)[V_0 - V(t)] \tag{3.2}$$

where

$$V_0 \;=\; \frac{(N_0\,\chi_\ell)\,V_N + R_C^{-1}\,V_C}{N_0\,\chi_\ell + R_C^{-1}} \tag{3.3}$$

V_0 is the resting potential produced by the leak and CLVC currents, between the Nernst and clamp potentials, equivalent to a membrane with two leaky channel species at different Nernst potentials. Here, one Nernst is the V_N established by the K^+ concentration gradient ($\sim 40\,mV$), and the other Nernst-like potential is the voltage assigned to the CLVC.

Merging leak and clamp terms in this way, V_0 effectively becomes input that can be assigned chosen values, as is done with V_C, and $\left(N_0\,\chi_\ell + R_C^{-1}\right)$ becomes the resistance. In the absence of channels, the membrane equation reduces to an equation for charging/discharging a capacitor,

$$C\frac{dV}{dt} \;=\; \left(N_0\,\chi_\ell + {R_C}^{-1}\right)[V_0 - V(t)] \tag{3.4}$$

When V_0 is constant, 3.4 has the analytical solution

$$V(t) = V_0 + (V_r + V_0)\, e^{-t\,(N_0\,\chi_\ell + {R_C}^{-1})/C} \tag{3.5}$$

where V_r is the initial value of the membrane voltage.

Equation 3.2 is useful because it separates the RC currents from the channel current:

$$C\frac{dV}{dt} = I_{ch} + I_{C\ell} \tag{3.6}$$

where $I_{C\ell}$ is the effective clamp current – leak and channel – and the channel current I_{ch} is isolated from all other terms.

In separating the currents in this way, it becomes possible to describe measurements of the membrane voltage in terms of RC input and channel response.

3.4 One-pulse input

Summation in the Artificial Axon is accomplished with CLVC "pulses" controlled in LabVIEW. The pulse protocol is described here. All pulses begin with the membrane at a low resting potential V_r, where channels are closed and not inactive. The CLVC value is increased to a voltage that brings the membrane potential to some depolarizing level $V_0 > V_r$ for a controlled length of time. At the end of this pulse, the CLVC value is brought back down so that the membrane potential returns to V_r.

One CLVC pulse that is sufficiently high in voltage or wide in time will open channels and result in one of two membrane behaviors. After the pulse, either $dV/dt < 0$, in which case the AA "fires," or $dV/dt > 0$, the AA does not fire, where V is the membrane potential of the Axon. The number of open channels determines which of these two will occur. In terms of currents, either $|I_{ch}| > |I_{C\ell}|$ (Axon fires) or $|I_{ch}| < |I_{C\ell}|$ (does not fire).

3.4.1 CLVC overwhelms channel current

Figure 3.1(b) is an example of membrane voltage behavior when $|I_{ch}| < |I_{C\ell}|$ after one pulse. In (a) there are no open channels, and thus the effect is simply the charging and discharging of the membrane capacitance, with an RC timescale given by the membrane capacitance $C \sim 192\,pF$ and the CLVC resistance $R_C = 100M\Omega$. In (b) the square pulse stimulus is longer ($40\,ms$ instead of $30\,ms$), and the response is different. The pulse is long enough so that the number of channels that open can compete with the current from the clamp. When the clamp voltage is brought back down to $-125\,mV$, at some point after the pulse there are

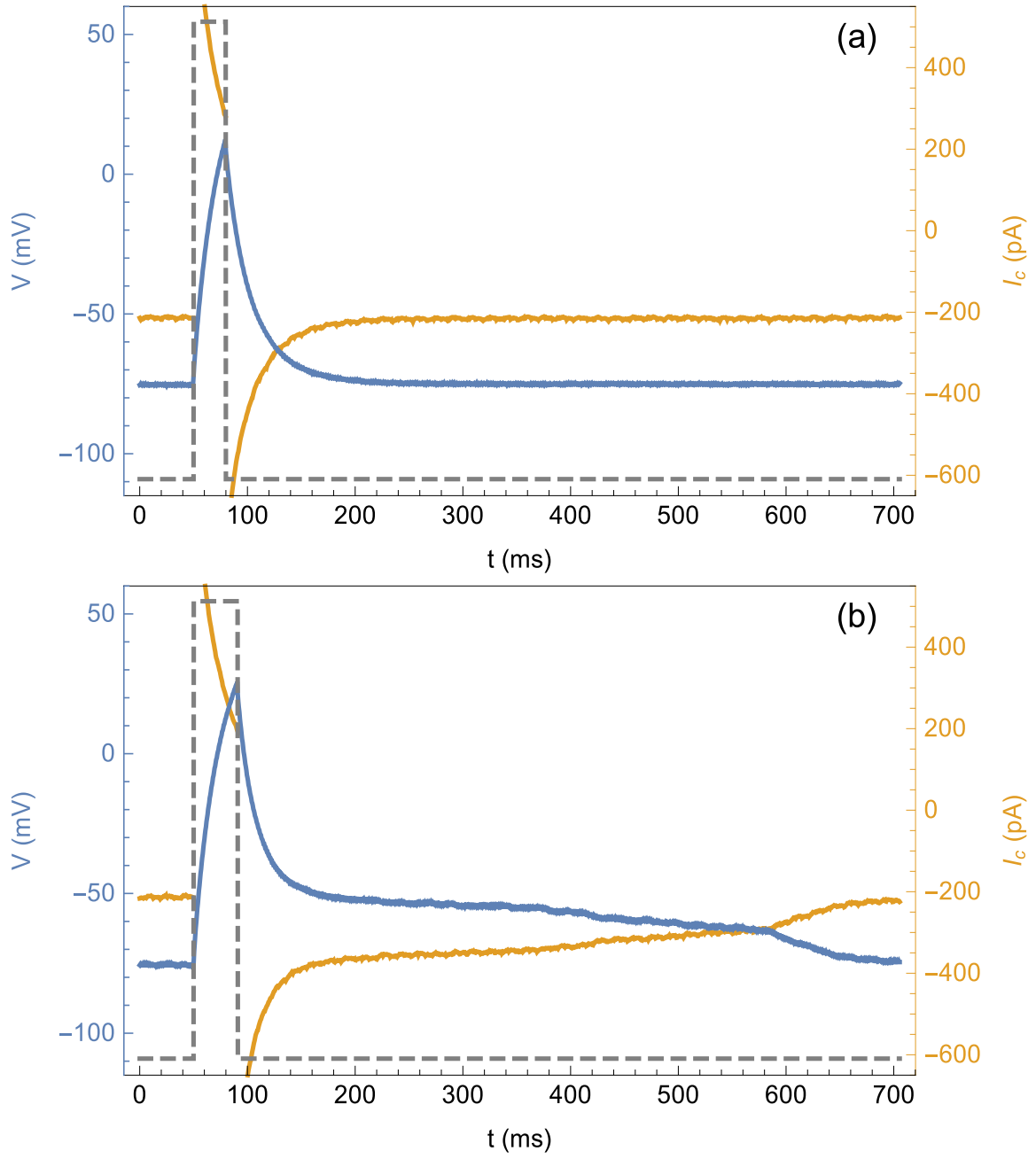

Figure 3.1: Membrane voltage response to one CLVC pulse. The dotted line represents the input (the CLVC voltage protocol), the blue trace is the measured Axon voltage V(t), and the yellow trace is the current through the CLVC. In both (a) and (b) the CLVC protocol is a square pulse from $-109\,mV$ to $54\,mV$, but the pulse width is $30\,ms$ in (a) and $40\,ms$ in (b), the latter being sufficient to open some channels. The CLVC resistance is $R_C = 100M\Omega$.

enough channels open to compete with the clamp but not overwhelm it; dV/dt¡0 because $|I_{ch}| < |I_c|$. The membrane potential remains low and returns to V_r as channels close.

3.4.2 Channel current overwhelms CLVC

Figure 3.2 (b) is an example of membrane voltage behavior when $|I_{ch}| > |I_{C\ell}|$ after one pulse. After the clamp is pulled back down to $V_C = -125\,mV$ (at $t \sim 100\,ms$) the Axon voltage V(t) continues to climb, because channels are open and the channel current overwhelms the clamp current. V(t) does not quite reach the Nernst potential $V_N \sim 40\,mV$ because of this competition. The subsequent decrease of V(t) is due to channel inactivation. These traces are essentially deterministic and can be repeated many times.

It is worth noting that channel behavior in the Artificial Axon is independent of the input shape in height and width. In Figure 3.1(b), for instance, a narrow/high input pulse opens some channels. It is possible to produce the same behavior with a wide/low pulse, opposite to the input given in those measurements. In Figure 3.2(b) a wide/low pulse results in Axon firing, but a narrow/high pulse can also make the Axon fire. Oppositely-shaped input measurements were taken but are not shown here. This input shape independence also applies to multiple-pulse inputs, as is done in the measurements for the section below.

In biological neurons, the action potential is defined as a "stereotyped response" [Koc99] because its amplitude is independent of input shape. This input independence is essential for frequency coding in brain computations. Firing rate in the Artificial Axon is described in a later chapter.

3.5 Two-pulse input

In giving the Artificial Axon a two-pulse protocol, the chosen criteria for a second CLVC pulse are as follows. (i) the max V_C value for the second pulse must equal the value for the first pulse; the heights must be the same. In choosing values to change systematically in a two-pulse protocol (height, width, separation), equal pulse heights keeps the protocols

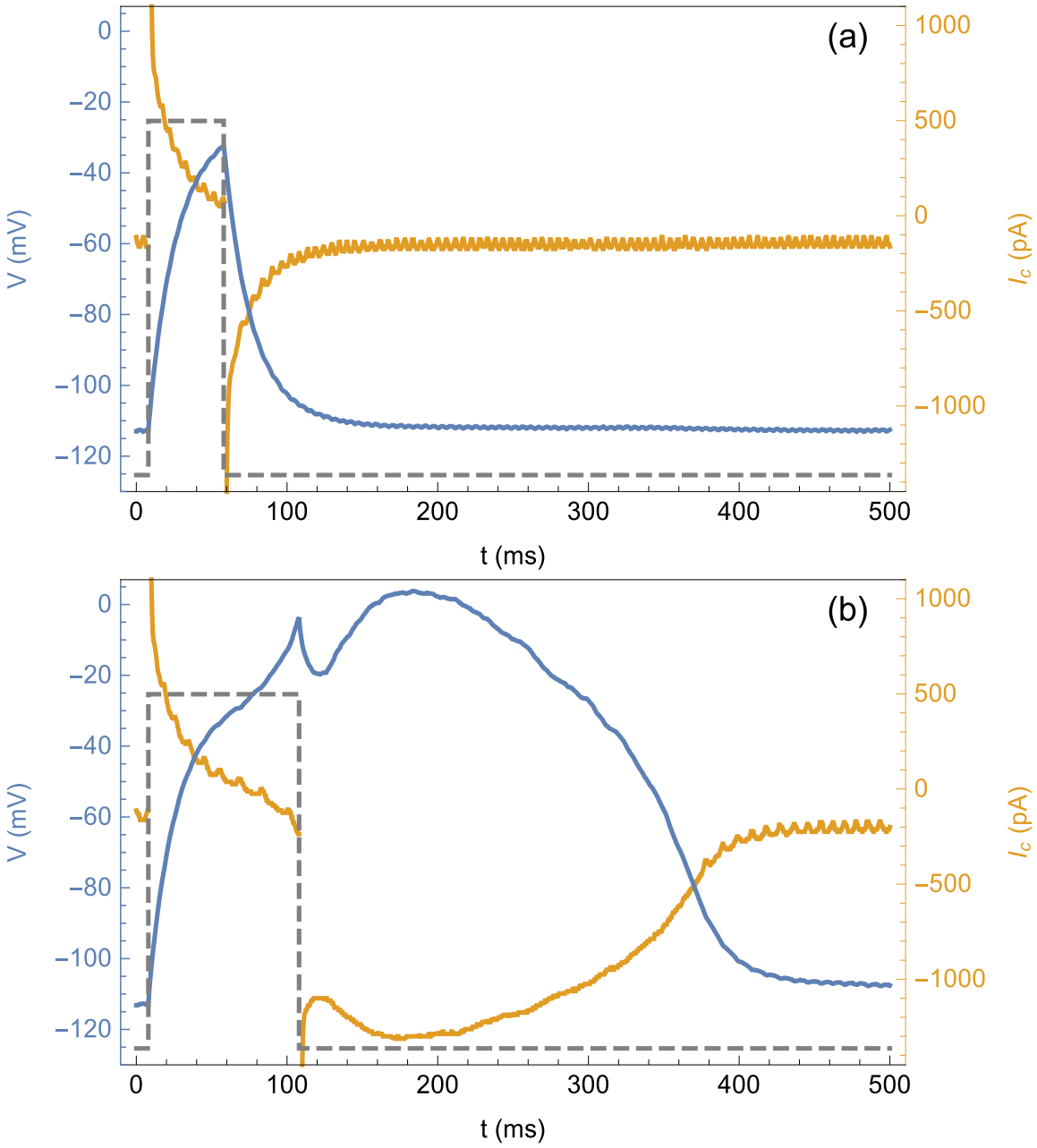

Figure 3.2: Response of the Artificial Axon to a sub threshold (a) and above threshold (b) stimulus. In both (a) and (b) the CLVC protocol is a square pulse from $-125\,mV$ to $-25\,mV$, but the pulse width is $50\,ms$ in (a) and $100\,ms$ in (b). The CLVC resistance is $R_C = 100\,M\Omega$, and from the sub threshold $V(t)$ trace, fitting with the membrane equation with closed channels ($p_O = 0$), the Axon values are $C = 192\,pF$ for the membrane capacitance and $R_l = 1.2\,G\Omega$ for the leak resistance.

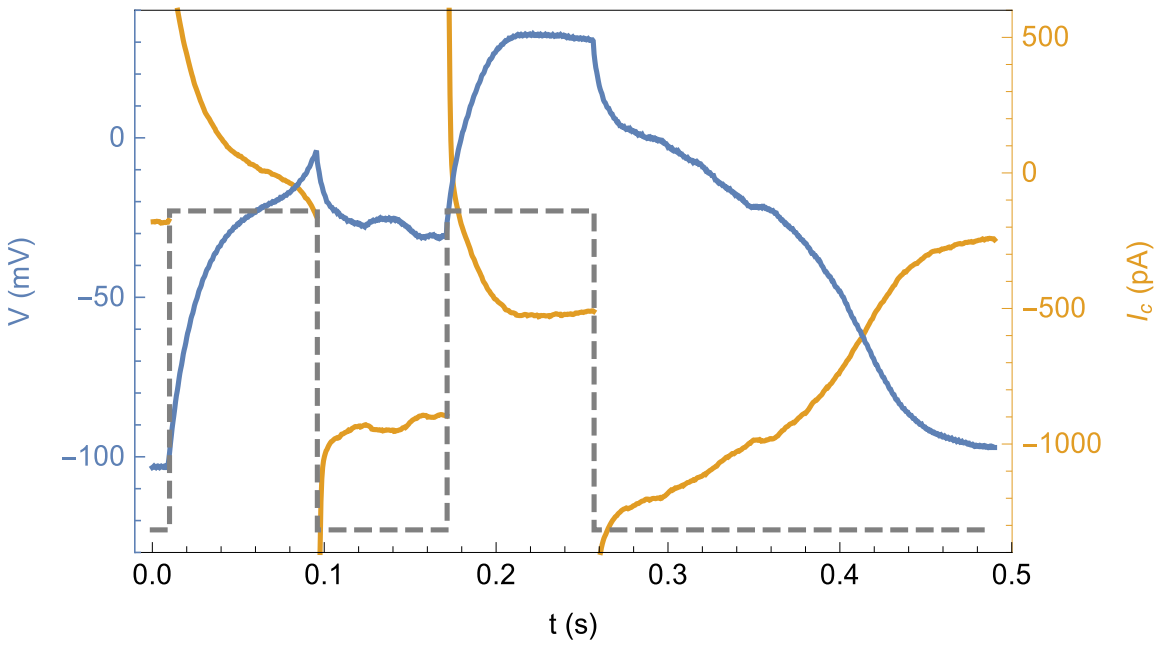

Figure 3.3: Coincidence detection with the Artificial Axon. Two sub threshold pulses (dotted line) in close proximity cause the Axon to fire. The first pulse induces opening of some channels, but the channel current cannot overwhelm the clamp (which has the role of the Na^+ gradient in the real neuron) absent the second pulse. The CLVC protocol is two identical pulses from $-123\,mV$ to $-23\,mV$, of width $86\,ms$ and $80\,ms$ apart. The CLVC resistance is$R_C = 100\,M\Omega$, $C = 210\,pF$ and $R_\ell = 0.7\,G\Omega$.

simple, given that the objective is to produce summation behavior in the system. (ii) pulse separations must be roughly equal to or greater than the width of the first pulse. Separations less than one pulse width begin to make two pulses effectively one pulse. The CLVC needs time to pull the membrane voltage down after the first pulse; in reducing the time to the next pulse, it becomes meaningless to call this two separate pulses.

3.5.1 Channels open after first pulse

Two sub-threshold pulses in close proximity will cause the system to fire, implementing an AND operation or coincidence detector. An example is shown in Fig. 3.3 where each $86\,ms$ long pulse alone is sub-threshold, but two such pulses $80\,ms$ apart cause firing. After the first pulse, $dV/dt < 0$ because $|I_{ch}| < |I_{C\ell}|$; without the second pulse, the membrane potential

would continue to decrease and return to V_r. But during the second pulse, $|I_{ch}| > |I_{C\ell}|$ until channels begin to inactivate.

3.5.2 Channels closed after first pulse

Summation of pulses that individually do not open channels is presented here. In all the measurements thus far, channels open after only one pulse. But in this system, with these channels, it is possible to observe firing in summation of pulses that individually do not open channels. In Figure 3.4, high and narrow input pulses open channels after the second pulse. However, high/narrow pulses are not exclusively the only input combination to achieve this behavior. Measurements have been accomplished with wide/low input but are not shown here.

The pulses in Fig. 3.4 cannot individually open channels. One pulse is $20\,ms$ wide and $727\,mV$ high. At the end of the first pulse, the membrane voltage decays exponentially, which implies that $I_{ch} \approx 0$ and thus no channels are open. At the end of the second pulse in Fig. 3.4(b), channels do open, but not enough channels open to overwhelm the CLVC. In Fig. 3.4(c), the pulses are now $20\,ms$ apart, and the result is $|I_{ch}| > |I_{C\ell}|$ after the end of the first pulse: the AA fires.

3.6 Discussion

3.6.1 Model

The channel contribution to the membrane potential is modeled by adding a V_C protocol to the membrane equation. The constant V_C term is replaced by

$$V_C \;\rightarrow\; V_{C1} + (V_{C2} - V_{C2}) \sum_{i}^{n} \Theta(t - t_i)\,\Theta(t_i + t_0 - t) \tag{3.7}$$

where V_{C1} is the resting potential V_r and V_{C2} is the pulse height, t_i is the start time of the pulse i, and t_0 is the pulse width.

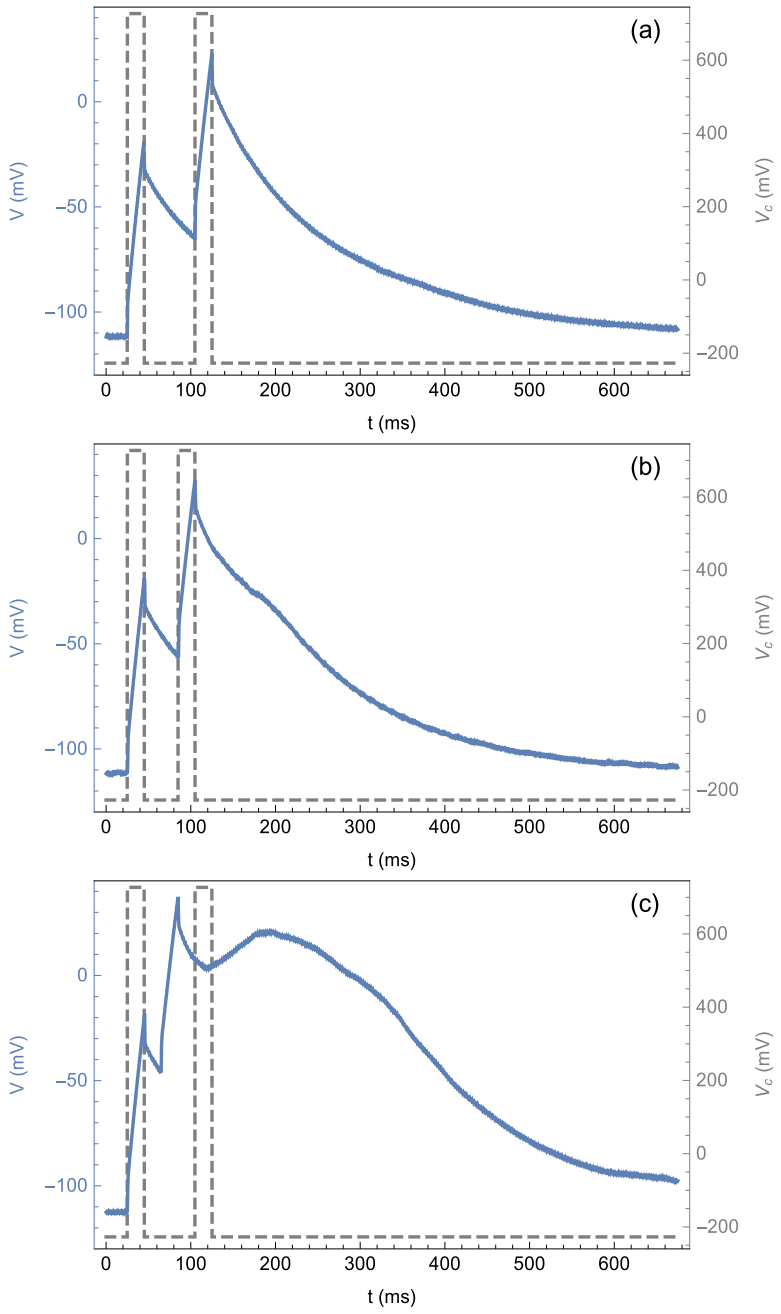

Figure 3.4: Multiple pulses to open channels. An individual pulse is insufficient to open channels. Two of these pulses must be close in time to open channels. One pulse is from $-109\,mV$ to $727\,mV$, of width $20\,ms$. The CLVC protocol is two such pulses at different separations. In (a), the pulses are $60\,ms$ apart and channels do not open. In (b) the pulses are $40\,ms$ apart, and some channels open, but not enough to overwhelm the CLVC. In (c) the pulses are $20\,ms$ apart and the Axon fires.

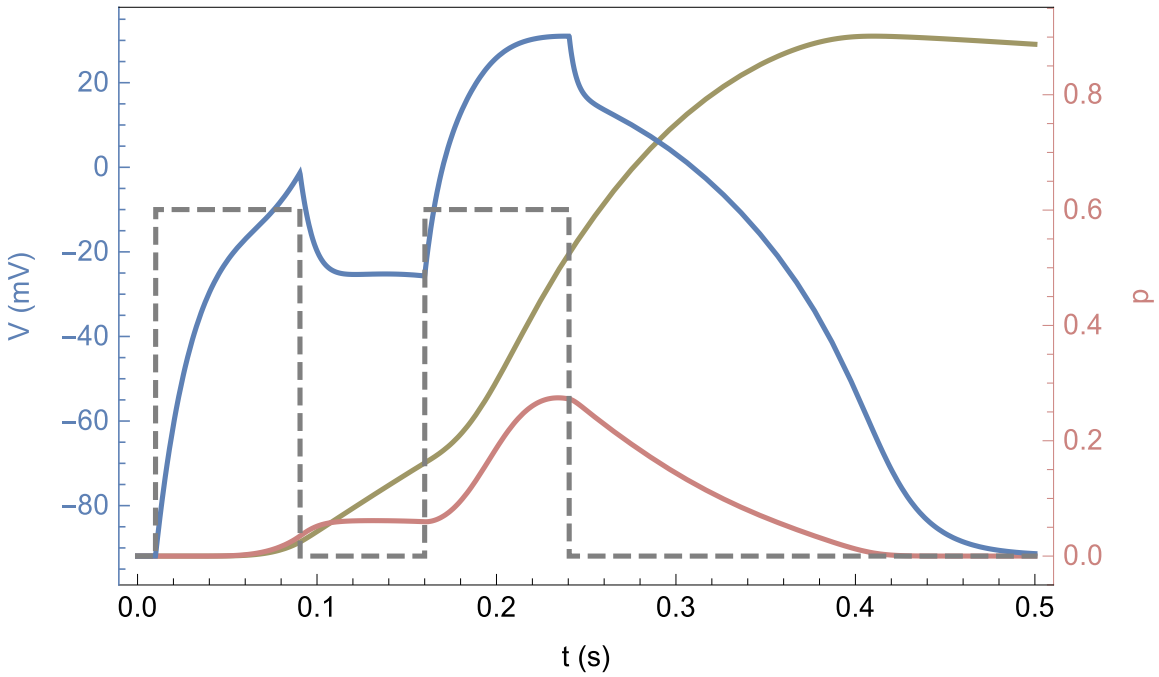

Figure 3.5: Simulation of two-pulse input. The rate constant values in this simulation are based on a fit for channel measurements not presented in this thesis. The coral-colored line represents the fraction of open channels, and the green line represents the fraction of inactive channels. The resemblance in shape across voltage and time of this simulation to the measurement in Fig. 3.3 suggests that the probability traces demonstrate how channels contribute to the membrane potential in measured data. The CLVC protocol is two identical pulses from $-91\,mV$ to $-10\,mV$, $81\,ms$ wide and $70\,ms$ apart. The Axon values are $V_N = 40\,mV$, $V_r = -92\,mV$, $R_C = 100\,M\Omega$, $C = 210\,pF$, and $\chi_\ell = 0$.

Figure 3.5 is an example of a simulated membrane potential with a V_C protocol. The rate constant values in this simulation are based on a fit for channel measurements not presented in this thesis. All values chosen for this simulation are listed here. The pulses are wide/low, with pulse height $-10\,mV$, width $81\,ms$ and separation $70\,ms$. The Axon values are $V_N = 40\,mV$, resting potential $V_r = -92\,mV$, $R_C = 100\,M\Omega$, $C = 210\,pF$, and leak conductance $\chi_\ell = 0$, chosen for simplicity and the reason why V_C and V_r membrane values are the same at rest. The channel rate constants are $\alpha' = 0.42\,\alpha$, $\beta' = (0.42)^{-1}\beta$, $k'_{CI} = 1.8\,k_{CI}$, $k'_{IC} = 1.8\,k_{IC}$, $k'_{CO} = 7\,k_{CO}$, $k'_{OC} = 7\,k_{OC}$, where the unprimed values are those previously reported in [SCM09]. Channel number $N_0 = 1000$.

The simulation in Fig. 3.5 complements the measured Axon voltage in Fig. 3.4. Even though the simulated channel values are not fit to Fig. 3.4 data, and the traces for simulated and measured membrane voltage differ in scale across V and t, the traces appear identical in shape, which suggests that the simulated and measured channel behavior is the same. Therefore the open and inactive state probability traces that are used to produce the simulation provide an explanation for the membrane potential behavior in Fig. 3.5.

After the first pulse in Fig. 3.4, enough channels are open so that $|I_{ch}| < |I_{C\ell}|$. The fraction of inactive channels continues to rise and the fraction of open channels continues to decrease, accounting for $dV/dt < 0$. The second pulse opens more channels so that $|I_{ch}| > |I_{C\ell}|$ after the end of the pulse. The membrane potential remains above rest until all channels are inactive.

The simulation in Fig. 3.5 is only one example of the membrane voltage reproducibility. The traces in Figures 1-3 of this chapter may also be simulated. Like in the example above, the measured and simulated Axon voltages will be identical in shape.

3.6.2 Future Work

The next logical step is to add more Artificial Axons to replace the CLVC as the pre-synaptic neuron(s). Only two Axons are used in the work done in this thesis. However, to build a network of logic gates will require three or more Axons, connected as two for input, one for

output, to do the simplest calculation of a logic gate. Additionally, implementing inhibitory input will allow for more complex calculations.

These additions necessitate the construction of a novel connection between Artificial Axons, essentially an artificial synapse. While current work toward an artificial synapse is electronics-based [al11, al13, al17], the goal of our work is to move away from electronics toward a chemical and biological solution. Replication of synapse machinery is an area of active study [DF03, UL05, BH16, KKR11], but anything that resembles a biological artificial synapse in the Artificial Axon would be something of the distant future. Many of the mechanisms involved in the steps from action potential at the terminals to vesicle fusion are still not well understood. The work toward an artificial synapse in the immediate future would be in a direction that takes concepts of what the synapse does, but does not resemble a real synapse.

For the work done in this thesis, and for suggested work to be done in the immediate future, Axons are connected electronically. These connections will be discussed in future chapters.

CHAPTER 4

Propagation of the action potential

Axons interconnect the network of the brain. Axons send action potentials between specialized areas of the brain – $\sim$ centimeter distances – and down the length of the human body; the longest axons in the body are $\sim$1 meter in length, in the sciatic nerve.

In this chapter I briefly discuss the physics of the membrane potential on an axon. I discuss the connection between two Artificial Axons to propagate an action potential from one Axon to the other. I present a measurement of successful propagation in our system and discuss the advantages and disadvantages associated with the KvAP ion channel in propagation. I end the chapter with a model of propagation in the Artificial Axon and discuss the future of the AA in a larger network.

4.1 The cable equation

Fig. 4.1 illustrates an infinitesimally small axon patch overlapped with an equivalent circuit for one ion channel species (K^+). dR_r represents the resistance from the one ion channel species, the membrane patch capacitance is dC, and the Nernst potential is V_N. The resistance dR_z come from the interior axon solution. This resistance is proportional to (area)$^{-1}$, so the resistance inside the axon is non-negligible but the outside resistance can be ignored. The voltages $V(z)$ are measured from the top wire to the bottom wire. The axon as a whole is represented by many elements dz connected along the axon's axial direction z.
To find the potential $V(z,t)$ for some point along the axon, we must identify the currents in the circuit. There is a current $I_z(x)$ across dR_z when the potentials to the left and right of the element dz are different. This current is

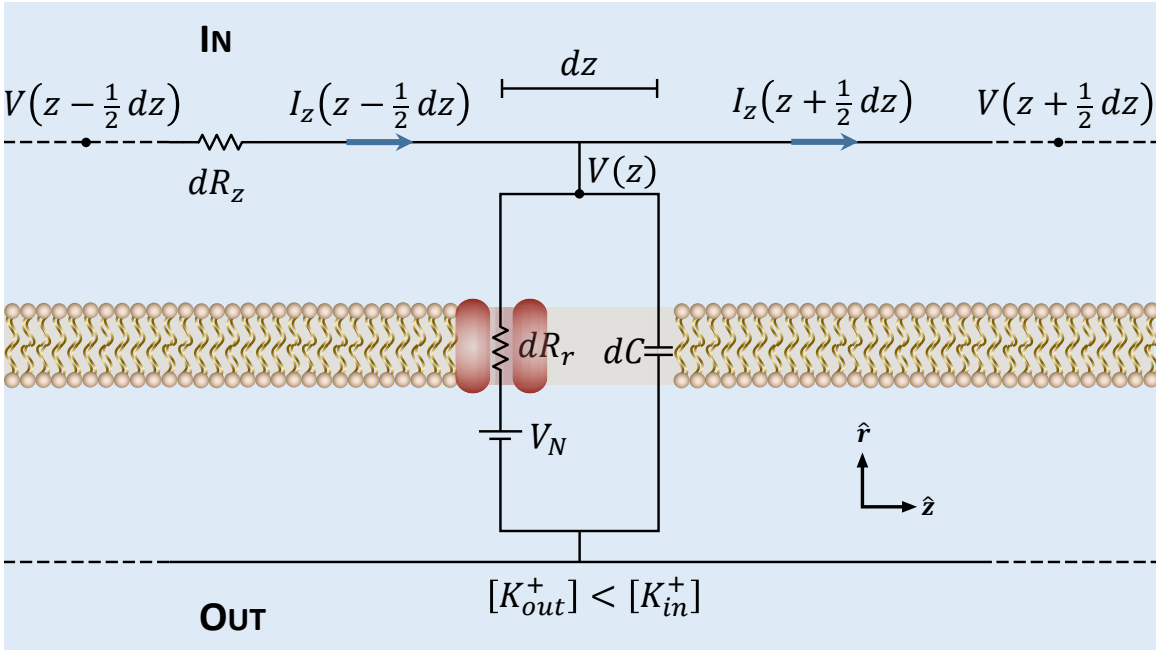

Figure 4.1: Membrane patch of an neuron axon and an equivalent circuit. dR_r is the resistance of the ion-channel, dC is the membrane capacitance, dR_z is the resistance of the solution inside the axon, and V_N is the Nernst potential created by the K^+ concentration gradient across the membrane. The axon is modeled by a series of dz components connected along the axon's axis.

$$I_z(z) \;=\; \frac{V(z-\frac{1}{2}dz) - V(z+\frac{1}{2}dz)}{dR_z} \tag{4.1}$$

An assumption in this model is that the axon is uniform along z. Therefore, R-C axon elements are proportional to length z, since resistance and capacitance come from the lipid and proteins in the axon. The element dR_z is rewritten as ${c_0}^{-1}dz$, where the constant c_0 is inverted for convenience later. Eqn. 4.1 becomes

$$I_z(z) \;=\; -c_0 \frac{dV}{dz} \tag{4.2}$$

By conservation of charge, the current into the element dz must equal the current out:

$$I_z(z-\tfrac{1}{2}dz) - I_z(z+\tfrac{1}{2}dz) \;=\; (dR_r)(V - V_N) \;+\; (dC)\frac{dV}{dt} \tag{4.3}$$

The LHS is re-written using eqn. 4.2

$$I_z(z-\tfrac{1}{2}dz) - I_z(z+\tfrac{1}{2}dz) \;=\; -\frac{dI_z}{dz}\,dz \;=\; c_0\,\frac{d^2\,V}{dz^2}dz \tag{4.4}$$

The two terms on the RHS in eqn. 4.3 are the current across the element dR_r and the changing charge on the capacitor over time.

As was done in eqn. 4.1, the R-C elements in eqn. 4.3 are re-written as $dC \;=\; c_2\,dz$ and $dR_r \;=\; (c_1\,dz)\chi$, where χ is the conductance of one ion channel, and c_1 is the number of channels per unit length. Combining these re-writes with eqns. 4.3 and 4.4 yields

$$c_0\,\frac{d^2\,V}{dz^2} \;=\; c_1\,\chi(V_N - V) + c_2\frac{dV}{dt} \tag{4.5}$$

The solution to eqn. 4.5 depends on the treatment of χ. If χ is treated as constant, then eqn. 4.5 has no traveling wave solutions.

Traveling wave solutions emerge from eqn. 4.5 when χ is given the voltage dependence of ion channels by way of some function $chi(V)$. If χ is modeled to represent one channel

species, an travelling wave – essentially the action potential – spontaneously propagates down the z-axis [Nel03]; a two-channel model of χ results in propagation to a stimulus [HH52].

In the Artificial Axon, we use one channel species and a CLVC, which takes the role of the second species in returning the membrane potential to rest after a stimulus or an incoming action potential.

4.2 Propagation in the Artificial Axon

4.2.1 The experimental setup

Figure 4.2 illustrates the connections that propagate an action potential between two Artificial Axons. The design and connection hardware was developed in the Zocchi lab by G. Zocchi and A. Ariyarante [AZ16]. The swtich S that connects the AAs is the Magnecraft W172DIP Reed Relay, and the component A is the Low-noise precision FET op-amp AD795. This high-impedance op-amp is connected to the electrode used for recording the membrane potential. The capacitor C_{in} function is analogous to empty axon membrane in the cable equation, and R_{in} function is analogous to the resistance of the bulk solution inside the axon. In Fig. 4.2, C_{in} is parallel to the membrane capacitance of Axon 1, C_1. Therefore, C_{in} adds to the Axon 1 membrane capacitance as $C_{in} + C_1$. This added capacitance C_{in} is not a necessary addition, but it does add an degree of tune-ability to the connection.

Both Artificial Axons are clamped in these propagation experiments. The alternative approach would be to clamp only the AA that initiates the action potential (Axon 1), and to float the receiving AA (Axon 2). However, this approach requires a small R_{in} so that the CLVC of Axon 1 can sustain the Axon 2 membrane potential at rest. However, when R_{in} is small, the time separation between spikes in a propagated action potential is small [AZ16]. Therefore it is not obvious that an action potential is propagated, and that instead Axon 2 is not just simply following the potential in Axon 1. But if R_{in} is too large with Axon 2 floating, then a small leak $N_0\chi_\ell$ in Axon 2 will result in spiking and inactivation of its ion channels, and leak-free AA preparations are not possible at the moment. To change

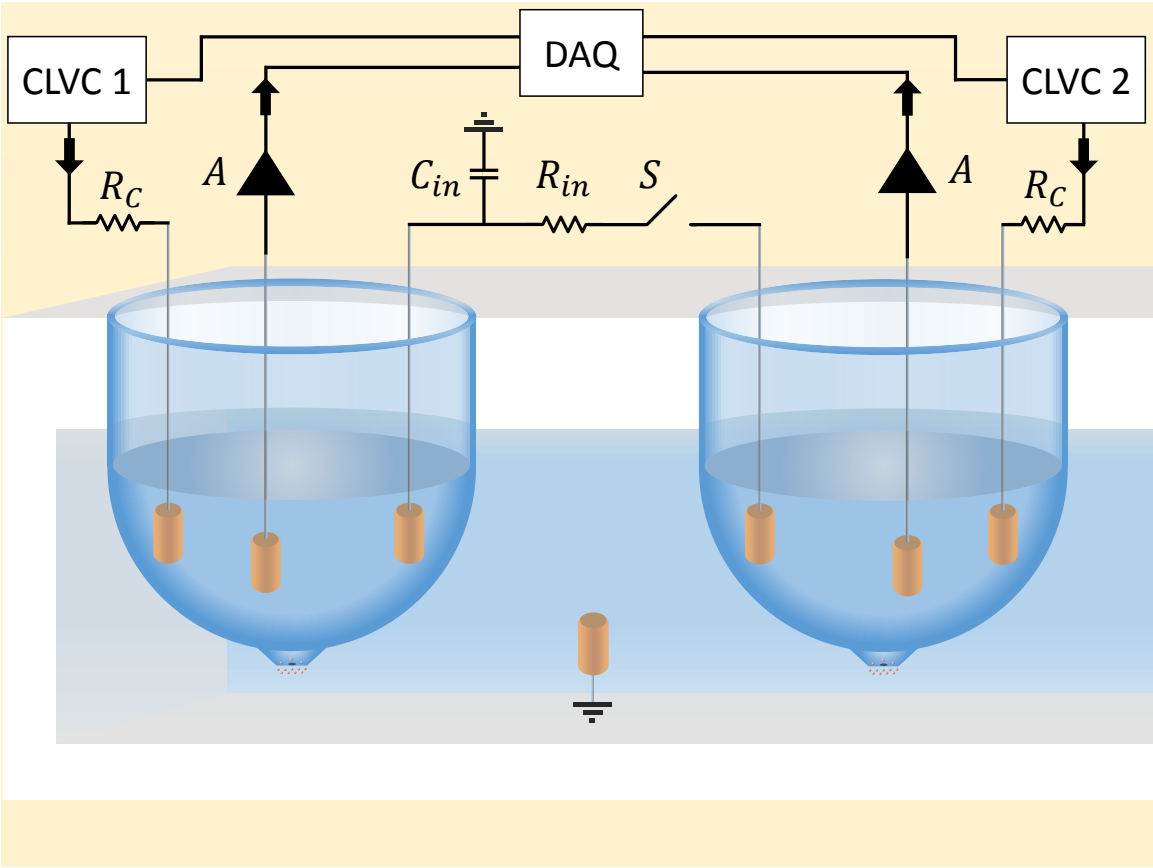

Figure 4.2: Connection diagram for propagation of an action potential between to Artificial Axons. The capacitor C_{in} function is analogous to empty axon membrane between two patches of ion channels in a neuron, and the resistor R_{in} function is analogous to the resistance of the bulk solution inside the axon. The switch S connects the two AAs, and the component A is a high-impedance op-amp.

the spike separation under these conditions requires the ability to tune R_{in}. In the present hardware, R_{in} is tuned using dual in-line package (DIP) switches that burst membranes while switching; it is the physical switching that causes the bursting. Digital switches would solve this bursting problem, but there are electronic current leak concerns in digital switches that must be explored and resolved before changing the hardware. Therefore, to produce a significant separation between spikes at the moment, we use a large resistance R_{in} and clamp both Artificial Axons.

4.2.2 Results: Propagation across two Artificial Axons

This section provides a lengthy and detailed description of the CLVC protocol required to produce propagation between two Axons. The series of CLVC steps prepares the system in a state from which propagation can be obtained; these steps are needed because the electrophysiological and channel parameters are not tune-able in a preparation, and inactivation specifically is the largest concern. The channels must be kept at a low rest potential or else the channels will inactivate. A potential solution to this problem is to increase the Nernst potential, so that the spike from one Axon is sufficiently strong as input to the next Axon. This will require future exploration in the Artificial Axon to determine what limitations would arise from dramatic increases to the Nernst potential. To my point: a larger Nernst potential, coupled with a solution to R_{in} tuning, may render this CLVC protocol unnecessary. At present, I describe the CLVC protocol that produces propagation between two Axons with the present system and its conditions.

One propagation measurement is shown in Figure 4.3. The solid curves are the membrane potentials $V(t)$, and the dashed lines are the CLVC protocols V_C. An action potential is propagated from the AA directly connected to C_{in} (Axon 1, blue trace) to the AA across the resistor R_{in} (Axon 2, yellow trace) (See Fig. 4.2). In Fig. 4.3(a) the AAs are connected and in Fig. 4.3(b) the Axons are disconnected. Both AAs fire when they are connected, and only Axon 1 fires when they are disconnected. The measurement in (a) was taken first, and (b) followed $\sim 20\,s$ after. The connecting component values are $C_{in} = 100\,pF$ and $R_{in} = 1\,G\Omega$;

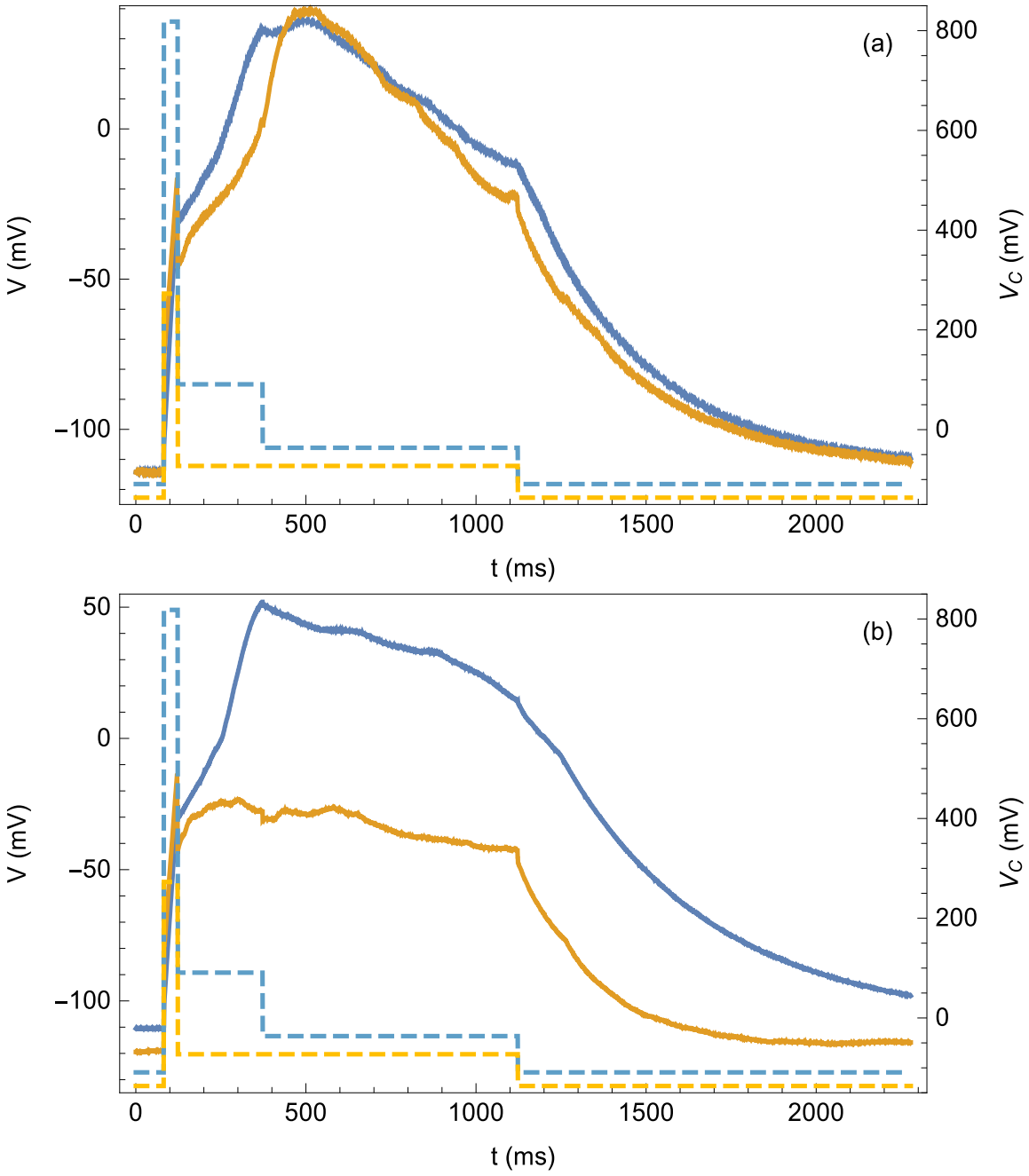

Figure 4.3: Measurement for action potential propagation across two Artificial Axons. The solid blue trace is the membrane potential for Axons 1, and yellow is for Axon 2. The dashed lines are the CLVC protocol for each Axon (described in the text). Membrane potential is measured on the left y-axis and CLVC is measured on the right. In (a) the Axons are connected (see Fig. 4.2) and Axon 2 fires when Axon 1 fires. In (b), the Axons are disconnected and Axon 2 does not fire.

both CLVC values are $R_C = 2\,G\Omega$. The CLVC protocols and membrane potential responses are described below.

For $t < 82\,ms$, the membrane voltages are held below $-100\,mV$, where channels are in the active state. For reference, we shall call this the *low-rest* step. The clamp values for Axons 1 and 2 are $(V_{C_1}, V_{C_2}) = (-109\,mV, -136\,mV)$. In the $\sim 20\,s$ between the measurements in (a) and (b), the leak in both Axons increases; the membrane potentials at *low-rest* for both Axons are higher in (b) compared to (a). These leaks are small and do not affect the AA's responses to input. The CLVC protocol was repeated multiple times after these measurements for both connected and disconnected Axons.

Axon 2 cannot fire from *low-rest*; Axon 1 stimulus cannot bring the Axon 2 potential to threshold. The resistance R_{in} must be decreased to achieve propagation in Axon 2 from *low-rest*, at the cost of the action potential spike-time separation between Axons. Therefore, after the low-rest step, a thin, high pulse is applied separately to each AA, to increase the resting potentials to values where a spike in Axon 1 will induce firing in Axon 2. For reference, we shall call this the *high-pulse* step. For $40\,ms$, between $83\,s < t < 123\,ms$, CLVCs 1 and 2 are set to $-818\,mV$ and $-273\,mV$, respectively. Axon 1 requires a significantly larger input because it is directly connected to C_{in}, which adds an extra $100\,pF$ to Axon 1's membrane capacitance. The *high-pulse* step quickly steps the membrane potentials from *low-rest* to sub-threshold values ($\sim -50\,mV$ to $\sim -40\,mV$) that are near threshold ($\sim -30\,mV$ to $\sim -20\,mV$). Although this step ensures that the largest fraction of channels will contribute to propagation, it is not entirely a necessary step. I explain this point later in subsection 4.3.1.

After the *high-pulse* step, Axon 1 is stepped down to an above-threshold value. For $250\,ms$, between $84\,s < t < 123\,ms$, CLVC 1 is kept at $91\,mV$. For reference, we shall call this the *stimulus* step. This step produces the action potential that will be propagated to Axon 2 across the resistance R_{in}. The *stimulus* step in this particular measurement is $2\times$ higher than the Nernst potential, but propagation does not require the *stimulus* step to be so high. In separate measurements on the same membrane, the *stimulus* step is set to $-20\,mV$, and Axon 2 still reaches its maximum near its Nernst potential, $\sim 40\,mV$. I discuss *stimulus*

step selection later in subsection 4.3.1.

For reference, we shall call the next step *high-rest*. This is a sub-threshold step, where channels will not fire when coming from *low-rest*. After the *stimulus* step in Axon 1, CLVC 1 is brought to $-36\,mV$ for $750\,ms$; Axon 2 is stepped to *high-rest* ($-73\,mV$, $1\,s$) immediately after its *high-pulse* step. There are several important outcomes of this step. The first is the response by Axon 2 to the potential in Axon 1. When the Axons are disconnected, a few channels in Axon 2 open, but the Axon does not fire. When the Axons are connected, Axon 2 fires to its peak near the Nernst potential. This difference in response demonstrates that the Axon 2 is firing because of input from Axon 1, and that it is not behaving independently. The second outcome is the separation of spikes. This separation demonstrates that the spikes are separate action potentials, and that Axon 2 is not simply just following Axon 1. The third outcome is regeneration of the action potential. Both wells reach their peaks near the Nernst potential. The implication here is that the spike in Axon 2 would induce a similar spike in a third Axon near its own Nernst potential, propagating an action potential down the next well, and so forth.

The final step in the protocol is a return to the *low-rest* potential below $-100\,mV$, to increase the rate of recovery from inactivation and to repeat the protocol for another measurement.

4.3 Discussion

4.3.1 The CLVC protocol

The CLVC protocols for the measurements in Fig. 4.3 may be simplified to produce the same propagation behavior. The simplified protocols are as follows: *high-rest* for Axons 1 and 2 at $\sim -50\,mV$ for $t < 0$, followed by a brief *stimulus* step below $-10\,mV$ to Axon 1 at $t < 0$. The reason this protocol simplification will work lies in the KvAP behavior at *high-rest*. When active channels are stepped from *low-rest* at $t < 0$ to *high-rest* values as high as $\sim -40\,mV$ for $t < 0$, a majority fraction of the channels remain in the closed-active

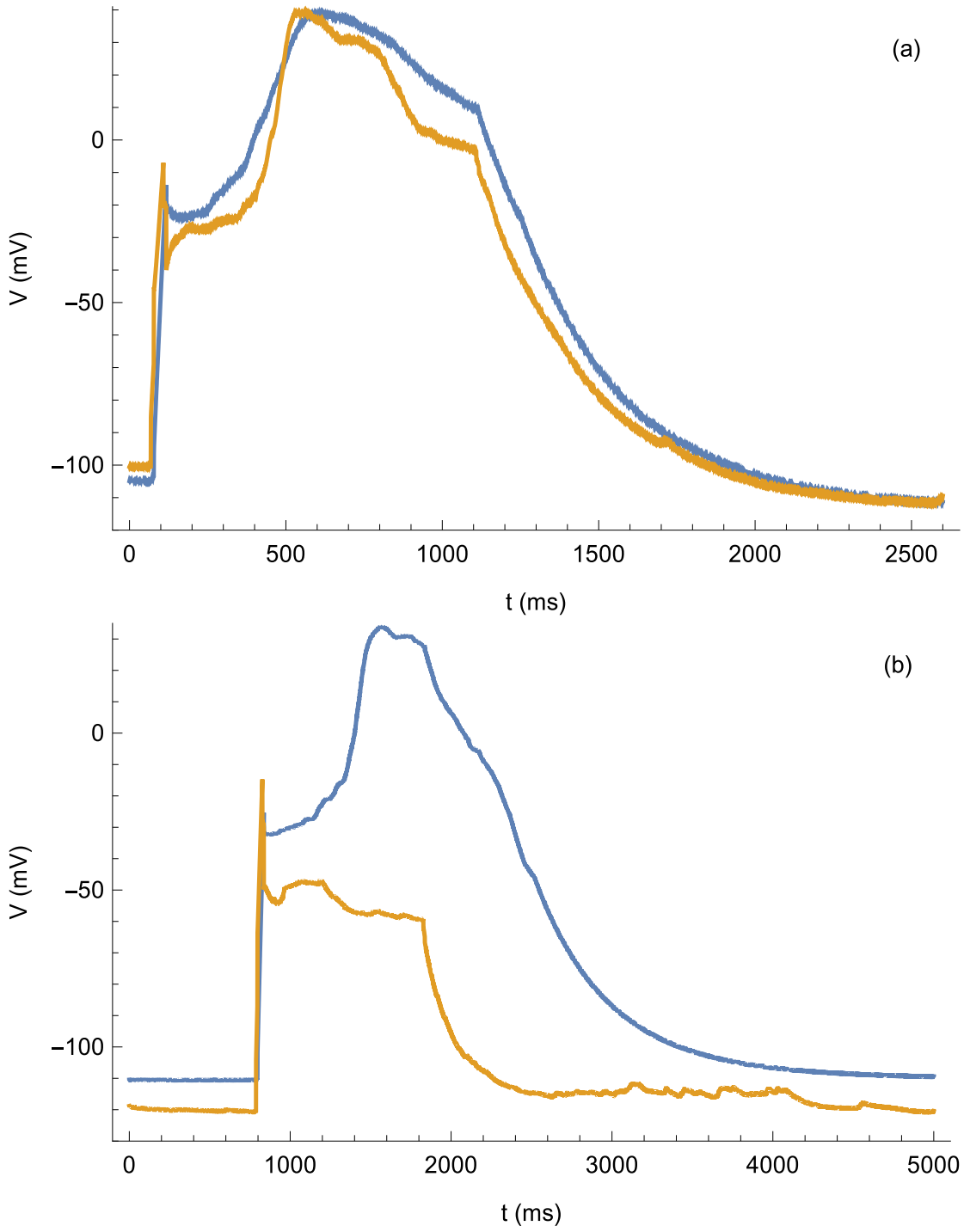

Figure 4.4: Second measurement for action potential propagation across two Artificial Axons. These measurements are for the same Axon preparations in Fig. 4.3. The CLVC protocols are also the same. The only difference in protocol is the *stimulus* step. In Fig 4.3, the CLVC is stepped to 91 mV for 250 ms. In the measurement above, the *stimulus* step is 18 mV for 500 ms.

state for $t \to \infty$. While a fraction of channels is lost to inactivation, it is possible to create conditions where the active channels in each Axon may propagate an action potential. This simplified protocol is implemented in the simulations of subsection 4.3.2 that follows.

The longer CLVC protocol in Fig. 4.3 was chosen over the simplified protocol for one glaring reason. This experiment was done before we fully understood how inactivation of this channel would behave in our Artificial Axon platform. At the time it was not clear whether channels would remain active at *high-step* voltages. Since the time these experiments were performed, we have a better model for the AA. We have used AA measurements to modify existing model parameters [SCM09] to better describe the KvAP in our system. A return to these propagation experiments in the future is worthwhile, in the pursuit of a viable network.

There is value in work toward improving the model of our system. As an example, consider the *stimulus* step in Fig. 4.3. As mentioned in section 4.3.1, this step is $2\times$ higher than the Nernst potential for Axon 1, but the purpose of the *stimulus* step is to get the Axon 1 potential above threshold enough to fire. While there are measurements with *stimulus* steps at $-20\,mV$, the measurement in Fig. 4.3 was chosen because it is cosmetically better for describing the channel behavior in the Axons during action potential progagation. Figure 4.4 is a measurement where all protocol values are the same except for the *stimulus* step. In Fig. 4.4, the CLVC value is $(-18\,mV,\ 500\,ms)$ instead of the $(91\,mV,\ 250\,ms)$ in Fig. 4.3. Here, Axon 2 "fires" before Axon 1, meaning that the action potential peak in Axon 2 comes before the peak in Axon 1. This may be fixed by decreasing the time width of the *stimulus* pulse, or changing some combination of CLVC values. Trial and error are involved in the search for the optimal width of the *stimulus* step. Simulation and modeling may inform how to optimize the network and behavior, and extracting these optimization techniques from the model is not trivial.

While our model and understanding of the KvAP behavior in our AA system has improved, experiments are crucial to further our understanding of the system. For example, during the *high-rise* steps in Axon 2 for the measurements in both 4.3(b) and 4.4(b), channels in Axon 2 do open and inactivate. The model and fits of AA action potential measurements suggest that the majority of channels in Axon 2 are still active. However this measurement

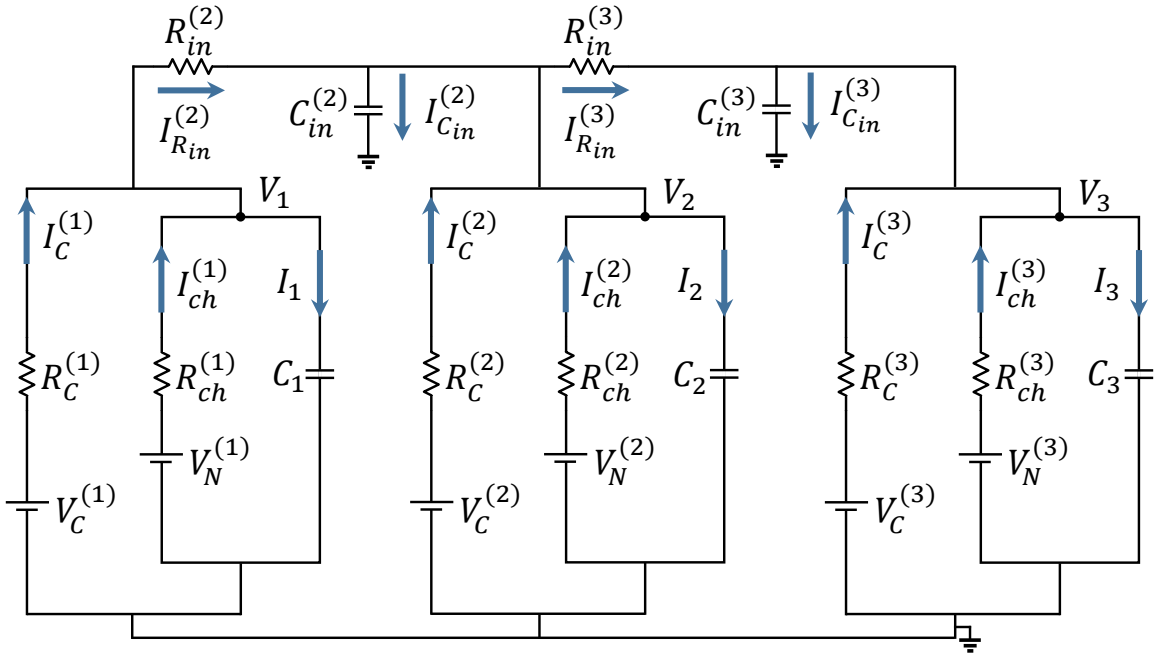

Figure 4.5: The equivalent circuit of three Artificial Axons connected by RC components for propagation of an action potential. R_{ch} is the resistance from the ion channels, C is the membrane capacitance, V_N is the Nernst potential. V_C and R_C are the CLVC voltage and resistance. An action potential is propagated from left to right. In this circuit, R_{in} and C_{in} order are switched compared to the measurements in Fig. 4.3 and Fig. 4.4.

in a propagation experiment has not yet been done. Therefore, whether (1) the channels may fire again or (2) all channels are inactive, is still unclear. Future experiments may confirm that what we see in the model and fits of AA action potential measurements do describe the channel behavior in propagation, or we may learn something new about the behavior of KvAP in our Artificial Axon.

4.3.2 Model

Figure 4.5 is an equivalent circuit for three Artificial Axons and their connections for propagation. C_i is the membrane capacitance for Axon i, and $R_{ch}^{(i)}$ is the channel resistance $\left(N_0^{(i)}\,\chi\right)^{-1}$, where $N_0^{(i)}$ is the channel number, and χ is the single-channel conductance for an open channel $(6\,G\Omega)^{-1}$. The Nernst potential $V_N^{(i)}$ is represented by a voltage source, $V_C^{(i)}$

and $R_C^{(i)}$ are the CLVC elements, and $C_{in}^{(i)}$ and $R_{in}^{(i)}$ are the external RC components that connect two Artificial Axons. The currents across all components is represented by I.

In the model, action potentials will be propagated from the left-most AA to the right. As such, the R_{in} and C_{in} components are reversed in this circuit representation compared to the measurements in Fig. 4.3 and Fig. 4.4. As was explained in section 4.2.1, the order is trivial. Consider the center Artificial Axon in the circuit. If more AAs are added to the circuit, these AAs will be identical to the center AA; each Axon i will be connected directly to a capacitor $C_{in}^{(i)}$ and a resistor $R_{in}^{(i+1)}$. The only AAs affected by the R_{in}-C_{in} order are the first and last. The first AA will require a larger stimulus if it is directly connected to C_{in}. If the last of n total AAs is not followed by components $R_{in}^{(n+1)}$ and $C_{in}^{(n+1)}$ in series, then its response to stimuli will be larger than internal AAs. Otherwise, successful propagation is not affected by the R_{in}-C_{in} order.

Capacitors C_i and $C_{in}^{(i)}$ are parallel, and can be written as $C_i + C_{in}^{(i)}$. The membrane equation becomes

$$\begin{aligned}\left\{(C + C_{in})\frac{dV}{dt} \;=\; N_0(p_O\,\chi + \chi_\ell)[V_N - V(t)] \;+\; \frac{1}{R_C}[V_C - V(t)]\right\}_i \\ +\; \frac{1}{R_{in}^{(i)}}[V_{i-1}(t) - V_i(t)] \;-\; \frac{1}{R_{in}^{(i+1)}}[V_i(t) - V_{(i+1)}(t)]\end{aligned} \tag{4.6}$$

In section 4.1, χ is treated as both constant and variable in different examples. Note that χ and χ_ℓ here are constants and p_O is voltage-dependent, as is the treatment in previous chapters.

Figure 4.6 illustrates action potential propagation across nine Artificial Axons for two different simulated channels. The figures for one simulated channel are displayed in one column. The green traces represent the membrane potentials for each AA in time, the blue traces represent the open probabilities p_O, and the yellow traces represent the inactivation probabilities. All Axons are individually clamped by V_C at *high-rest*$\}$ $(-50\,mV)$. No other stimulus is applied to any Axon, except for a brief stimulus pulse at $t = 0$ to the left-most AA in each simulation. The left-most Axon fires, and the action potential is propagated to

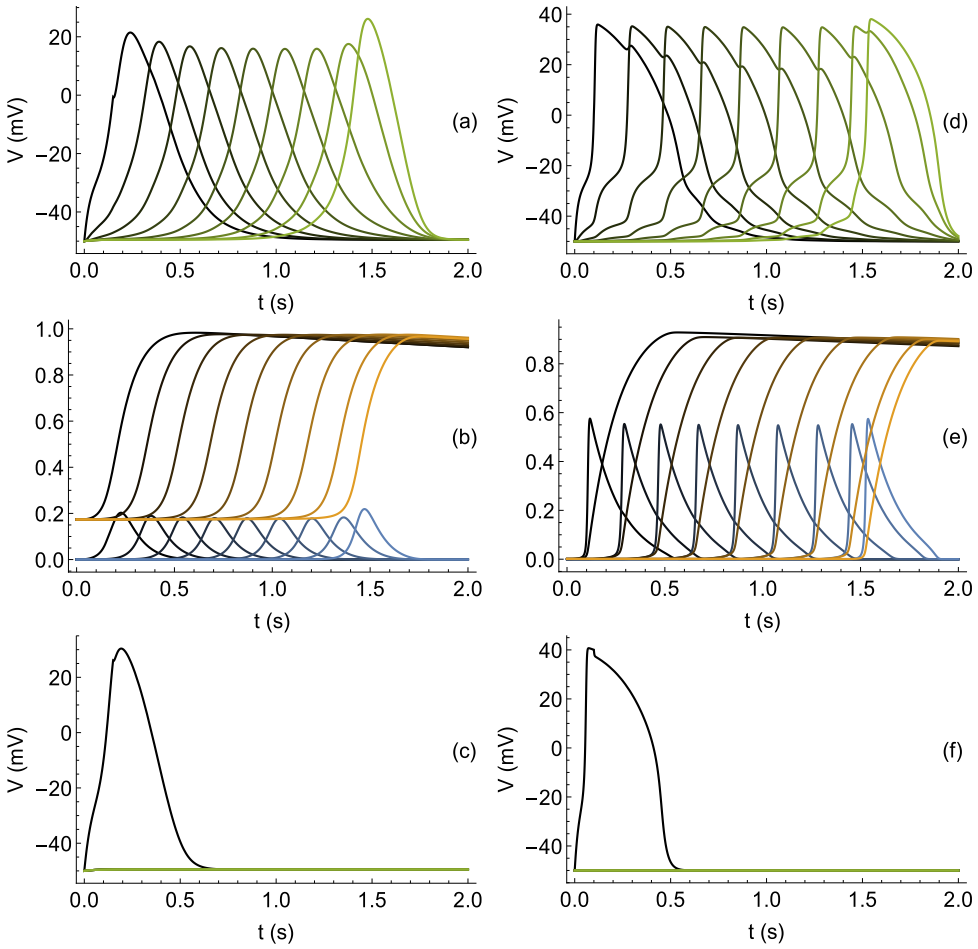

Figure 4.6: Two simulations of propagation across nine Artificial Axons. Each column corresponds to one simulation. The simulations use different channel and electrophysiological parameters; the parameters for the Axons in the left column are from the simulation in chapter 3 section 3.6.1, and those for the right-column Axon are from a fit for an AA action potential measurement. The green traces are the membrane potentials, the blue traces are open probability, and the yellow traces are inactivation. In (a) and (d) all Axons are connected, and in (c) and (f), the first Axon is disconnected from the downstream Axons. Two simulations are presented here to demonstrate the behavior of inactivation (yellow traces) at *high-rest* ($-50\,mV$). While there is $\sim 20\,\%$ inactivation in the left-column Axon at $-50\,mV$, inactivation does not prevent Axon firing from a $-50\,mV$ start point. These simulations suggest that the CLVC protocols in section 4.2.2 may be simplified to the CLVC protocol used in these simulations.

the last AA on the right. In (a) and (d), the Axons are connected by "reasonable" $R_{in} - C_{in}$ components; by this I mean values that propagate the action potential with large separation between spikes. The last action potential in (a) and (d) is higher because the ninth AA is not connected to a $C_{in}^{(10)}$ and $R_{in}^{(10)}$. In figures (c) and (f), the first R_{in} value in each simulation is made large, essentially disconnecting the first Axon from the others.

The KvAP rate constants for the simulated channel in the first column (channel 1) are from the simulation in the summation chapter; rate constants for the second channel (channel 2) are from a fit for a measurement in an AA action potential from another experiment – essentially a "borrowed channel" for this simulation. These parameters are not rigorously selected. Channel 1 is a loose fit for its measurement, and channel 2 parameters were modified to approximately fit the membrane behavior observed in the summation experiments. Despite this, the essential feature for propagation is present in both channel simulations: the majority fraction of channels remains active at *high-rest* membrane values. In channel 1 (Fig. 4.6(b)), 20% of channels are inactive at rest, and in channel 2 (Fig. 4.6(e)), the fraction of inactive channels is negligibly small. The expectation in a propagation experiment with this simple CLVC protocol would be that some fraction of channels will inactivate, but the majority would remain in the closed-active state, ready to fire from AA stimulus. However, it is still the case to the KvAP that recovery from inactivation requires a very negative resting potential, as can be seen in the inactivation figures. Before a spike, a majority of channels remain active. After the spike, channels are recovering from inactivation very slowly. At $\sim -50\,mV$, recovery from inactivation is $\sim 10\,s$, compared to the $\sim 1\,s$ timescale at voltages below $-100\,mV$. This inactivation timescale issue is one disadvantage to using the KvAP channel in a larger, future network.

4.3.3 Future work

An immediate improvement to the system would be the ability to tune R_{in} and C_{in}. As explained in subsection 4.2.1, R_{in} and C_{in} values cannot be changed once a lipid membrane is formed. But tuning ability would be necessary in a larger network, where not all Axon

preparations will be similar. Channel number, membrane capacitance, and leak are electrophysiological parameters that cannot be tuned in an Axon preparation, but these parameters determine an axon's ability to propagate an action potential for a given R_{in}-C_{in} combination.

An interesting set of questions arises here. We are seeing directly how much tuning is needed to just have propagation between two Axons, which is taken for granted in a fully developed neuron. The questions become: what drives the tuning mechanisms [HS98, Tur08] in the brain? What are the fundamental elements essential in tuning a neuron in the brain? In tuning a network? We see that the Artificial Axon and our constructivist approach in a future network may elucidate these elements and mechanisms.

KvAP's slow recovery from inactivation above $-100\,mV$ must also be addressed, if KvAP is to remain a candidate in the future expansion of our system. The time from rest to spike of KvAP channels in the AA is on the order of 100's of milliseconds, so the recovery from inactivation timescale must be brought down from $10\,s$ to (at maximum) a $1\,\mathrm{s}$ a timescale. As described at the top of section 4.2.2, a significant increase to the Nernst potential is a solution worth exploring as a solution. A second ion channel species the ideal solution, as it solves other problems to be discussed in future chapters. A more alternative to a second channel species is to reverse the connections between two Axons, so that positive input from one Axon brings the membrane voltage down below $-100\,mV$ in another Axon. It is conceivable to have multiple Axons work together to bring the potential down in one Axon in a reasonable amount of time. More discussion on this topic will be presented the next chapters.

CHAPTER 5

Firing Rate

A tunable firing rate is essential for information encoding by the neuron. Because the Artificial Axon has the same fundamental composition of the neuron, we expect a tunable firing rate to be essential to information encoding in a network of AAs. In this chapter, I show that the Artificial Axon can sustain firing rates over a range of input. First I show that the KvAP channel can recover from inactivation on the timescale of an action potential's rising edge. I then introduce a current clamp (CC) to produce input independently from the CLVC, and describe a few measurements with the CC. I implement a software trigger that mimics a second ion-channel species in polarizing the membrane for KvAP recovery from inactivation. The trigger is a temporary solution that nonetheless demonstrates the Axon's potential to fire as expected with a second species. Finally, I model the CC and trigger, and I propose an explanation for the behavior of active and inactive KvAP states in our firing rate measurements.

5.1 Firing rate in the neuron

Firing rates in the neuron are induced by depolarization events in the axon hillock that last longer than the width of one action potential. When Na^+ channels on a post-synaptic dentrite open, Na^+ rushes into the cell, depolarizing the soma with respect to the cell exterior. When the depolarization in the soma is large enough to reach the axon hillock – the most "threshold-sensitive" region of the neuron – the hillock "fires," and an action potential propagates down the axon. The hillock continues to fire for as long as the hillock is depolarized above threshold. The result is a train of spikes, and the inverse of the average

spike separation is called the *firing rate*. Firing rates are induced *in vitro* by injecting constant current directly into the axon hillock. The electrophysiology tool that injects the current is called the current clamp (CC). Constant CC input produces a constant firing rate, and increasing CC input produces increasing firing rates [BCP07].

The rate at which a neuron fires is controlled by the interplay between two circuit phenomena. The first is a resistor-capacitor response to input current. To charge the membrane, the input current competes with the channel-leak resistances and ion pumps that establish the resting potential. Second is the neuron microscopics. *Microscopics* refers to the behavior of active and inactive states of the channel species, which dynamically change the channel conductances.

A tunable firing rate is essential for information encoding by the neuron. *How* the neuron encodes information downstream is a subject of investigation with two main models. In one model, information is encoded in the firing rate itself (Rate Code model). In the other model, the information is in the precise timing of spike events (Temporal Code model). There is experimental evidence for both models [Fet97, GKM97]. What these models have in common is a firing rate that is tuned by the magnitude of input stimulus.

Because the Artificial Axon has the same fundamental composition of the neuron – lipid membrane capacitance and voltage-dependent conductance by way of the voltage-gated ion channel – we expect a tunable firing rate to be essential to information encoding in a network of AAs.

5.2 Recovery from inactivation and spike regeneration

Above a membrane potential $-100\,mV$, full recovery from inactivation is on a $\sim 10\,s$ timescale. Recovery from inactivation is asymptotic, thus membrane potentials below $\sim -120\,mV$ do not improve the recovery time. In a sequence of spikes, the membrane will spend most of the time above $-100\,mV$, and it is unclear whether KvAP can sustain a firing rate under these conditions. The measurement described below is a test for KvAP behavior in a sequence of such spikes.

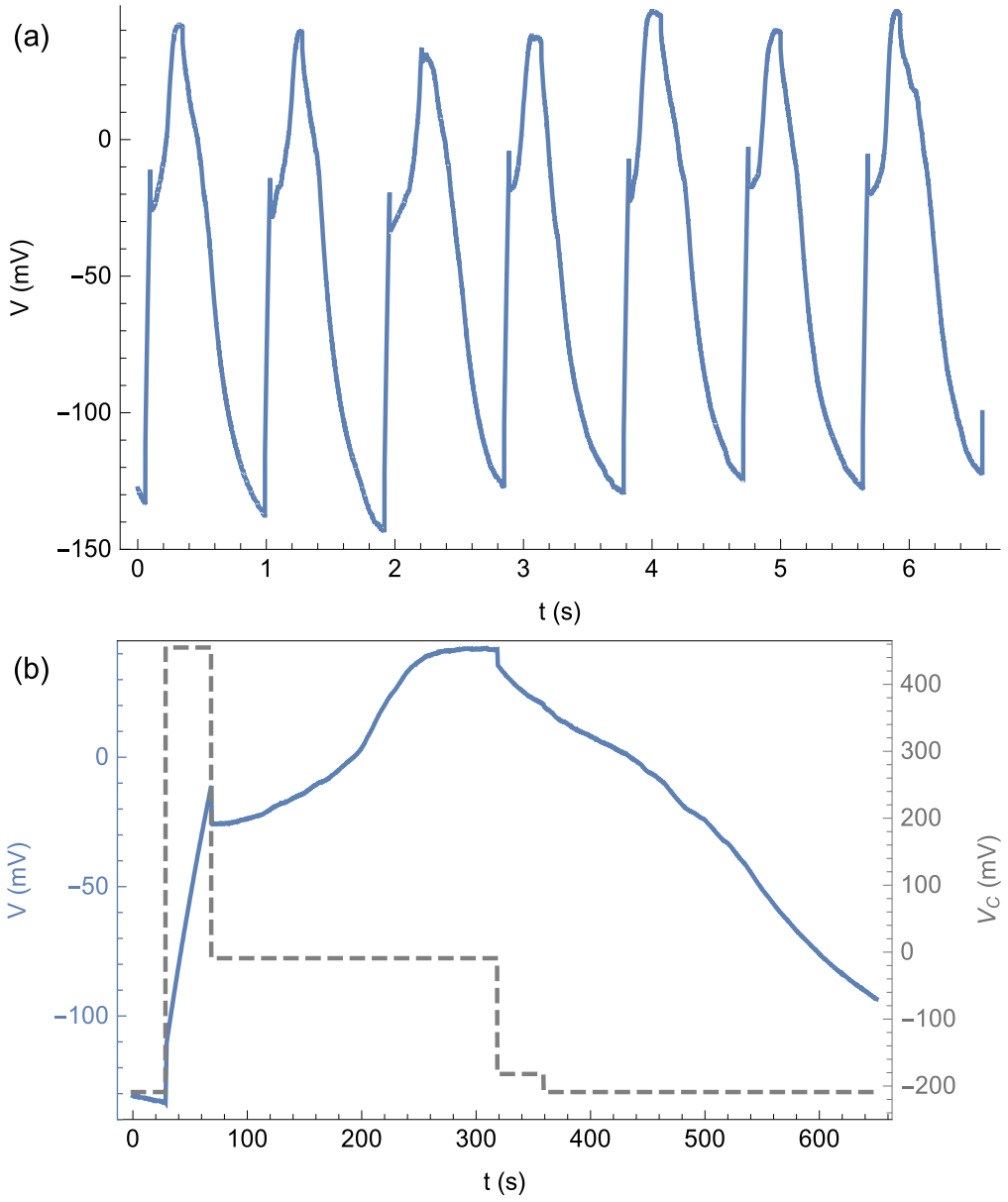

Figure 5.1: A sequence of action potentials from a CLVC protocol. Multiple spikes are shown in (a), and a single spike (blue trace) with the imposed CLVC protocol (gray steps) is shown in (b). The protocol is as follows. The CLVC value is moved from *low-rest* at $-209\,mV$ to at *high-pulse* step at $455\,mV$ for $40\,ms$ to bring the membrane potential to near-threshold for firing. Next is the *stimulus* step, protocol $(-9\,mV,\ 250\,ms)$, where the Axon fires toward the Nernst potential. CLVC is then brought down to $-182\,mV$ for $40\,ms$ (*low-pulse*), and then back to *low-rest* at $-209\,mV$ for $600\,ms$ so that channels may recover from inactivation and fire again. The protocol then repeats.

Figure 5.1 shows a sequence of spikes from a CLVC protocol. A line of several spikes is shown in (a), and one spike with superimposed CLVC protocol is shown in (b). The protocol is as follows, with terminology similar to subsection 4.2.2 of Chapter 4. The CLVC is stepped from $-209\,mV$ to $455\,mV$ for $40\,ms$; this step takes place in Fig. 5.1(b) shortly after $t = 0$. For future reference, we shall call this the *high-pulse* step. This step quickly brings the membrane potential to threshold. As discussed in section 4.3.1 of Chapter 4, this step is not necessary and is purely cosmetic. This step assures that a larger fraction of channels will contribute to the action potential compared to a step height that is closer near threshold for firing ($\sim -30\,mV$). However, the behavior in Fig. 5.1 would be the same without this step, in the sense that the channels will fire toward the Nernst, but just not as high.

After the *high-pulse* step, the CLVC is brought down to $-9\,mV$ for $250\,ms$, where the Axon fires toward the Nernst potential. For future reference, we shall call this the *stimulus* step. The small step that follows is a $40\,ms$, $-182\,mV$ pulse. Like the *high-pulse* step prior, this *low-pulse* step is also not necessary. It was put into the protocol for tune-ability, in the event that the un-tunable electrophysiological parameters of an Axon preparation – specifically leak and channel-number – are too large for the CLVC to overcome. In such a preparation, the *low-pulse* would be similar in absolute value to the *high-pulse* step.

Finally, the CLVC is brought down to *low-rest*, at $-209\,mV$ for $600\,ms$, and the protocol repeats. The Axon repeatedly spikes toward the Nernst potential with some random variation in height and no visible trend toward inactivation. Barring any detrimental changes in the electrophysiological parameters, the Axon should fire indefinitely. This measurement demonstrates that the KvAP is capable of recovery from inactivation enough to regenerate an action potential. Therefore, KvAP remains a viable candidate for study in our work toward a larger network of Artificial Axons.

5.3 The current clamp

A CLVC protocol is not an ideal stimulus in a network, where our goal is to move away from software control. Any stimulus will not step like a protocol, but rather will be approximately

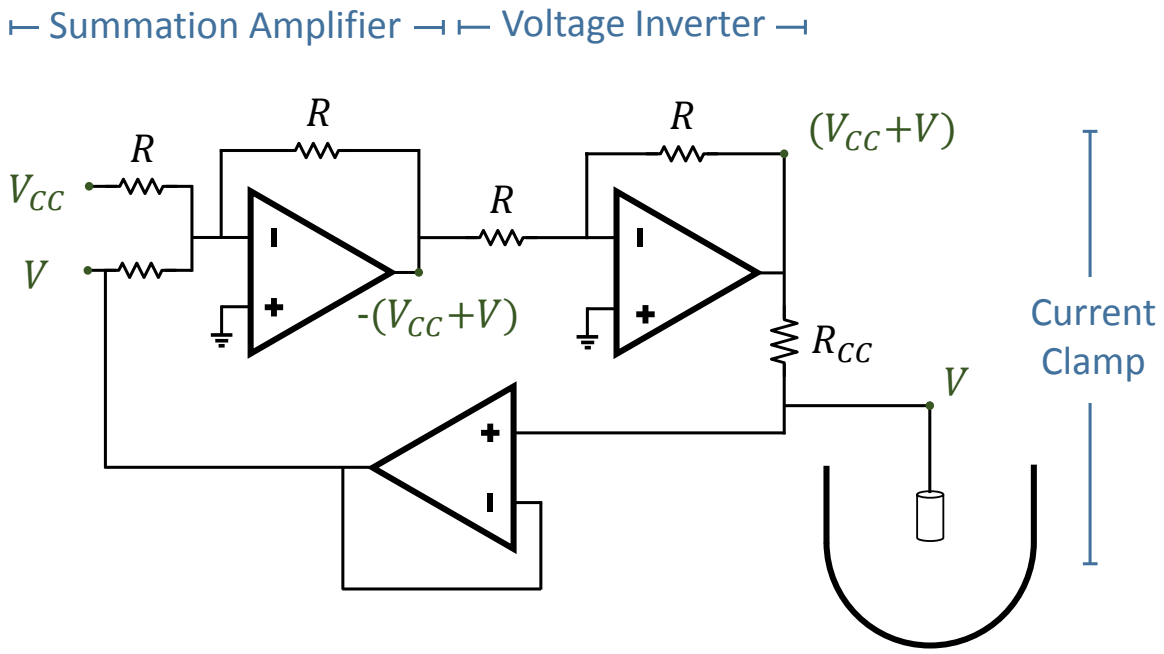

Figure 5.2: Schematic of the current clamp. All op-amps used are the low-noise FET precision op-amp AD795. The green dots represent the positions of the stated voltage values, also in green. The current clamp has three components: a summation amplifier circuit, a voltage inverter, and a high-impedance voltage follower. These components work together as follows. The potential difference between the voltage inverter and follower determines the current injected into the AA as $I_{CC} = V_{CC}/R_{CC}$ [VZ18].

constant input. In electrophysiology experiments, constant input to a neuron is given to the axon by a current clamp (CC). A current clamp takes as input a voltage V_{CC} and injects a constant current $I_{CC} \propto V_{CC}$ into the axon to produce firing in the neuron. Current clamp design and measurements in the Artificial Axon are described below.

5.3.1 Electronic design

A schematic of the current clamp is shown in Figure 5.2. All op-amps used are the low-noise FET precision op-amp AD795. The summation amplifier adds the command voltage V_{CC} to the membrane voltage V as $-(V_{CC} + V)$, and the inverter flips the voltage reference so that the sum is positive. The potential difference across the current clamp resistor R_{CC} is

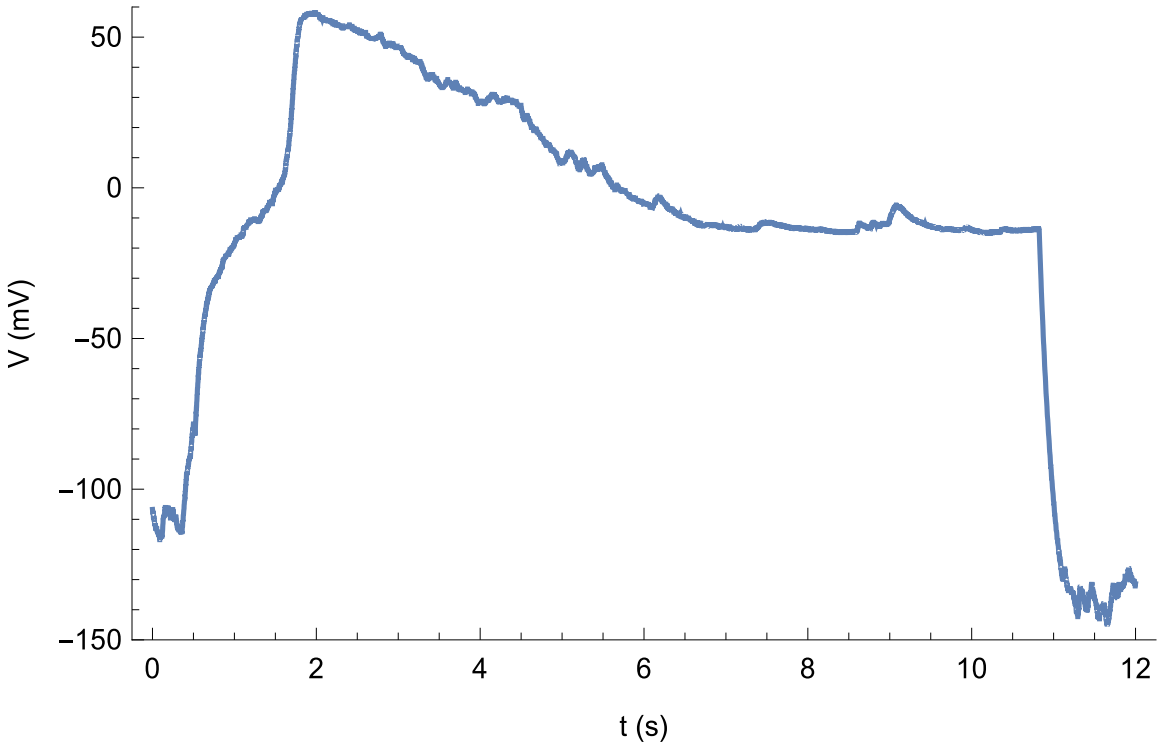

Figure 5.3: Figure 5.3 shows a measurement of an action potential induced in an Axon by a current clamp. $V_C = -227\,mV$ holds the potential at rest (-110 mV). At $t = 360\,ms$, the current clamp is switched on and injects a constant $100\,pA$ into the Axon, and then is switched off at $t = 10.8\,s$ after the channels have inactivated. $N_0\,\chi_\ell = (1.87\,G\Omega)^{-1}$, and $C = 250\,pF$.

V_{CC}, and the current injected is $I_{CC} = V_{CC}/R_{CC}$. The lowest op-amp in the figure is a high-impedance voltage follower that measures V for feedback to the summation amplifier [VZ18].

5.3.2 No trigger

Figure 5.3 shows a measurement of an action potential induced in an Axon by a current clamp. The CLVC voltage $V_C = -227\,mV$ holds the potential at rest (-110 mV). At $t = 360\,ms$, the current clamp is switched on and injects a constant $100\,pA$ into the Axon, and the Axon fires toward the Nernst potential. The CC is then is switched off at $t = 10.8\,s$ after all channels have inactivated. The competing CLVC, CC and leak put the membrane

rest potential at $-14\,mV$. The leak conductance $N_0\,\chi_\ell = (1.87\,G\Omega)^{-1}$, and the membrane capacitance $C = 250\,pF$.

Once the channels in Fig. 5.3 inactivate, the Axon cannot fire again. The membrane potential must be pulled down below threshold ($\sim -20\,mV$ to $\sim -30\,mV$) so that channels may recover from inactivation. Furthermore, as was discussed in section 4.3.2 of Chapter 4, channels recover from inactivation faster at larger, negative membrane values. The most ideal solution to this problem would be a second ion channel species in the same membrane with a salt gradient and Nernst potential in the opposite direction to the KvAP. While this is a future direction for our work with the Artificial Axon, a short-term solution is either in hardware or software.

5.3.3 Trigger

A software solution is written in LabVIEW. We call this solution the *trigger*, which works as follows:

$$\text{When } V \geq V_T,\ V_C^{(1)} \rightarrow V_C^{(2)} \text{ for } \tau_T > 0$$

V_T is called the *trigger voltage*, τ_T is the *trigger length* (units of time), and the $V_C^{(i)}$ are CLVC values. There are selection criteria for these trigger values. $V_C^{(1)}$ is some value that keeps the potential low, where channels are in the closed-active state. As discussed in subsection 4.3.1 of Chapter 4, the majority fraction of KvAP channels will move into the close-active state for $V < \sim -50\,mV$. However, $V_C^{(1)}$ values are typically chosen for $V < -90\,mV$, where channels will recover from inactivation more quickly. Without any outside stimulus, the membrane potential will remain low. The purpose of the trigger is to detect firing in the event that a current clamp input is large enough bring the membrane potential to threshold and thus induce an action potential. Therefore, the trigger value is chosen to be between $0\,mV < V_T < V_N$, where the channels are open and the axon is firing. $V_C^{(2)} < V_C^{(1)}$, where $V_C^{(2)}$ can pull the membrane voltage down to some large negative value, so that enough channel can quickly recover from inactivation to fire again. After some time τ_T, the CLVC returns to $V_C^{(1)}$ from $V_C^{(2)}$.

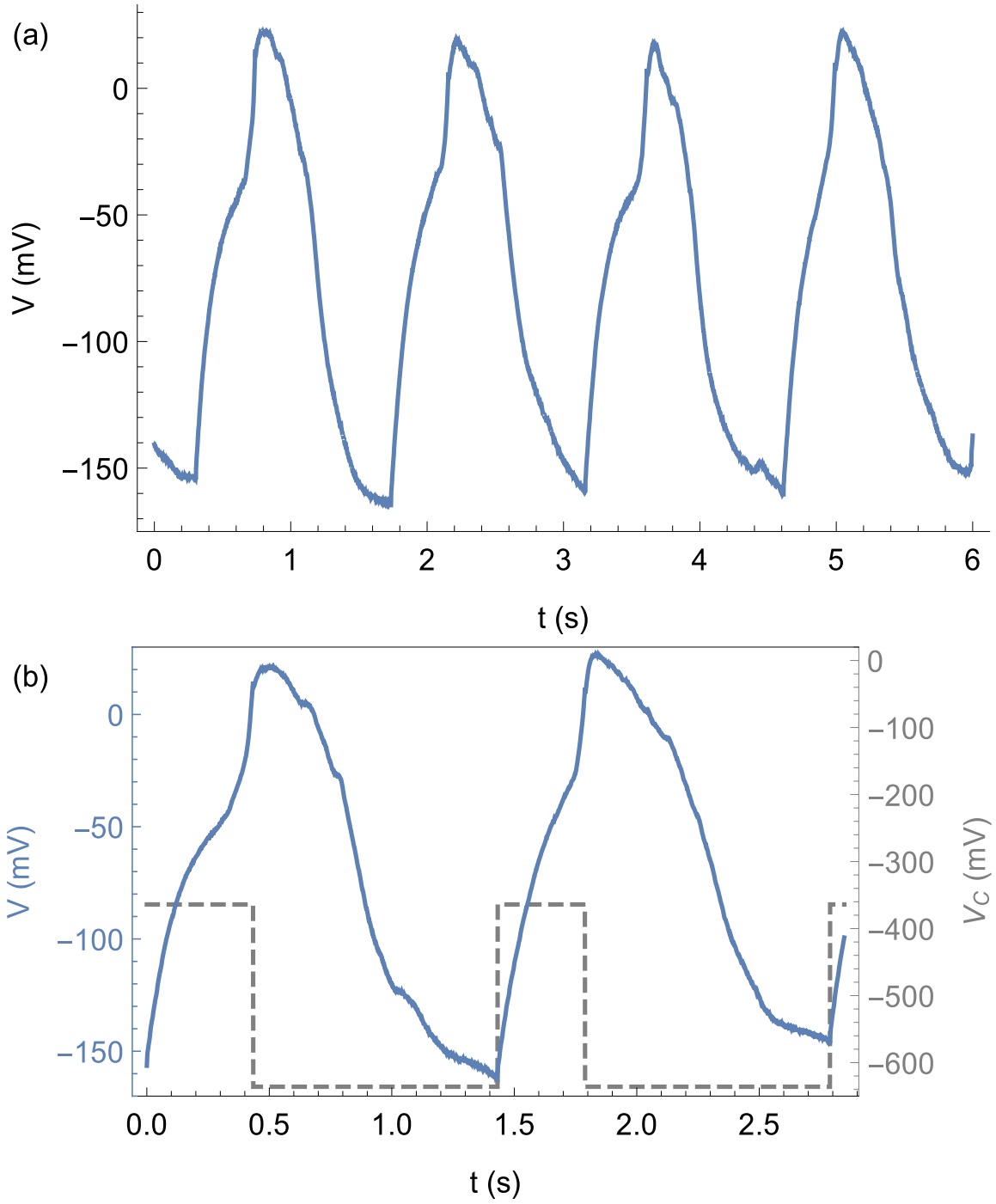

Figure 5.4: Membrane potential measurement with a CLVC, a CC and a trigger. A sequence of spikes is shown in (a), and two spikes (blue trace) with the imposed CLVC trace (gray steps) is shown in (b). The clamp values are $V_C^{(1)} = -364\,mV$, $V_C^{(2)} = -636\,mV$, $V_{CC} = 10\,mV$ ($I_{CC} = 100\,pA$), $V_T = 0\,mV$, and $\tau_T = 1\,s$.

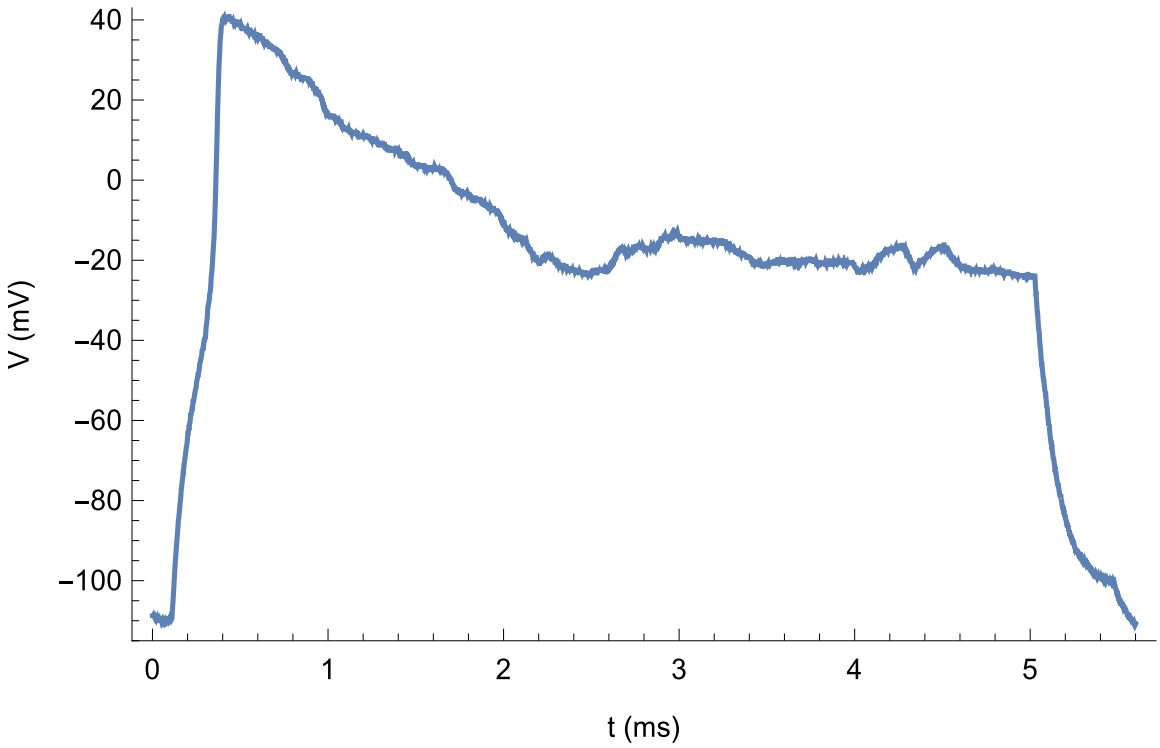

Figure 5.5: Measurement in Fig.5.4 with no trigger. All clamp and electrophysiological values are the same. After the Axon fires, the channels inactivate and the Axon cannot fire again.

Figure 5.4 shows a measurement of an Artificial Axon membrane potential with a CLVC, a current clamp and a trigger. A sequence of spikes is shown in (a), and two spikes (blue trace) with the imposed CLVC trace (gray steps) is shown in (b). Both the CC and CLVC are switched on at some time $t < 0$. The $V_C^{(i)}$ values are significantly larger than the rest potentials $V_r^{(i)}$ because the CLVC must compete with the CC and a large leak to keep the membrane potential low. $V_C^{(1)} = -364\,mV$, $I_{CC} = 100\,pA$ ($R_{CC} = 100\,M\Omega$), and leak conductance $N_0\,\chi_\ell = (1.78\,G\Omega)^{-1}$. In the absence of a CC current I_{CC}, as is the case in Fig. 5.5, this combination of clamp voltages and leak puts the rest potential at $V_r = -124\,mV$; when a CC current is present, as is the case in (a) and (b), $V_r = -29\,mV$ and the Axon fires. When the membrane potential becomes greater than $V_T = 0\,mV$, the CLVC value changes to $V_C^{(2)} = -636\,mV$ for $\tau_T = 1\,s$. After time τ_T, the CLVC value returns to $V_C^{(1)}$.

A brief note regarding the CLVC protocol in Fig. 5.1. In describing the measurement, I mentioned that the *high-pulse* and *low-pulse* steps are unnecessary. These steps were included to counter the inactivation of the KvAP channel, which was initially thought to be far less forgiving at voltages between $-90\,mV$ and $-50\,mV$. However, Fig. 5.4 demonstrates that enough channels remain open and recover from inactivation in the $\sim 1\,s$ between action potentials to continue firing. Therefore, the *high* and *low* pulses are purely cosmetic, in the sense that these quick steps in voltage will allow for more channels to recover from inactivation, and thus produce wider and higher spikes in firing. The CLVC protocol in Fig. 5.1 may be simplified by including only the *low-rest* and *stimulus* steps.

5.3.4 Changing firing rate

The measurements below demonstrate the Axon's ability to respond to a range of input. In this subsection I show that firing rate increases with increasing input current, and I propose an explanation for the behavior of active and inactive KvAP states in the spike train measurements.

Figure 5.6(a) shows six trains of spikes across time. $V_C^{(1)} = -125\,mV$ holds the mem-

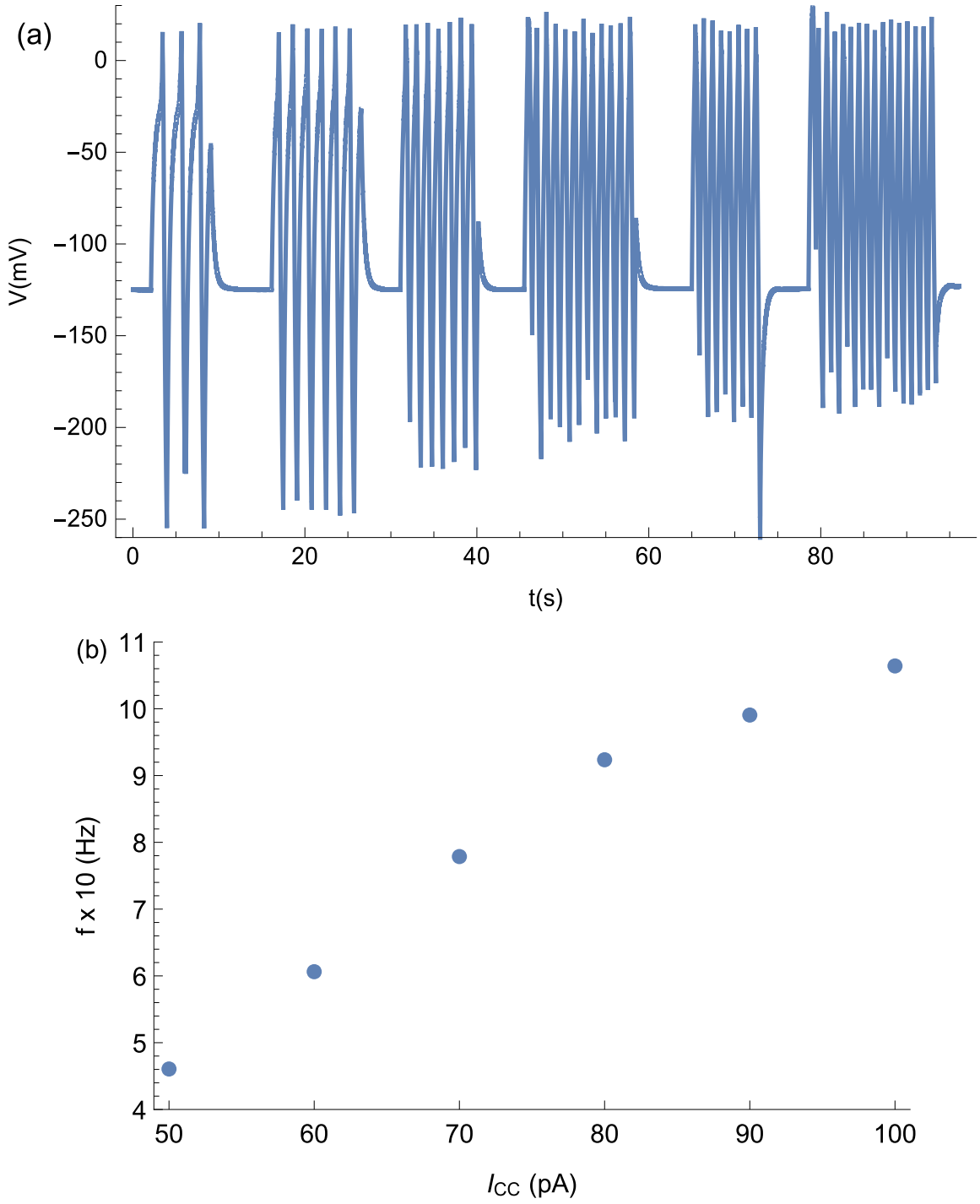

Figure 5.6: A series of spike trains induced by a CLVC, CC and trigger. $I_{CC} = 50\,pA$ in the first train, and I_{CC} increases by $10\,pA$ in the trains that follow. The membrane potential in time is plotted in (a), and the corresponding train frequencies are plotted with their currents in (b). All clamp values are constant. They are: $V_C^{(1)} = -125mV$, $V_T = 14mV$, $V_C^{(2)} = -459\,mV$, and $\tau_T = 500\,ms$.

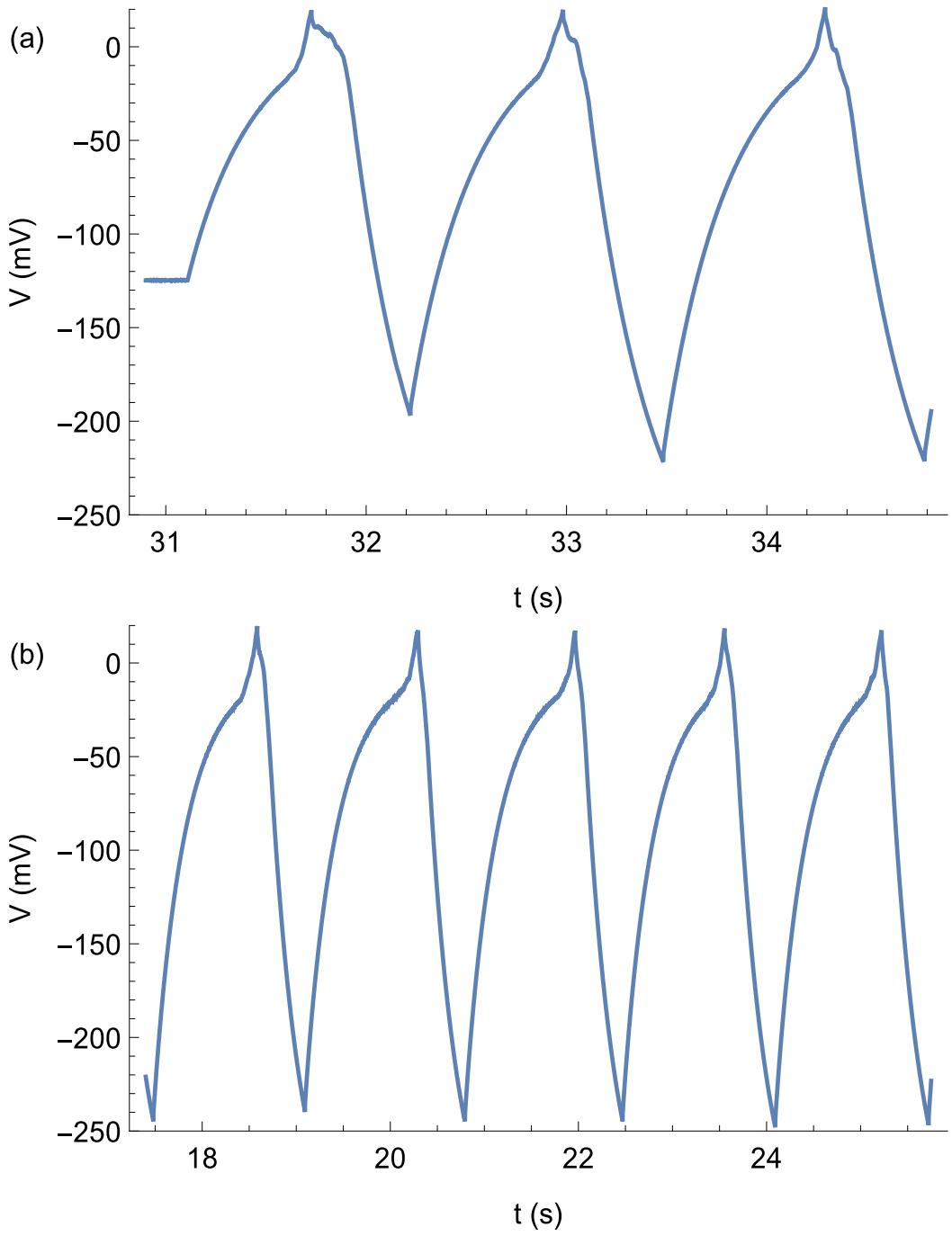

Figure 5.7: Several spikes from two different trains in Fig. 5.6. In (a) we see the first spike in a train, which has more open channels than the two action potentials that follow. By the third spike, active and inactive states "stabilize," and the spikes that follow are visually similar in channel contribution, with some variation but no visible trend toward inactivation. (b) is an example of spikes that have become stable in the channel contribution to firing.

brane potential at rest $V_r \approx -125\,mV$. A train is produced by a current clamp and trigger, with CC input increasing by $10\,pA$ between trains. $V_T = 14\,mV$, $V_C^{(2)} = -459\,mV$ and $\tau_T = 500\,ms$ are constant. As the injected current I_{CC} increases, the firing rate also increases. Fig. 5.6(b) is a plot of the frequency for each train, given its I_{CC} input. The firing rate is approximately linear, but then begins to flatten out for larger I_{CC} input. This leveling of the slope comes from the shrinking contribution of the channels, toward spikes that are predominantly the rising and falling RC edges from the clamps and trigger.

Fig. 5.7 shows a few spikes from two separate trains in Fig. 5.6. The train in (a) is for input $I_{CC} = 70\,pA$, and (b) is for input $I_{CC} = 60\,pA$. Compared to action potentials in Fig. 5.4, the channel contribution to firing is much smaller in Fig. 5.6. As discussed in subsection 4.3.1 of Chapter 4, there is a trial and error component to optimizing the channel contribution in an experiment. This optimization is not trivial, and to construct an optimization protocol would require further exploration of the model for our Artificial Axon. However, the aim of this experiment is to verify whether the Artificial Axon will respond without full inactivation to a range of input, and this measurement does demonstrate that this is the case. This measurement's combination of clamp choices is a viable solution to the changing-stimulus question.

Figure 5.7(a) shows the first pulse in a train. This first spike has a greater channel contribution than the two spikes that follow. I propose the following explanation for this behavior. Channels do inactivate in the first spike of the train, but some stability is reached between the oscillating fractions of channels in the active and inactive states, so that spikes further down the train will all have the same channel contribution. The measurement in (b) begins a few spikes after the first spike in the train, and channel contribution is visually about the same between spikes, with some variation but no visible trend toward inactivation. Active/inactive states in a spike train are modeled and simulated in the section below.

5.4 Discussion

5.4.1 Model

The new additions to be modeled in the AA are the current clamp and the trigger. The current clamp is included in the model as an extra current term $I_{CC} = V_{CC}/R_{CC}$ in the membrane equation. To simulate the trigger described at the top of subsection 5.3.3, the expression for the CLVC voltage input is

$$V_C^{(1)}\,\Theta\big[t - \big(\tau(t) + \tau_T\big)\big] + V_C^{(2)}\,\Theta\big[\big(\tau(t) + \tau_T\big) - t\big] \tag{5.1}$$

The behavior is as follows. Θ is the Heaviside step function, and τ is a time-dependent discreet variable. At the time t when the membrane potential in a simulation reaches $V \geq V_T$, the τ value is replaced with the time t. This effectively changes the CLVC value from $V_C^{(2)}$ to $V_C^{(1)}$ for the duration of τ_T.

The membrane equation for simulation becomes

$$\begin{aligned} C\frac{dV}{dt} \;=\; & N_0(p_O\,\chi + \chi_\ell)[V_N - V(t)] + \frac{1}{R_{CC}}V_{CC} \\ & + \frac{1}{R_C}\Big(V_C^{(1)}\,\Theta\big[t - \big(\tau(t) + \tau_T\big)\big] + V_C^{(2)}\,\Theta\big[\big(\tau(t) + \tau_T\big) - t\big]\Big) \end{aligned} \tag{5.2}$$

Figure 5.8 shows one simulated Artificial Axon with two different CC inputs. The traces in the top row are spike trains from different CC input, $100\,pA$ on the left and $80\,pA$ on the right. The bottom row figures illustrate the open probability (blue trace) and inactivation (yellow trace) for the membrane plot directly above each figure. The clamp values and electrophysiological parameters are identical to the measurement in Fig. 5.4, with the exception of the rate constants. The rate constants are not the closest fit to the measurements, but they are sufficiently similar to describe the behavior of the membrane potential and the open and inactive state probabilities. Prior to the first spike in a train, the channels are in the closed-active state. The first spike has a larger channel contribution than the spikes that follow, as was the case in the measurements in Fig. 5.5. Inactivation oscillates about some high value and does not show a trend toward complete inactivation.

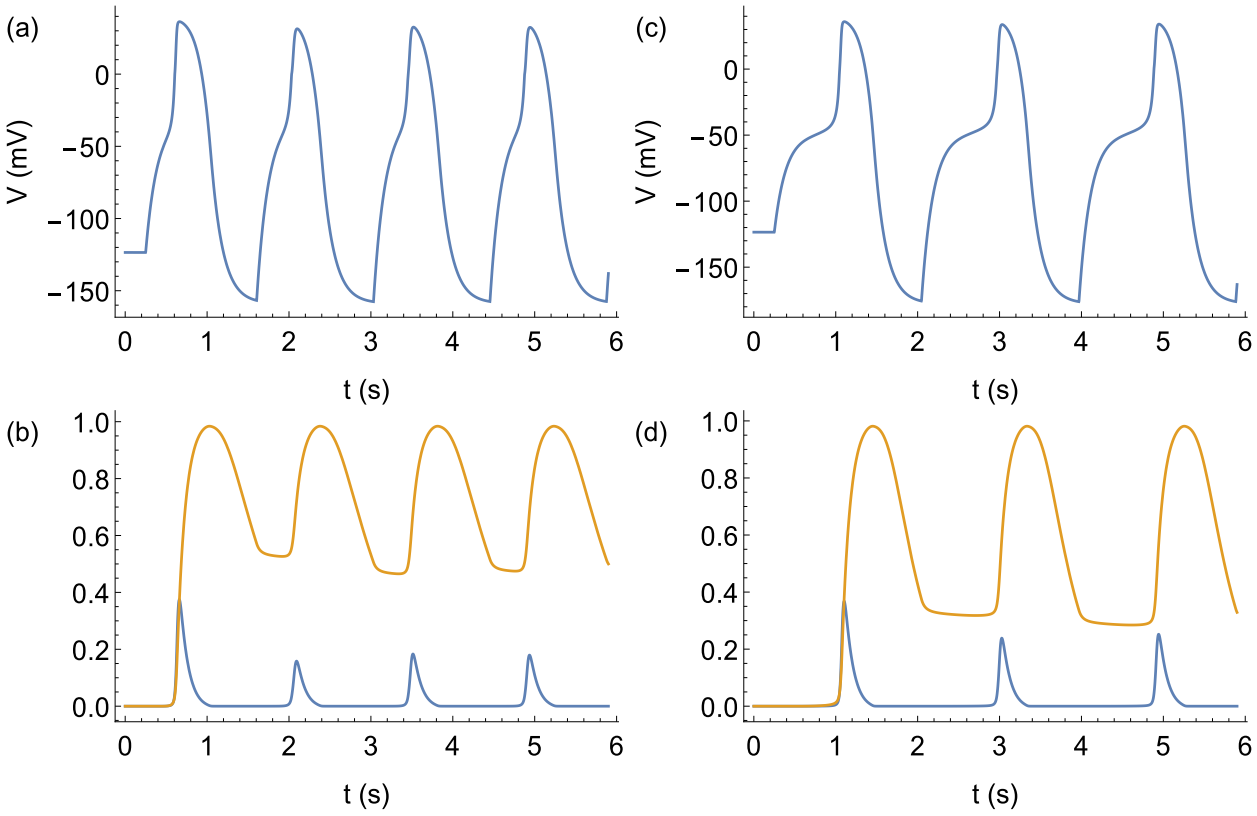

Figure 5.8: One simulated Artificial Axon with two different CC inputs. (a) is a spike train from CC input $100\,pA$, and (b) illustrates the channel open probability (blue trace) and inactivation (yellow trace). Not shown is a trace for the closed-active state, which makes the sum of probabilities equal to 1 at all points in time. (c) and (d) are corresponding simulations for CC input $80\,pA$. Electrophysiological parameters and clamp values are identical to those in Fig. 5.4. The rate constants in the simulation are not a perfect fit, but the fit is sufficient to describe the membrane and channel behavior.

5.4.2 Future work

As mentioned in subsection 4.3.3 of Chapter 4, a second ion-channel species is the ideal solution slow inactivation at potentials above $-100\,mV$, and two connected Axons with inverted input is a more tangible solution in the short-term. In the work for this chapter, the second species is also an ideal solution to the trigger. While a second channel is a future goal of the lab, the direction of my work is toward connections between Axons to make one complete computational unit as described in section 5.1. I present my work on Axon connections in the chapter that follows.

CHAPTER 6

Synapse

The connection between two neurons in the brain is called the *synapse*. In this connection, (i) a pre-synaptic action potential is translated into a current that is injected into the post-synaptic neuron, and (ii) the "machinery" involved in each neuron's rest and action potential does not see other neurons; the inner-workings of each computational unit is kept separate.

In this chapter I present an electronic synapse design to connect two Artificial Axons – a current clamp and voltage-dependent switch. I discuss measurements of two Artificial Axons connected by a synapse at different synapse strengths. Then, I discuss a circuit built in the lab to connect two Axons to each other with two synapses. I propose two Axons with two synapses as one computational unit in a network (what I call a *node*), which eliminates the need for a trigger or for a second ion channel species (at least at present). This connection scheme is presented in simulations. Finally, I present simulations with more synapses and nodes to build a self-contained spike loop that is not driven by external input, what I call an *oscillator*. The oscillator brings immediate practical use as a method of information storage in a future network of Artificial Axons.

6.1 Synapse in the neuron

The synapse in the brain is the space between two neurons, where the pre-synaptic neuron releases neurotransmitters into the synapse that induce K^+ current injection into the post-synaptic neuron. When an action potential reaches an axon terminal, membrane depolarization at the terminal opens calcium channels, and Ca^+ ions enter the pre-synaptic membrane. Calcium ions result in neurotransmitter-filled vesicles inside the pre-synaptic

neuron to release their contents into the synapse; the mechanism for calcium influx to vesicle fusion is not fully known [BPS92, FKG01, PSM06, KKR11]. Neurotransmitter in the synapse binds to receptors on ligand-gated ion channels in the post-synaptic membrane. This binding opens the channels, and ion current flows through the cell.

The chemical processes in the synapse are a means to inject current into the post-synaptic neuron. A logical step in development of a synapse for the AA is to use the existing current clamp. A CC connection also keeps the CLVCs from influencing other Axons, much like the chemical synapse and separation prevents the neuron machinery that maintains rest potentials in pre- and post-synaptic Axons from influencing each other. In the section that follow, I discuss a synapse design used in the lab to connect two Axons.

6.2 Electronic synapse for the Artificial Axon

Fig. 6.1 is a circuit diagram for the synapse we use to connect two Artificial Axons. When the membrane voltage $V_{pre} > 0$, the switch S closes and the current clamp injects a current into the post-synaptic Axon. This diagram excludes some resistors and expands only the components responsible for switching the synapse on and off. A complete and expanded diagram is presented in the next figure. In Fig. 6.1, both op-amps are the Low-noise precision FET op-amp AD795, and the switch in between the op-amps the Magnecraft W172DIP Reed Relay. We refer to this switch as the *synapse switch*, to identify it among the other switches in the circuit. A_1 is a voltage follower for the pre-synaptic Axon membrane potential V_{pre}, which functions as a high-impedance op-amp that prevents the summation amplifier in the current clamp (see Fig. 5.2) from injecting current into the pre-synaptic Axon. The A_1 output is connected to the relay and to op-amp A_2, what we refer to as the *saturation op-amp*. Saturation in A_2 provides the minimum $10\,mA$ required to flip the relay switch; the Axons are connected when $V_{pre} > 0$ and disconnected when $V_{pre} < 0$. When the Axons are connected, V_{pre} is input for the CC, such that the current injected in to the post-synaptic Axon is $I_s = V_{pre}/R_s$, where R_s is the current clamp resistance in Fig. 5.2.

A_1 also serves another function. When the relay switches, it produces an induction spark

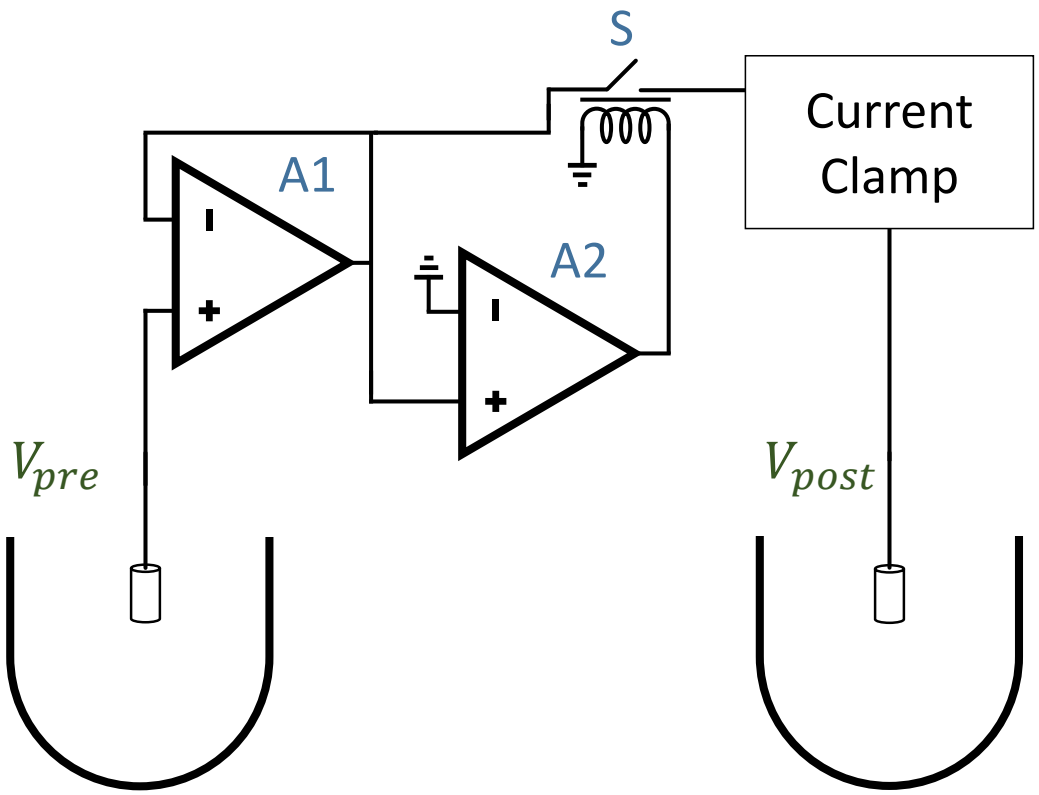

Figure 6.1: An electronic synapse switch for the Artificial Axon. A_1 and A_2 are the Low-noise precision FET op-amp AD795, and the relay is the Magnecraft W172DIP-5 Reed Relay. A_1 is a high-impedance op-amp, and A_2 drives the relay switch. When $V_{pre} > 0$, the current clamp injects current $I_s = V_{pre}/R_s$ into the post-synaptic Axon (see Fig.5.2).

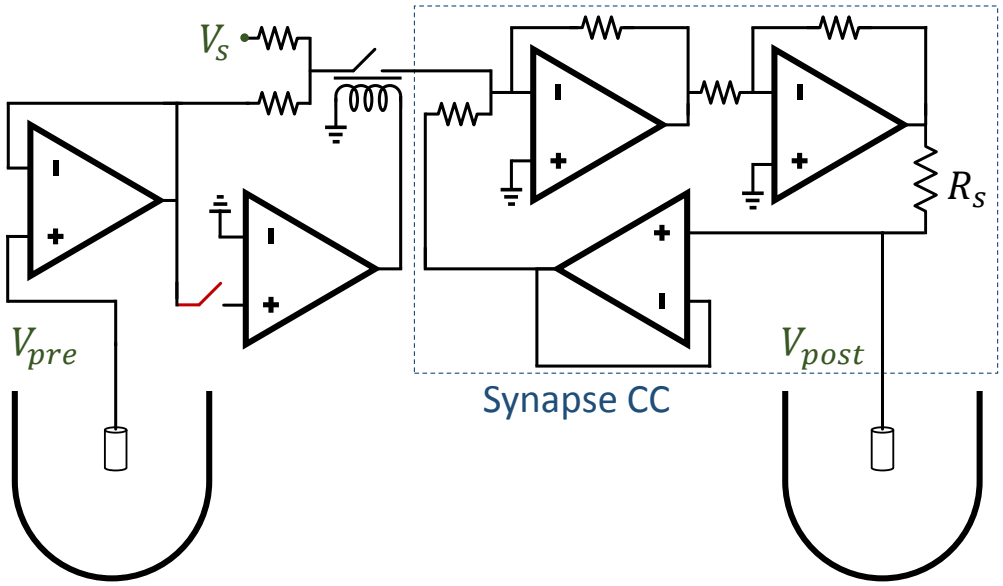

Figure 6.2: This is the same *synapse switch* and current clamp in Fig. 6.1 with one shifted connection. The inputs to the summation amplifier in the CC (see Fig. 5.2) are separated from the rest of the CC by the relay in the synapse. The switch in red is a reed relay that disconnects the two Axons from each other. V_s is an input voltage supplied by a DAQ to amplify the synapse strength by $I_s = (V_{pre} + V_s)/R_s$, where I_s is the current injected into the post-synaptic Axon. All unlabeled resistances are the same resistance $R = 100\,k\Omega$.

that injects current into the pre-synaptic Axon and charges its membrane. A_1 maintains V_{pre} output for both the relay and the saturation op-amp, working against these induction sparks.

An expanded connection diagram for the synapse is shown in Fig. 6.2. The synapse is identical to the current clamp design in chapter 4, except the summation amplifier input is on one side of the *synapse switch*, and the rest of the CC is on the other side. But the output is the same; when $V_{pre} > 0$, the switch closes and the current clamp injects current $I_s = V_{pre}/R_s$ into the post-synaptic Axon. From this point on, *synapse CC* will refer to the part of the CC in the blue, dashed box.

There are two additions to the circuit. The first is a switch between the high-impedance and saturation op-amps, highlighted in red in the diagram, which we simply call the *con-*

nection switch. This switch is a Magnecraft W172DIP Reed Relay, and it is driven by an Infineon BSP 75N. The *connection switch* connects/disconnects the Axons from one another, and its placement in the circuit is crucial. Like the *synapse switch* in Fig. 6.1, switching in the *connection switch* relay produces an induction spark that injects current into the post-synaptic Axon through the *synapse CC*. Its placement in Fig.6.2 does not affect the post-synaptic Axon.

The second addition to the circuit is the post-synaptic Axon input voltage V_s, provided by a DAQ. In this configuration, the input to the *synapse CC* is $V_{pre} + V_s$. The electrophysiological parameters in an Axon preparation are not tunable, and this V_s addition provides the system with tuning ability in the synapse strength. The alternative – and admittedly favored – method of synapse tuning is multiplicative, such that the input to the *synapse CC* is $\alpha\, V_{pre}$, where α is the tunable parameter. α may be tuned by either R_s or by software, where the input V_{pre} is measured by a DAQ that then returns $\alpha\, V_{pre}$ for input to the *synapse CC*. A software solution is something we attempt to avoid in our work when possible. Our aim with the Artificial Axon is to move away from computer software decision and computation toward a neuron-like network that is based in biology and the microscopics of the neuron. Tuning resistance has its problems in our present setup, as mentioned in section 4.2.1, but these issues may be resolved in future work. Synapse amplification by addition of V_s is a temporary compromise until resistor-tuning issues are explored and resolved.

In summary, the current injected by the synapse is $I_s = \alpha\Big(V_{pre} + V_s\Big)\Theta(V_{pre})$, where Θ is the Heaviside step function and $\alpha = \Big(R_s\Big)^{-1}$.

6.3 Measurements with the electronic synapse

6.3.1 Un-tuned synapse

Fig. 6.3 is a measurement of two Axons connected by the synapse in Fig 6.1. When $V_{pre} > 0$ for the pre-synaptic Axon (blue trace), the *synapse switch* closes and the *synapse CC* injects current $I_s = V_{pre}/R_s$ into the post-synaptic Axon (yellow trace). The smooth, dark-yellow

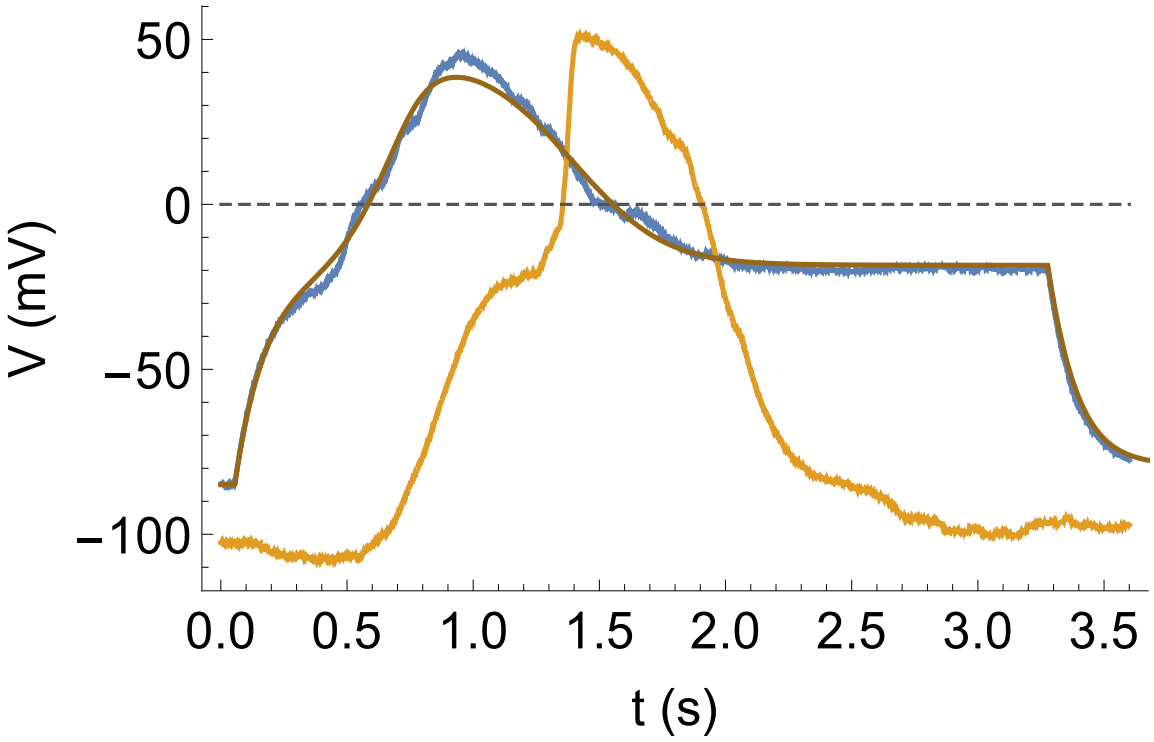

Figure 6.3: Two Axons connected by a synapse. The blue trace is the membrane potential for the pre-synaptic Axon, the dark-yellow line over the trace is a fit for the pre-synaptic Axon, and the lighter yellow trace is the membrane potential for the post-synaptic Axon. There are no triggers in this experiment, and $V_s = 0$. The CLVCs hold their respective Axons at rest. Shortly after $t = 0$, CC_{pre} is switched on, inducing a spike in the pre-synaptic Axon. When $V_{pre} > 0$ at $t \approx 0.5\,s$, the synapse injects current into the post-synaptic Axon until $V_{pre} < 0$ at $t \approx 1.5\,s$. The post-synaptic Axon fires, and V_2 remains high until the channels fully inactivate. At $t \approx 3.3\,s$, CC_{pre} is switched off and V_{pre} returns to rest. The electrophysiological parameters found in the fit are $N_0 = 461$, $C = 175\,pF$, $\chi_\ell = (68\,G\Omega)^{-}1/N_0$, and $V_N = 56\,mV$. The clamp values are provided in the text.

line over the pre-synaptic Axon trace is a fit line, and the dashed line across $0\,mV$ is a visual aid for the overlap between synapse input and post-synaptic firing. There are no triggers in this measurement, and $V_s = 0$. The CLVCs hold their respective potentials at rest, and are constant throughout the measurement. A current clamp in the pre-synaptic Axon (CC_{pre}, not to be confused with the *synapse CC*) delivers a stimulating pulse to induce firing. CC_{pre} is switched on shortly after $t = 55\,ms$, injecting $I_{CC} = 90\,pA$ into the pre-synaptic Axon, which brings the membrane above threshold to $-23\,mV$, and the Axon fires. The *synapse CC* injects current into the post-synaptic Axon shortly after $t \approx 0.5\,s$ when V_{pre} crosses $0\,mV$. The synapse stops injecting current at $t \approx 1.5\,s$ when V_{pre} crosses $0\,mV$ again. The post-synaptic Axon fires and V_{post} remains high after synaptic input ends. V_{post} slowly returns to rest as channels inactivate. CC_{pre} is switched off at $t \approx 3.3\,s$, and V_{pre} returns to rest. The clamp values are $R_{CC}^{(pre)} = 100\,M\Omega$, $R_s = 500\,M\Omega$, $V_{CC}^{(pre)} = 9\,mV$, $V_C^{(pre)} = -364\,mV$, and $V_C^{(post)} = -273\,mV$.

The measurement in Fig. 6.3 did not require a change in the synaptic strength; the chosen $(R_s)^{-1}$ provided sufficient amplification for post-synaptic firing. However, not every pair of Axon preparations will be as compatible. The following measurement is one such example.

6.3.2 Tuned synapse

Figure 6.4 shows a synapse measurement at two different strengths. The spikes in the top figure are from the pre-synaptic Axon, and the bottom figure shows the different responses of the post-synaptic Axon. When the synapse strength is too weak (V_s small), the post-synaptic Axon will not fire (blue traces). When V_s is made $\sim 2\times$ larger, the post-synaptic Axon fires (yellow traces). There is a negligible offset in the synapse switching voltage, but it is worth mention because it is noticeable in the figures. The synapse switches on at $\sim -0.5\,mV$ and switches off at $\sim -1.5\,mV$. The source of this offset in the synapse electronics is not known, but it is small and therefore ignored. The clamp and electrophysiological parameters for these two Axons are as follows. $V_C^{(pre)} = -155\,mV$, $R_C = 2\,G\Omega$, $V_C^{(post)} = -123\,mV$,

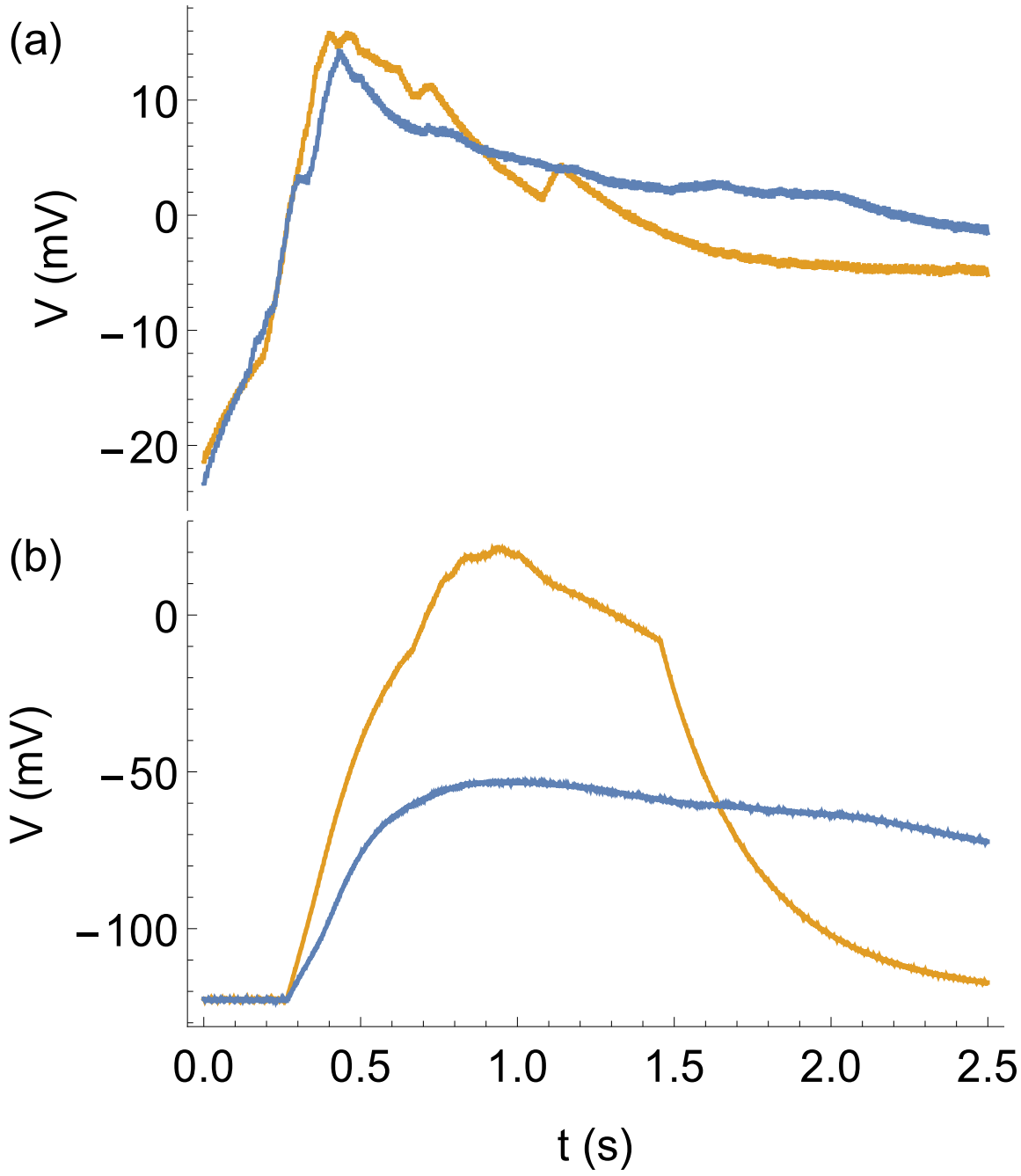

Figure 6.4: A synapse measurement at two different strengths. The top and bottom figures are for pre and post-synaptic Axons, respectively. V_s is too small in the blue traces to induce firing in the post-synaptic Axon. When V_s is made $\sim 2\times$ larger (yellow trace), the post-synaptic Axon fires. There is a negligible offset in the V_{pre} switching value; the synapse switches on at $\sim -0.5\,mV$ and switches off at $\sim -1.5\,mV$. The clamp values are listed in the text.

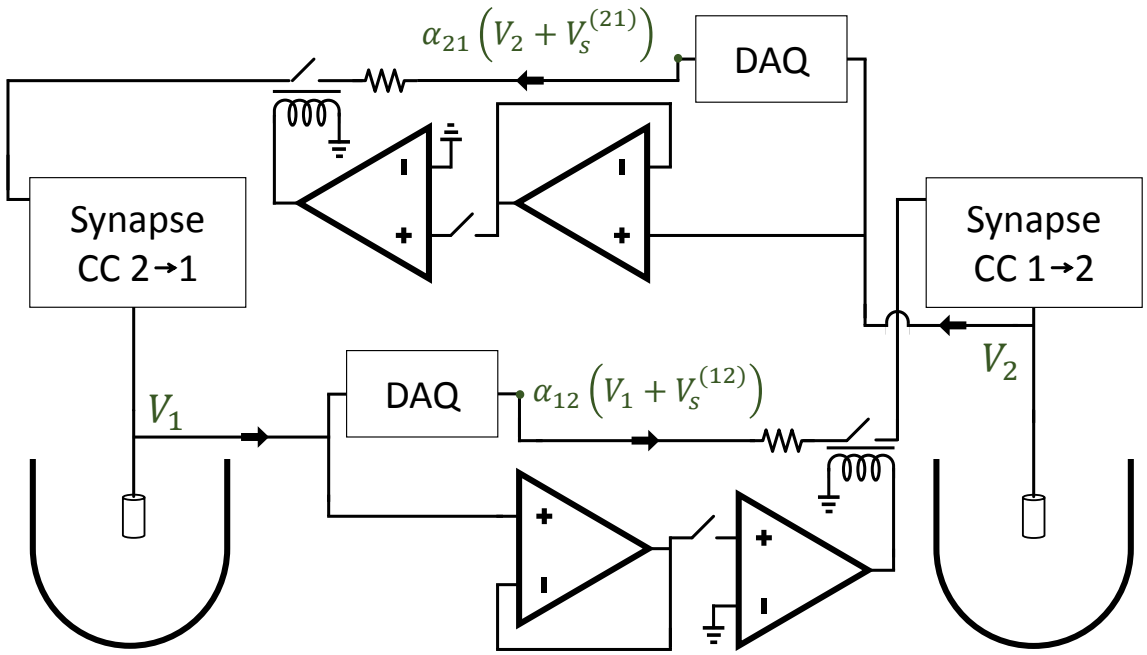

Figure 6.5: Two Axons connected by two synapses. Two synapses connect two Artificial Axons such that each Axon receives input from – and provides input to – the other Axon. The bottom synapse takes input from Axon 1 and outputs to Axon 2, and the top synapse takes input from Axon 2 and outputs to Axon 1. The DAQs change the synapse strengths, so that the output current from the CC is $I_{ij} = \left(R_s^{(ij)}\right)^{-1} \alpha_{ij} \left(V_i + V_s^{(ij)}\right) \Theta(V_i)$, where index i refers to the pre-synaptic Axon, j is for the post-synaptic Axon, and Θ is the Heaviside step function.

$CC_{pre} = 7\,mV$, $R_{CC}^{(pre)} = 100\,M\Omega$, and $R_s = 500\,M\Omega$. $V_s = 10\,mV$ in the blue traces, and $V_s = 23\,mV$ in the yellow traces.

6.4 Adding electronic synapse connections

The electronic synapse design in Fig. 6.1 is a viable connection that may be used to connect many Artificial Axons to each other in a future network. At present, there are interesting directions for exploration with two Axons and two synapses. Figure 6.5 is a diagram for a circuit built in the lab for exploration in the near future. The Axons are connected such that the sypapse input to V_i is $I_{ij} = \left(R_s^{(ij)}\right)^{-1} \alpha_{ij} \left(V_i + V_s^{(ij)}\right) \Theta(V_i)$, where index i refers to the pre-

synaptic Axon, j is for the post-synaptic Axon, and Θ is the Heaviside step function. The bottom synapse in the circuit provides input from Axon 1 to Axon 2, and the top synapse gives input to Axon 2 from Axon 1. The DAQs receive as input the membrane potential V_i and put out $\alpha_{ij}\left(V_i + V_s^{(ij)}\right)$. Note that if a DAQ is removed from the circuit, and the floating wires are connected to each other, the modified circuit is identical to the synapse in Fig. 6.2. The DAQ amplifies the signal by multiplication and addition, and these amplifications may be done by hardware. For example, V_s can be tuned with an external power source, α can be tuned by implementing changeability in the synapse resistance R_s, and the input to the synapse can be made negative (inhibitory input) by implementing a voltage inverter with op-amps. While our aim in the lab is to move away from software control of the Axon, we have demonstrated that this synapse design may function with electronics hardware alone; the software input here is an issue of convenience.

Some experiments with this circuit design are proposed in the section below.

6.5 Discussion

6.5.1 Model

As mentioned in section 6.2, the synapse current contribution I_s to a post-synaptic Axon is

$$I_s = {R_s}^{-1}\big(V_{pre} + V_s\big)\Theta\big(V_{pre}\big) \tag{6.1}$$

The membrane equation with synapse term for one Axon is

$$\begin{aligned} C\frac{dV}{dt} \;=\; & N_0(p_O\,\chi + \chi_\ell)[V_N - V(t)] \;+\; \frac{1}{R_C}[V_C - V(t)] \;+\; \frac{1}{R_{CC}}V_{CC} \\ & +\; \frac{1}{R_s}\big(V_{pre} + V_s\big)\Theta\big(V_{pre}\big) \end{aligned} \tag{6.2}$$

The last term in eqn. 6.2 is excluded if the Axon is pre-synaptic.

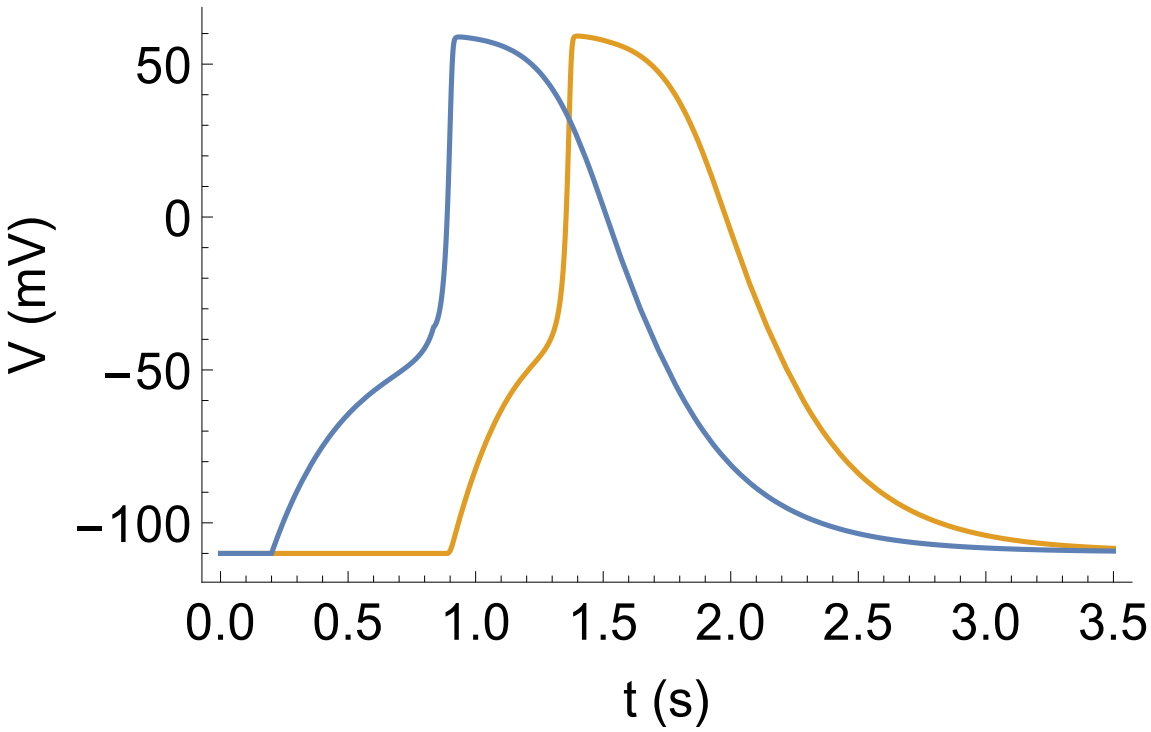

Figure 6.6: Simulation of two Axons connected by a synapse. The pre-synaptic Axon is the blue trace, and the post-synaptic Axon is the yellow trace; firing in the pre-synaptic Axon induces firing in the post-synaptic Axon. The Axons are held at rest with CLVCs. A stimulating current $ICCpre =$ from $< t <$ brings the pre-synaptic Axon to firing. While $V_{pre} > 0, /mV$, the synapse injects current I into the post-synaptic Axon. The channel parameters are taken from the simulations in section 5.4.1. In this simulation, V_N is raised to $60\,mV$ and $N_0 = 10^3$.

6.5.1.1 One Synapse

Figure 6.6 shows a simulation using eqn. 6.2 for two Axons connected by a synapse. The post-synaptic Axon (yellow trace) fires from input by the pre-synaptic Axon (blue trace). Both Axons are held at rest ($-110\,mV$) with their respective CLVCs ($R_C = 2\,G\Omega$). A stimulating pulse is applied to the pre-synaptic Axon with a CC_{pre} current $I_{CC}^{(pre)} = 36\,pA$ from $t = 200\,ms$ to $t = 835\,ms$. This stimulating pulse brings the pre-synaptic potential to threshold and the Axon fires. While $V_{pre} > 0\,mV$ between $888\,ms < t < 1.514\,s$, the synapse injects a current $I_s = R_s^{-1}(V_{pre})$ into the post-synaptic Axon, with $R_s = 1.2\,G\Omega$. The post-synaptic Axon fires, and both Axons return to rest after the CLVCs can overwhelm the channel current by inactivation. The electrophysiological, clamp, and channel parameters are taken from the simulations in section 5.4.1 of chapter 5, with exceptions in the Nernst potential and channel number: $V_N = 60\,mV$, and $N_0 = 10^3$.

6.5.1.2 Candidate for a complete biological node in a network

By *complete biological node*, I mean a unit of computation in the Artificial Axon where the rising and falling edges of an action potential use the microscopics of one or two ion-channel species, in place of a single channel species and a trigger (see section 5.3.3). The circuit in section 6.4 may produce such a unit. In this node candidate, one synapse provides excitatory input, and the other synapse provides inhibitory input. The result is one rising membrane potential edge from external stimulus, and one falling edge from inhibitory synaptic input. This is a neuron-like action potential, controlled by channel microscopics, able to carry information by way of a firing rate. I elaborate on the behavior of this node in the simulations and descriptions below.

The plots Fig. 6.7 show one simulation of two Axons connected by two synapses to produce an action potential. The Axon connections are modeled after the circuit in section 6.4. The Axon in (a) (AA_{full}) is stimulated to fire by an external pulse. AA_{full} provides excitatory input to the Axon in (b) (AA_{pol}) through one synapse, and the AA_{pol} provides polarizing, inhibitory input to AA_{full} through the other synapse. The result is an action

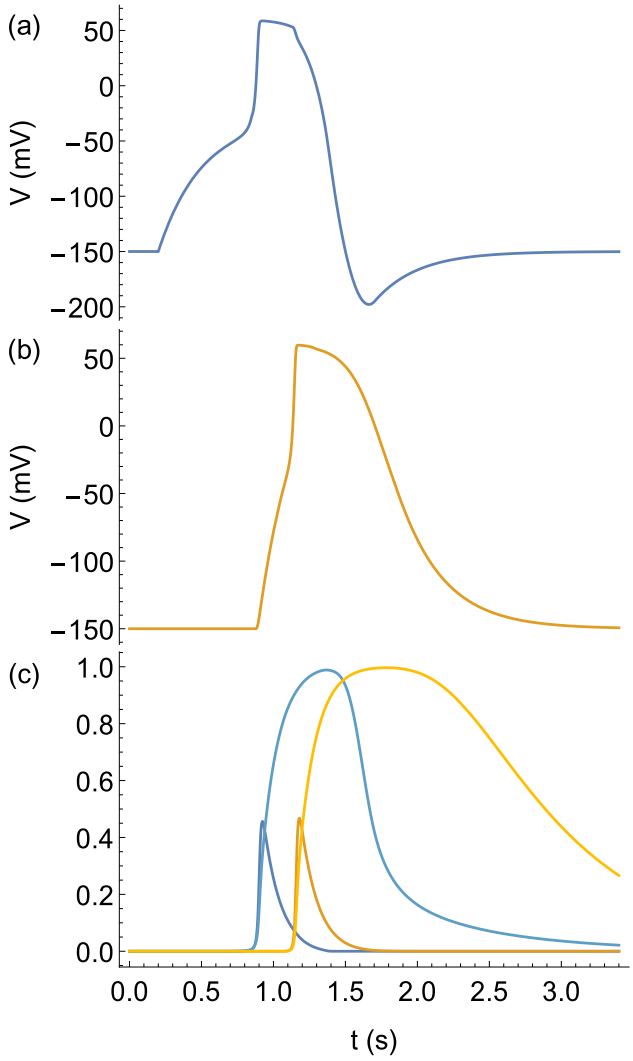

Figure 6.7: Two Axons connected by two synapses in a candidate network-node. The Axon in (a) excites the Axon in (b) with positive synapse current, and the Axon in (b) polarizes the Axon in (a) with negative synapse current. The outcome is an Axon (a) action potential with rising and falling edges from the ion channels and not from a trigger. Figure (c) plots p_O and inactivation in time for both Axons. The blue and light-blue traces are p_O and inactivation in Axon (a), respectively. The yellow traces in (c) are for the Axon in (b).

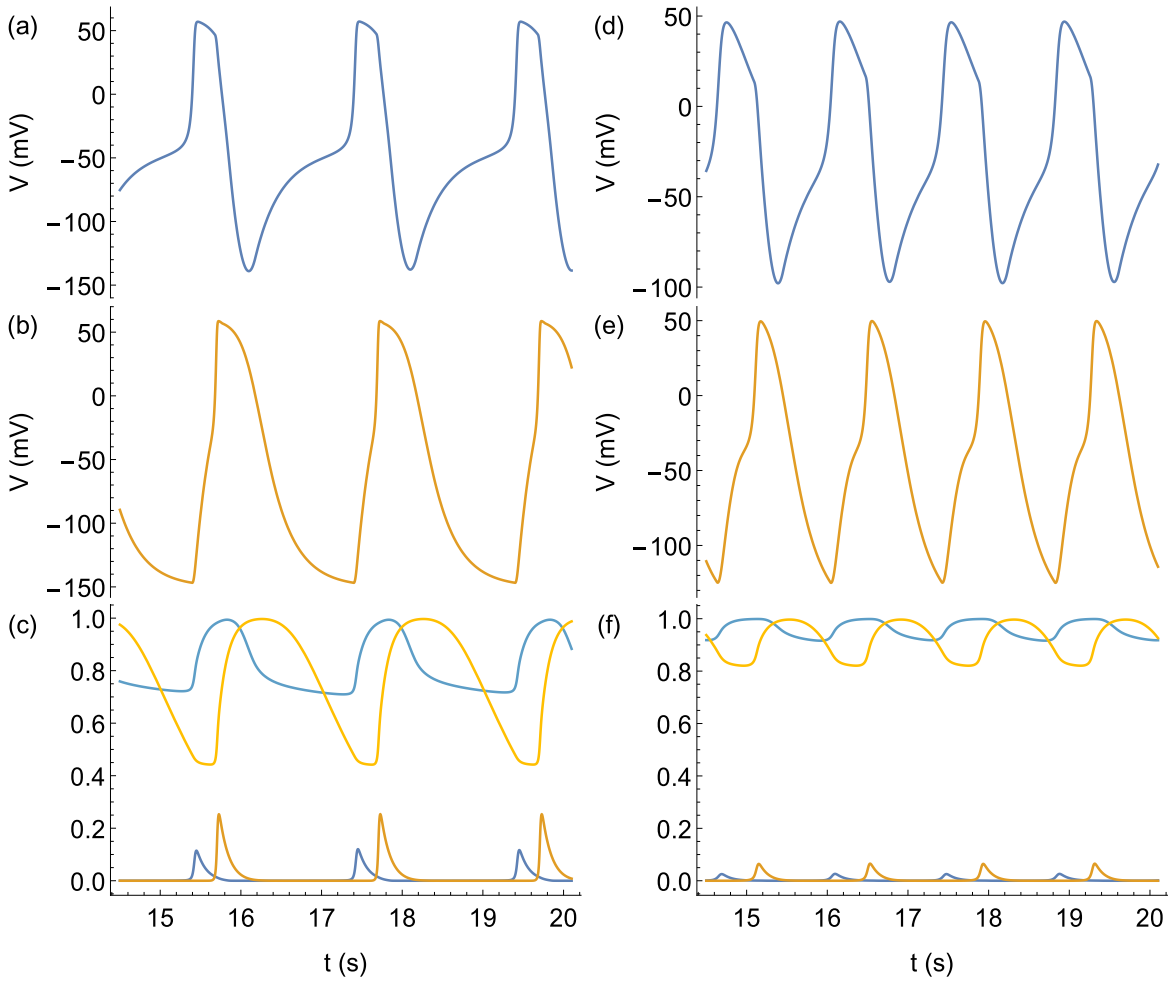

Figure 6.8: Simulation for one node's response to constant CC inputs. This is the same node from Fig. 6.7. (a)-(c) show the response to a constant $50\,pA$ input to AA_{full}, and (d)-(f) show the response to $60\,pA$ input. This node's key features as a computational unit are (i) the firing rate changes with changing input, and (ii) the firing rates are maintained with no trend toward inactivation.

potential in one Axon (AA_{full}) with a rising and falling edge produced by ion channels. The external pulse to $AArise$ is a constant $60\,pA$ that is applied for $650\,ms$ between $200 < t < 850\,ms$. When the AA_{full} potential V_{full} crosses $0\,mV$, the excitatory synapse injects into AA_{pol} a current ${R_s}^{-1}\,V_{full}$, and AA_{pol} fires. When the AA_{pol} potential V_{pol} crosses $0\,mV$, the inhibitory synapse injects into AA_{full} a current $-{R_s}^{-1}\,V_{pol}$, polarizing AA_{full} below the resting potential. This hyper-polarization is useful in firing rates, where sustained current stimuli will compete with the inhibitory synapse input to AA_{full}. Figure (c) illustrates the open probabilities and inactivation for the Axons. The darker traces are the open probabilities p_O, and the lighter traces are the inactivation curves for the same-colored p_O traces (blue-blue for AA_{full}, yellow-yellow for AA_{pol}). $R_s = 500\,M\Omega$, and all other parameters are identical to those used in Fig. 6.6.

Figure 6.8 show the same Axons' response to constant CC input. Figures a-c are the node's response to $50\,pA$ input to AA_{full}, and figures d-f correspond to a constant $60\,pA$ input. This node has the same behaviors sought in the Artificial Axon in chapter 5 for a unit of computation in a future network. Mainly, the firing rate changes in response to changing stimulus, and the firing rate is maintained with no visible trend toward inactivation. The simulation suggests that inactivation oscillates from full to partial inactivation as the membrane potentials move from Nernst to low-rest below $-100\,mV$. The input range for a firing rate with no eventual inactivation is $47\,pA - 60\,pA$. This range can be expanded by tuning the parameters. The electrophysiological parameters – leak, channel number, membrane capacitance and rate constants – cannot be tuned in a physical Axon preparation. Expansion of the firing rate range therefore relies on the tuning of clamp parameters – resistances and voltage inputs – as well as the Nernst potential. Parameter tuning in firing rate optimization requires future work with the model.

I note that the connection scheme presented here for a network node is an immediate solution to our single-channel species system. As I have mentioned many times, our aim is to move away from electronics in the Artificial Axon, and this direction includes the connections between Axons. However, in the immediate future the connection scheme in this subsection does provide a "brain-like" node that responds with the microscopics of a neuron. At present,

this node candidate is a worthwhile pursuit in our system.

6.5.1.3 Oscillators

Oscillators in the brain and their role is an active area of study in navigation, memory and sleep, among other functions [HCD09, KLL11, DPB10, BCP16, BD04]. Oscillators play a role in rhythmic motion like breathing, walking, and chewing [Kuo02, BHG15], and short-term information storage [LI95, BD04]. While there are many unanswered questions on the topic [ZAD18, SSL12, SWC13], oscillators are known to play significant roles on micro- to meso- to macroscopic scales, in terms of the neuron number involved [Wan10, CCM09, BMS11, SKP01].

Simulations of interconnected Artificial Axons suggest that our system may support sustained oscillations. By *oscillations* I refer to the ability to maintain a firing rate in two or more Axons that is sustained by input from the participating Axons only, and not with some form of perpetual outside stimulus. Information storage is a practical and immediate use for oscillators in our Artificial Axon in a small-scaled network of a few nodes. The implementation of an oscillator would transition the ability of our network from simple stimulus-response computation in real-time to information storage for processing at later times. An oscillator would allow our system to perform computations with input received in the past, in contrast to computations with incoming stimuli as it is received in real-time.

Figure 6.9 shows a simulation for an oscillator with four Axons. A $70\,pA$, $500\,ms$ stimulating pulse is applied to Axon 1 (the thicker, blue trace) at $t = 0$, and all Axons fire in a sequential loop indefinitely. Axon 2 is the yellow trace, Axon 3 is green, and Axon 4 is orange. The Axon connection (pre-synaptic $\rightarrow$ post-synaptic) is $1 \rightarrow 2 \rightarrow 3 \rightarrow 4 \rightarrow 1$. The Axon parameters are all identical, all Axons are held at rest with CLVCs, and all have a trigger at $V_T = 0\,mV$ that switches V_C from $V_C^{(1)} = -150\,mV$ to $V_C^{(2)} = -1\,V$ for $400\,ms$. The Axon parameters are the same as Figure 6.8, except for the synapse resistance $R_s = 300\,M\Omega$. All synapses are identical and excitatory.

The oscillator in Fig. 6.9 is achieved with four Axons, and this is likely the minimum

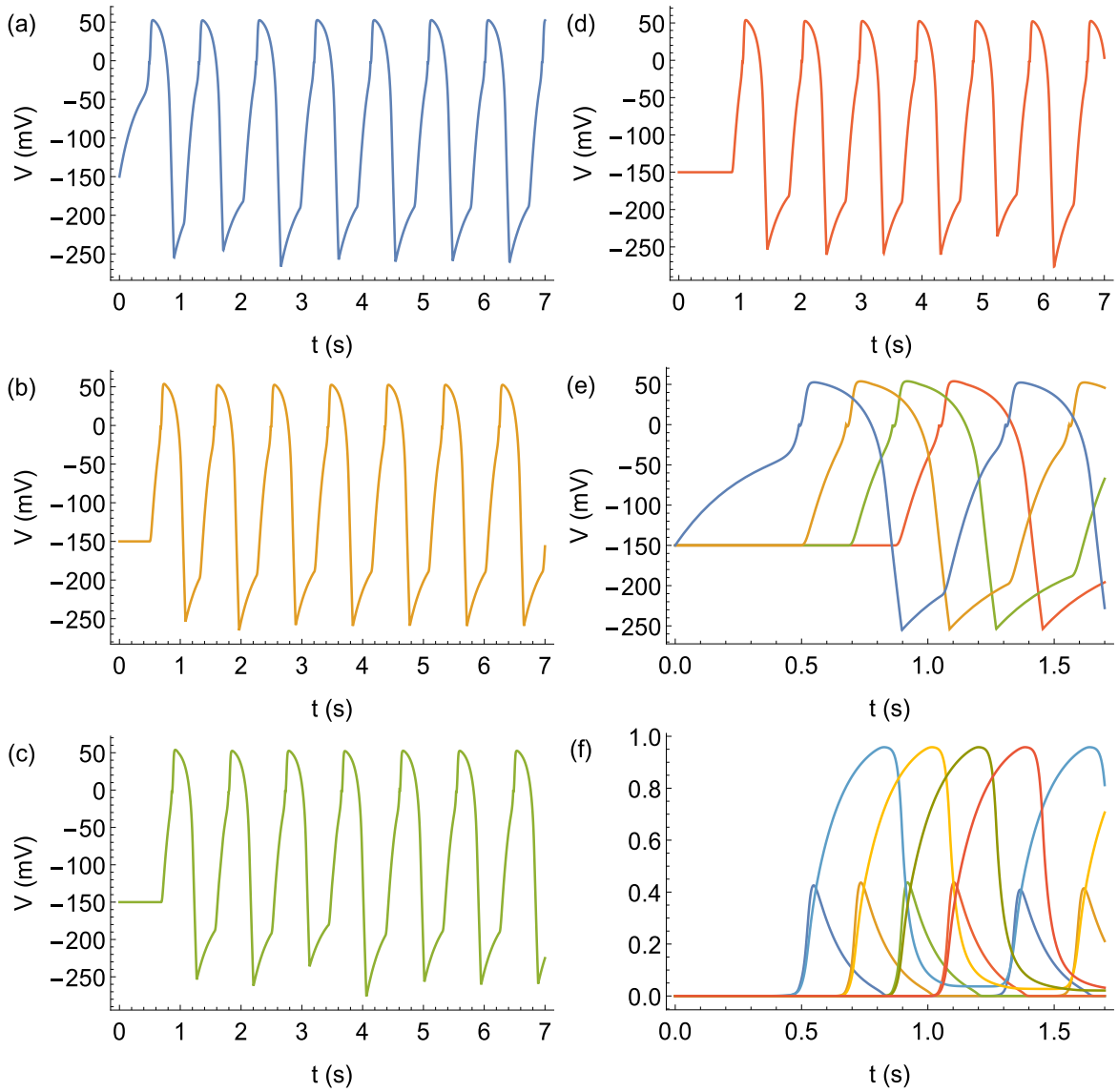

Figure 6.9: Oscillator with four Axons and 4 excitatory synapses. Axon 1 is the blue trace, Axon 2 is yellow, Axon 3 is green and Axon 4 is orange. The Axons are connected (pre-synapse $\rightarrow$ post-synapse) in a loop as $1 \rightarrow 2 \rightarrow 3 \rightarrow 4 \rightarrow 1$. A $70\,pA$, $500\,ms$ pulse is applied to Axon 1. Consequently, all Axons fire consecutively and indefinitely. When an Axon fires, a trigger pulls the potential down to a large negative value for channel recovery from inactivation. (d) displays only the first few spikes. In (e), a dark-colored trace corresponds to p_o for an Axon of the same color, and the lighter-colored trace is the inactivation for the same Axon. All channel and electrophysiological parameters are identical to Fig. 6.8, with exception to $R_s = 300\,M\Omega$.

number to produce an oscillator. Rather, four nodes (section 6.5.1.2) is likely the minimum to produce an oscillator. An oscillator cannot be produced with two Axons and the present synapse design because of the overlap in polarization between two connected Axons. In Fig. 6.9 (b), when a post-synaptic Axon spikes, for some small time the pre-synaptic Axon's potential is above $0\,mV$ simultaneously with the post-synaptic Axon. While conditions may be found that minimize this overlap, the post-synaptic Axon potential will still remain high while the pre-synaptic Axon is being pulled low to recover channels from inactivation. If these two Axons are connected directly to one another, neither Axon will allow the other's potential to be pulled low for inactivation recovery, and the Axons will not oscillate. The reason is because the present synapse injects current only when the pre-synaptic Axon is firing. To produce an oscillator with two Axons will require a new synapse design, where the peak output persists for some time after the pre-synaptic spike ends. The aim is a separation in time between the pre and post Axon spikes sufficient to allow channels in both Axons to recover from inactivation. An oscillator with three Axons is also likely not possible. The first Axon to spike must experience a large $V_C^{(2)}$ to recover channels from inactivation in time for the third spike. However, it would be difficult – and has been impossible in brute force simulations – for the synapse to inject sufficient current in Axon 1 to induce a new spike. This problem is specific to the ion channel KvAP and its requisite large negative potentials for recovery from inactivation. Another channel that recovers at a faster rate or a smaller negative potential may yield a three-Axon oscillator.

I note, however, that an experimental attempt to produce an oscillator with two or three Axons is still a worthwhile endeavor in spite of these simulations. Experiments in the work presented in past chapters have informed and improved the model through new channel parameters in the fits of new measurements. In work toward an oscillator with two Axons, we may uncover a new behavior by the KvAP in the Artificial Axon.

Increasing the number of Axons allows for an oscillator with no trigger nor need for active de-polarization of the membranes. Figure 6.10 is a simulation with six Axons and no trigger. With six Axons there is sufficient time between pre-synaptic inputs for the Axons to recover from inactivation. The connections and Axon positions are identical to Fig. 6.9 with a few

additions and one resistor value change. Axons 1 through 4 are same colors, and Axon 5 is added in purple and Axon 6 is brown. Axons 1 and 4 are disconnected, and Axons 5-6 are added to the end of the loop such that the new end-connections are $\rightarrow 5 \rightarrow 6 \rightarrow 1$. The resistor $R_s = 400\,M\Omega$.

The software triggers may be eliminated, and the number of Axons required reduced to 4, if we introduce inhibitory input synapses to the oscillator. Figure 6.11 is such an oscillator. The Axons provide excitatory input via the connection scheme $1 \rightarrow 2 \rightarrow 3 \rightarrow 4 \rightarrow 1 \rightarrow$, and inhibitory input by $4 \rightarrow 3 \rightarrow 2 \rightarrow 1$, and the Axons in the oscillator fire indefinitely with no aid from triggers. The connection scheme is shown above (a), where (+) and (-) correspond to excitatory and inhibitory input, respectively. The colors assigned to each Axon are identical to Fig. 6.9, as is the small pulse delivered to Axon 1 at $t = 0$. The parameters for Fig. 6.11 and Fig. 6.10 are identical; the only differences are the trigger and the inhibitory connections.

6.5.2 Future work

There are two immediate hardware directions that would improve the flexibility of the present synapse in accounting for differences between pre and post-synaptic Axon preparations that are detrimental to an experiment's success. First, the ability to adjust the voltage at which the switch becomes active. At present, the synapse switches at pre-synaptic potential $0\,mV$. In this synapse hardware, adjustment to the synapse switching voltage is a matter of changing the reference connection in the saturation op-amp. In Fig. 6.1, the saturation op-amp is referenced to ground, thus making the synapse switching voltage $0\,mV$. The reference point can be made adjustable by connecting the op-amp to an external voltage source or a DAQ instead of ground. The second hardware direction: expansion in the width of synapse input. It is mentioned in subsection 6.5.1.3 above that oscillators with two or three Axons may not be possible because of the overlap between pre and post synaptic spikes. This is a consequence of synapse design, whereby the synapse injects current only while the pre-synaptic Axon is spiking. The ability to expand synapse input in time, beyond the falling

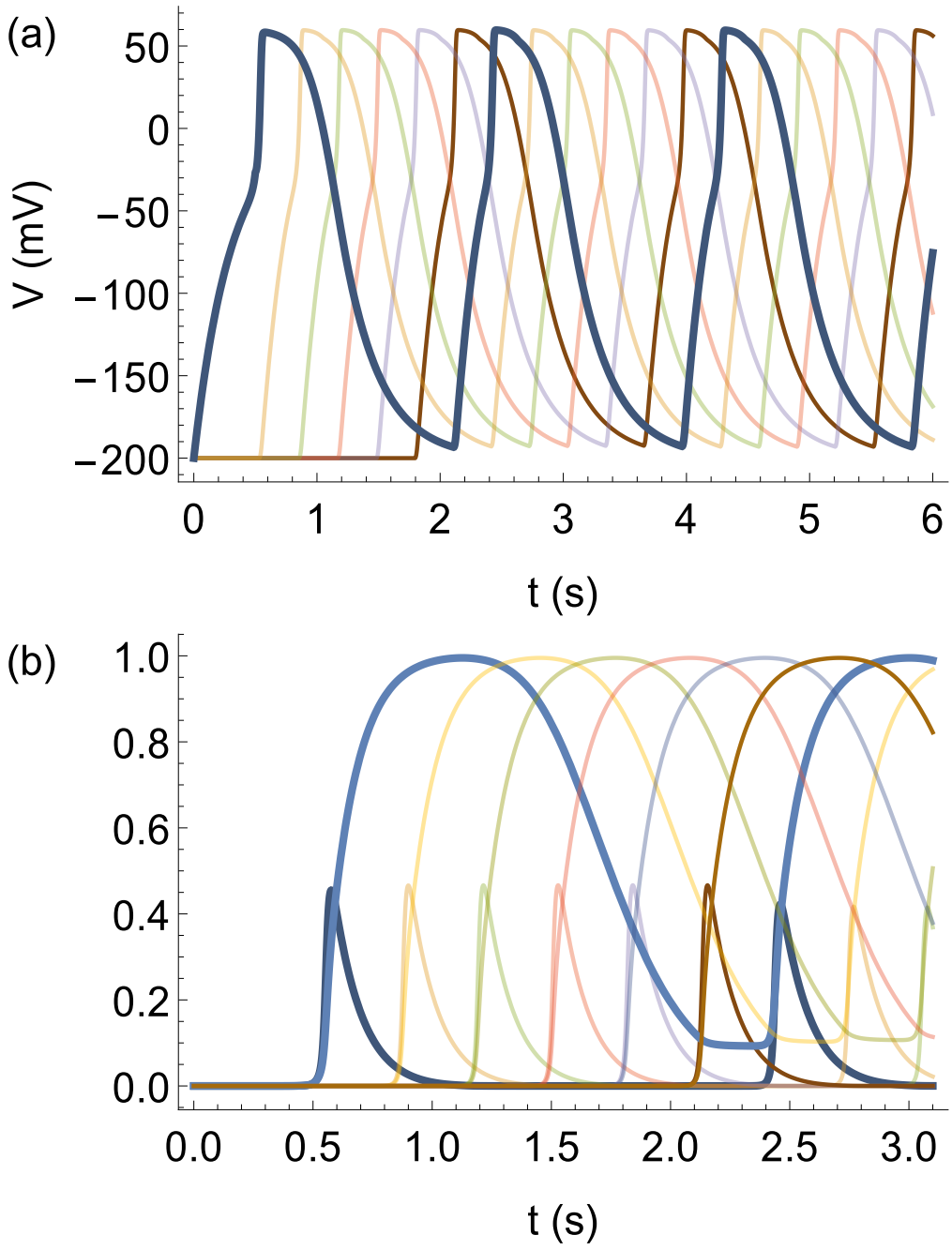

Figure 6.10: Oscillator with six Axons and no triggers. The thick blue trace is Axon 1, and the others in the background are Axons 2 (yellow), 3 (green), 4 (orange), 4 (purple) and 5 (brown). The Axon connection loop goes $1 \to 2 \to 3 \to 4 \to 5 \to 6 \to 1$. Axon 1 is stimulated to fire with a $100\,pA$, $500\,ms$ pulse, and the Axons fire sequentially and indefinitely. The channel and electrophysiological constants are identical to each other at to Fig. 6.9, but the synapse resistor value here is $R_s = 400\,M\Omega$.

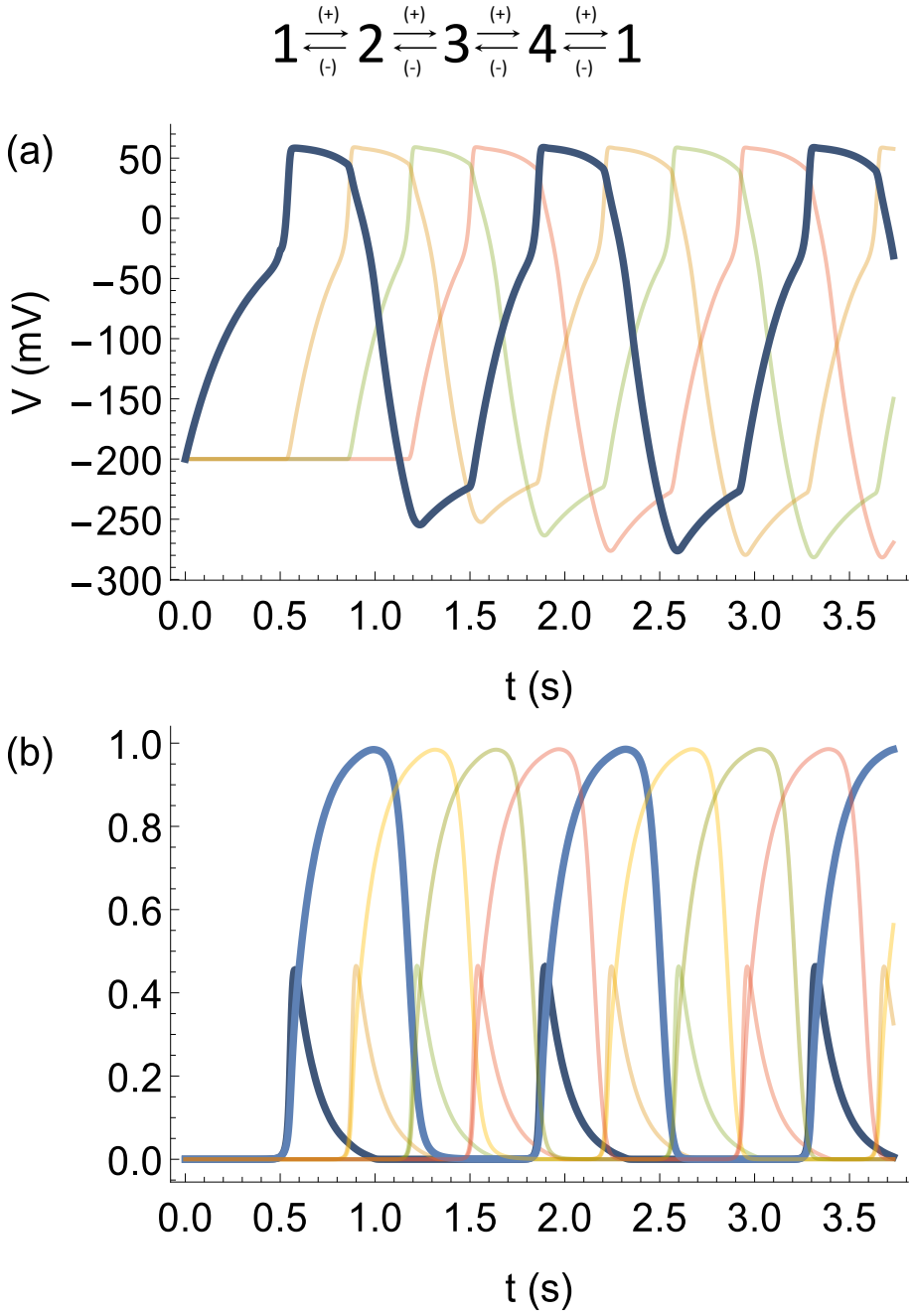

Figure 6.11: Four Axons connected by inhibitory and excitatory input to produce an oscillator. The connection scheme is shown above (a), where (+) corresponds to excitatory input and (-) corresponds to inhibitory input. In this connection scheme, the Axons fire indefinitely with no trigger. A small pulse is applied to the first Axon, after which there is no intervention in the circuit. The Axon color scheme and excitatory pulse in this figure are identical to Fig. 6.11, and the parameters for this figure are identical to Fig. 6.10 (with exception in the inhibitory synapses).

edge of the pre-synaptic spike, would minimize the number of required Axons to produce an oscillator and add an element of timing control in a future network.

As mentioned at the end of chapter 3, we aim to move away from electronics toward a chemical and biological synapse. How an action potential at the axon terminal translates to neurotransmitter release is an active area of study [DF03, UL05, BH16]. And while our solution may involve neurotransmitter vesicles and SNARE proteins to resemble the machinery of a real neuron, our synapse solution may be in a direction that does not resemble a real synapse.

CHAPTER 7

Navigation

In the preceding chapters, I have shown that the Artificial Axon is a computational unit with properties of the neuron. I have shown that the Axon is a threshold detector and a logic gate. I have shown that the Axon can maintain an input-dependent firing rate, which is essential in neuron communication and computation in downstream neurons. Now I show that a simple network of Artificial Axons is capable of performing a task. Namely, I use two Artificial Axons to steer an RC car toward a light source.

In this chapter, I describe the protocols, algorithms and hardware developed to achieve this navigation task. I discuss the noise and biases in the trajectory of the car, and I explain the mechanism responsible for successful navigation. I end with the model and a simulation of the navigating car, and I discuss the complexity that arises from this simple network.

7.1 Overview of the electronic system

Two Artificial Axons navigate an RC vehicle to a light source. Photodiodes mounted on the car receive light from the source. The photodiode sends its voltage output to the AA for processing, essentially functioning as the "eyes" of the car. Figure 7.1 shows a diagram of the system. The AAs sit on an optical table in the lab; communication with the car is by radio waves. The remote control car is modified with two sets of photodiodes ("eyes") accepting light from the right (R) and left (L) side of the car, respectively, and corresponding voltage-to-frequency converters (VFCs) and transmitters. Following for example the signal from the R photodiode, its voltage output is converted to frequency (in the kHz range) by the VFC and transmitted; this signal is received by a receiver on the optical table converted to voltage

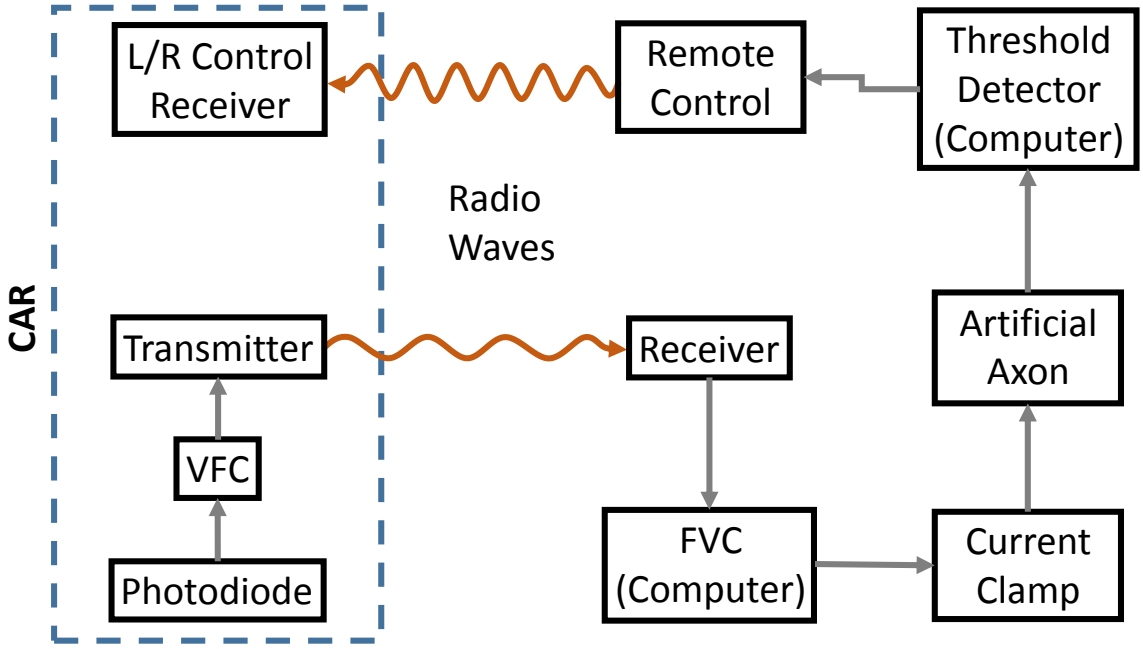

Figure 7.1: System block diagram. The complete system consists of two such circuits, one for the right (R) photodiodes and AA and one for the left (L) components. VFC: voltage to frequency converter; FVC: frequency to voltage converter.

by another VFC, and used as the input to a current clamp, or "synapse", which injects a proportional current (in the tens of pA range) into the right (R) axon. Action potentials in the AA trigger a threshold detector which inputs into the remote control module of the car the signal to turn the wheels to the right. We use the actual remote control of the toy car, and so the same receiver and right/left control built into the car. A similar but independent pathway conditions the signal from the left photodiode set. In summary, this system realizes a very simple analogue control protocol: each time the R axon spikes, the wheels of the car are turned to the right and stay there until the next signal comes in, and similarly for the L axon, which turns the wheels to the left. Action potentials in the R/L axon are induced by the light intensity falling onto the R/L photodiode set. So while all the peripheral systems are, at the moment, electronic, the "decision making algorithm" is implemented by ionics.

There is no interaction between the two AAs in this realization, and the only property of the AA which we really exploit is the "integrate-and-fire" dynamics. The system has a degree of stochasticity (due to the relatively small number of ion channels in the axons), lots

of noise which is not only thermal in origin, makes many mistakes, has many defects, and ends up looking "biological."

7.2 Electronic system components

7.2.1 Photodiode eyes of the car

The Burr-Brown OPT301 integrated photodiode and amplifier is chosen for several reasons. It is low-noise, takes low supply current, has a wide response angle, and has high responsivity. The photodiode's large voltage supply range, between $\pm 2.25\,V$ to $\pm 18\,V$, confers flexibility in connecting this photodiode with smaller supply-voltage components. Furthermore, a larger maximum supply voltage translates to increased resolution in detecting light intensity differences. The built-in amplifier minimizes the common noise problems of discrete designs, it keeps the circuit compact, and is tunable in voltage responsivity by a change the transimpedance resistance R_F. The amplifier's saturation recovery time is $\sim 1\,ms$, negligible compared to the $\sim 100\,ms$ RC and channel-opening timescales of the artificial axon. The photodiode output V_p is used in the simulations at the end of the chapter. A detailed description of the photodiode behavior is provided here. The photodiode voltage output $V_p(r,\phi)$ depends on the distance r from the light source. The output follows the following equation:

$$V_p(r,\phi) \;=\; (V_S - V_b)\left[\Theta[r_0(\phi) - r] + \frac{{r_0}^2(\phi)}{r^2}\Theta[r - r_0(\phi)]\right] + V_b \tag{7.1}$$

V_b is the voltage contribution from background light, and V_S is the saturation voltage, the maximum voltage output by the photodiode amplifier. For the OPT301, the saturation voltage value is the supply voltage. When the output value reaches the saturation voltage, light intensity stops increasing the output value V. The saturation distance $r_0(\phi)$ is measured from the light source and corresponds to the point where V transitions from saturation behavior to $1/r^2$ dependence. This distance r_0 depends on ϕ, the angle of incidence for light rays on the photodiode surface, measured relative to the normal. The voltage output at

$r > r_0$, with $V_b = 0$, follows the ohmic equation

$$V_p \;=\; iR_F = (R_\lambda{}' P') \tag{7.2}$$

R_F is the tunable gain resistance for the amplifier, R'_λ is the responsivity of the photodiode at an arbitrary angle ϕ, and P' is power at the photodiode surface from a light source. The intensity at the photodiode surface is related to the distance r by

$$\frac{P'}{A} \;=\; \frac{P}{\frac{1}{2}4\pi r^2} \tag{7.3}$$

where A is the photodiode area, P is the source power, and the factor $\frac{1}{2}$ accounts for the light over a hemisphere; LEDs on a chip emit light in only one direction. R' expanded has the form

$$R_\lambda{}' \;=\; \frac{R_\lambda \, cos(\phi)}{1 + e^{a(|\phi| - \phi_0)}} \tag{7.4}$$

The constant R_λ is the maximum responsivity at some wavelength, when $\phi = 0$. At small angles, the cosine term is explained geometrically by a reduction in photodiode surface area for incoming photons. At larger angles, the sides of the photodiode package block the light path from source to photodiode surface, sigmoidally reducing responsivity. The sigmoid constants a and ϕ_0 are specific to OPT301, with values $a = 9.7\, rad^{-1}$ and $\phi_0 = 43°$. Combining eqn. (7.2) with (7.2) and $V_b = 0$, the photodiode voltage is written as

$$V_p(r, \phi) \;=\; \frac{A}{2\pi} \frac{R_\lambda \, cos(\phi)}{1 + e^{a(|\phi| - \phi_0)}} \frac{R_F P}{r^2} \tag{7.5}$$

Comparing the constants in eqns 7.5 and 7.1 yields

$$\frac{A}{2\pi} \frac{R_\lambda \, cos(\phi)}{1 + e^{a(|\phi| - \phi_0)}} R_F P \;=\; (V_S - V_b) {r_0}^2 \tag{7.6}$$

Fig. 7.2 shows a measurement of photodiode output with a calculated fit using eqn. 7.6. The source is a $728\, mW, 730\, nm$ LED at incidence angle $\phi = 0$. The photodiode area

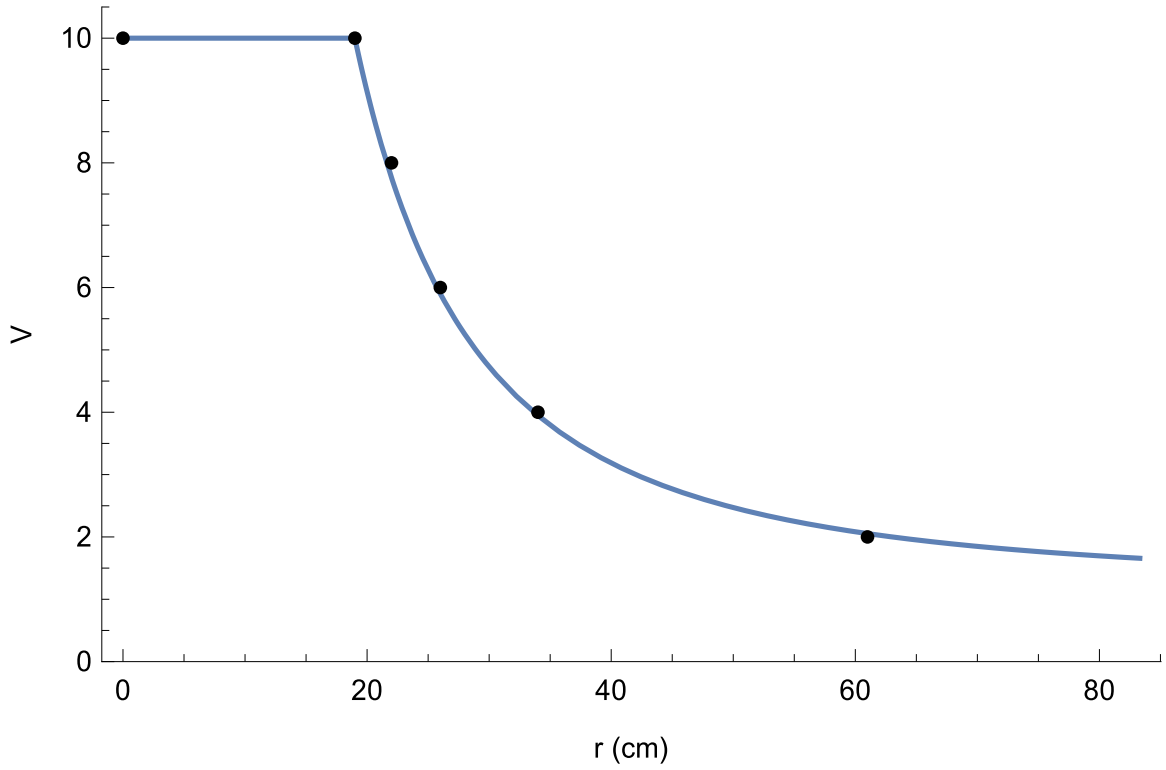

Figure 7.2: Measured photodiode output $V(r, 0)$ with fit. Equations 7.1 and 7.6 fit the output behavior and saturation distance r_0 very well. $V_S = 10\,V$, $V_b = 1.2\,V$, $P = 728\,mW$, $\phi = 0$, $R_F = 1\,M\Omega$, $R_\lambda = 0.52\,A/W$, and $A = 2.29 \times 2.29\,mm$.

is $2.29 \times 2.29\,mm$, its responsivity R_λ at $730\,nm$ is $0.52AW^{-1}$, R_F is the $1\,M\Omega$ built into the amplifier, the supply voltage is $10\,V$ and the background light response is 1.2 V. For $r < 19\,cm$, the photodiode amplifier is saturated and its output is at the supply voltage. At distances $r > 19\,cm$, the output voltage decreases with the intensity of the source as r^{-2} until only the background light contribution remains.

For turn input in one direction, three photodiodes are positioned at 90° relative to each other. This arrangement is shown in Fig. 7.4 for right turns. One photodiode faces the direction of forward motion, another is oriented 180° relative to the first in the backward direction, and the third is perpendicular to the other two, facing outward. The ground pin of one photodiode is connected to the amplifier output of the next. The result is one output voltage from all three photodiodes, equal to the sum of their individual outputs. This summed output is the turn input to one Artificial Axon. With this arrangement of

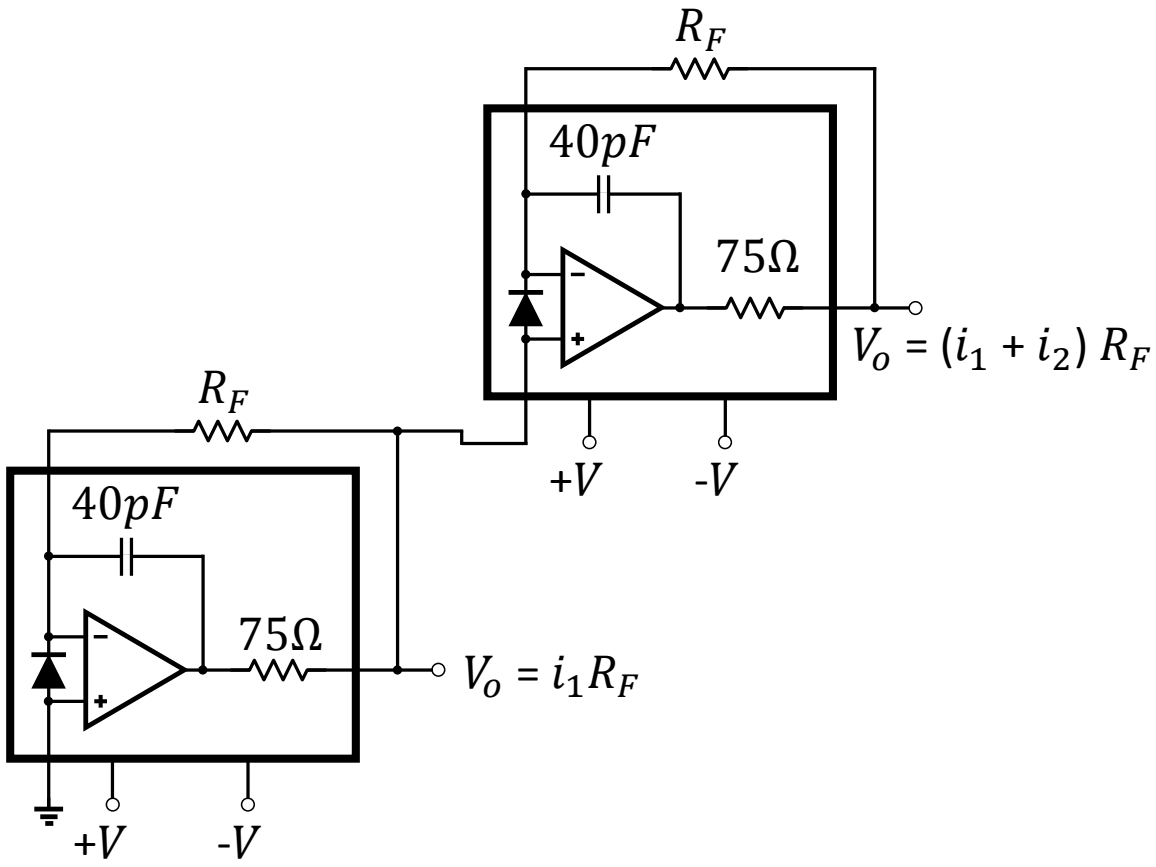

Figure 7.3: Photodiode and amplifier circuits. There are two OPT301 photodiodes in this diagram. The output of the first photodiode is equal to $V_0 = i_1 R_F$, where R_F is external to the photodiode and i_1 is the photodiode current. The output pin of the first photodiode is connected to the ground pin of the next. The output of the second photodiode is the sum of the individual outputs, equal to $V_0 = i_1 R_F + i_2 R_F$. More photodiodes can be added by continuing to connect in this way, from output pin to ground. The final output to be sent to the Artificial Axon is the sum $V_o = \Sigma_n i_n R_F$. In the navigation circuitry specifically, $V\pm = \pm 12\, V$ and $R_F = 44\, M\Omega$.

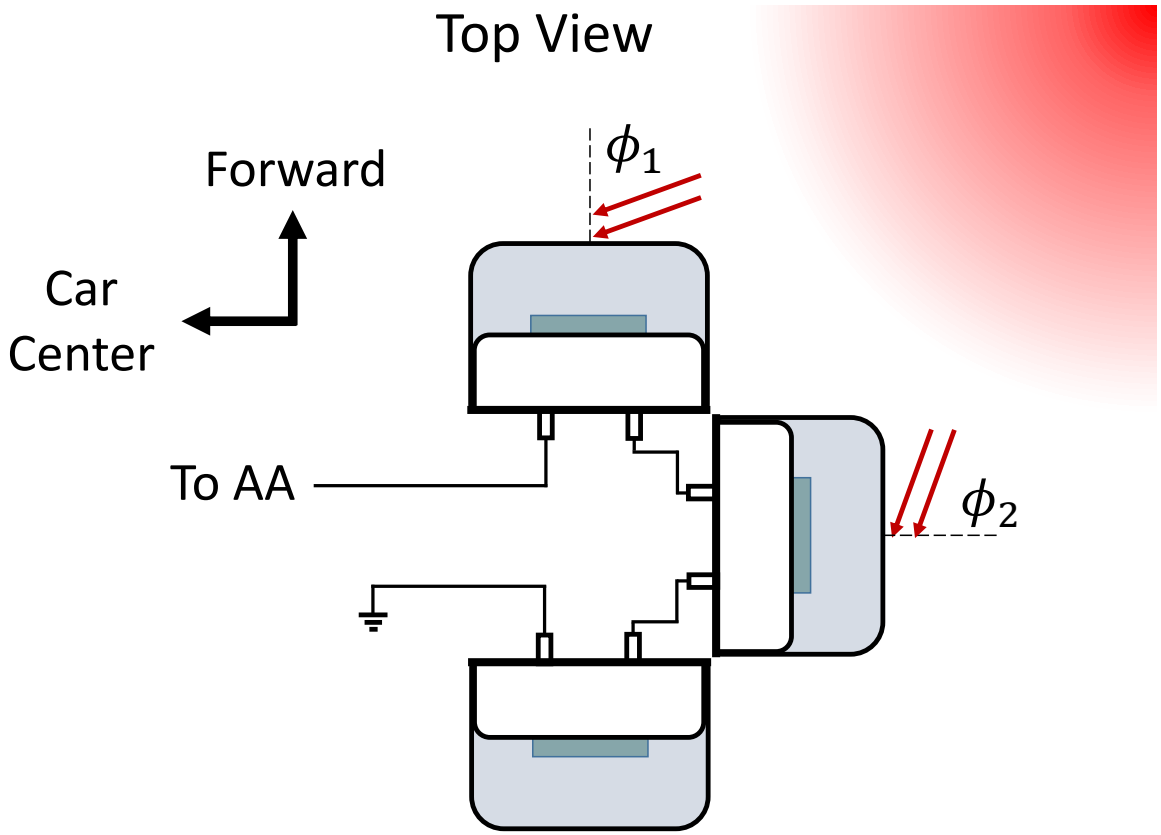

Figure 7.4: Top-view schematic of the photodiode arrangement for right-turns.

photodiodes and connections, if the light source in Fig. 7.4 was to the left of the car, the right photodiodes would output no turning voltage and the car would turn left toward the light source. As another example, if the light source is in the NE direction, the forward and outward-facing photodiodes contribute input to the AA for right turns. The backward-facing photodiode is in the dark and therefore does not contribute to the AA input.

Figure 7.5 demonstrates that three photodiodes is sufficient to maintain a high relative responsivity for a 300° viewing angle. The y-axis represents the r-independent relative responsivity of the 3-photodiode arrangement. On the x-axis, 0° is measured from the outward-facing photodiode at incidence angle 0°. The drops in responsivity between the photodiodes are small if the spacing between photodiodes is small. For more sensitive experiments, photodiodes may be added at positions $\pm\pi/4$. But for the purposes of these experiments, three photodiodes is sufficient.

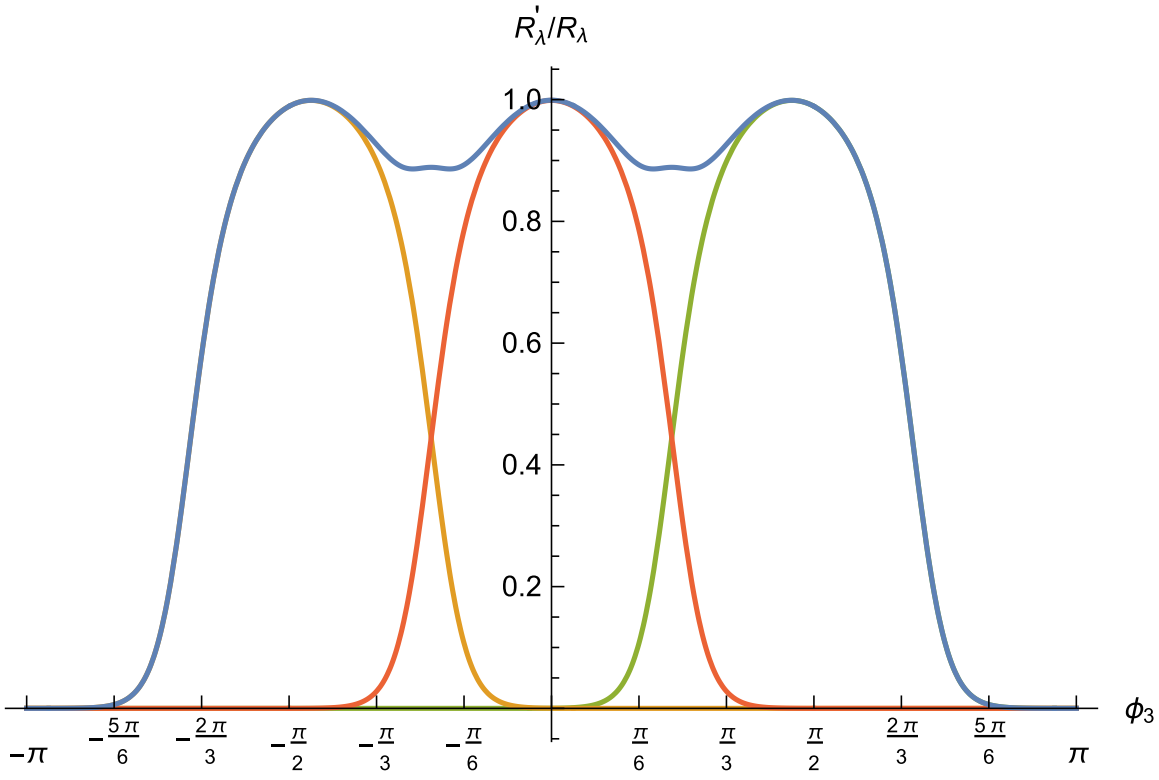

Figure 7.5: Photodiode relative responsivity for turning in one direction. The photodiodes are oriented at 90° from each other, facing forward, backward and outward. The sum of individual outputs combine to produce one input to the artificial axon. This sum is represented by the blue trace, while the yellow, orange and green traces represent individual photodiode outputs. The x-axis angles are referenced from the outward-facing photodiode's incidence angle $\phi = 0°$.

7.2.2 The light source

There are two criteria in choosing an LED light source. The first is lab space, where the navigation task is performed, and the second is photodiode amplifier saturation distance $r_0(\phi)$. The lab space is 4 meters by 4 meters, and the chosen LED must have enough power to give sufficient input to the AA for firing at ~ 5 meters from the photodiode. Although it is not necessary, the chosen saturation distance at normal incidence is the full $r_0(0) \approx 5\,m$. Equation 7.6 is used to select an LED that will satisfy these criteria, taking into consideration the efficiency of LED sources, which are typically at 20%. Specifically, a transimpedance resistance $R_F = 44M\Omega$ is chosen so that the photodiode amplifier saturates at 5 meters from a $625\,nm$, $100\,W$ LED light source. The photodiode responsivity R_λ at $625\,nm$ is 0.45.

7.2.3 Heating and background

Heating and background in the high-wattage LED are minimized with an active heat sink and brightness shields, respectively. Silicone thermal grease is applied to the interface between the LED and a heat sink for improved thermal conduction. Background refers to reflection of light from the floor and walls that adds a constant to the photodiode voltage output and is roughly independent of car orientation. The CLVC competes with this background and membrane leaks to keep the axon at the resting potential, and struggles when leaks alone are large. A brightness shield above the LED lowers background from reflection of the ceiling and walls, and a shield below the LED reduces background from floor reflection. Walls and reflective surfaces are covered with black tarps for background reduction. In total, shielding reduces the background to less than 5% of the photodiode amplifier saturation voltage.

7.2.4 The voltage-to-frequency converter

The Burr-Brown VFC32 voltage-to-frequency converter (VFC) converts the photodiode voltage output to a digital pulse input for the wireless transmitter. The connection diagram for the VFC is shown in Fig. 7.6. The VFC output f_{out} is made linearly proportional to input from the photodiode by choice of R_1. For a full-scale voltage input

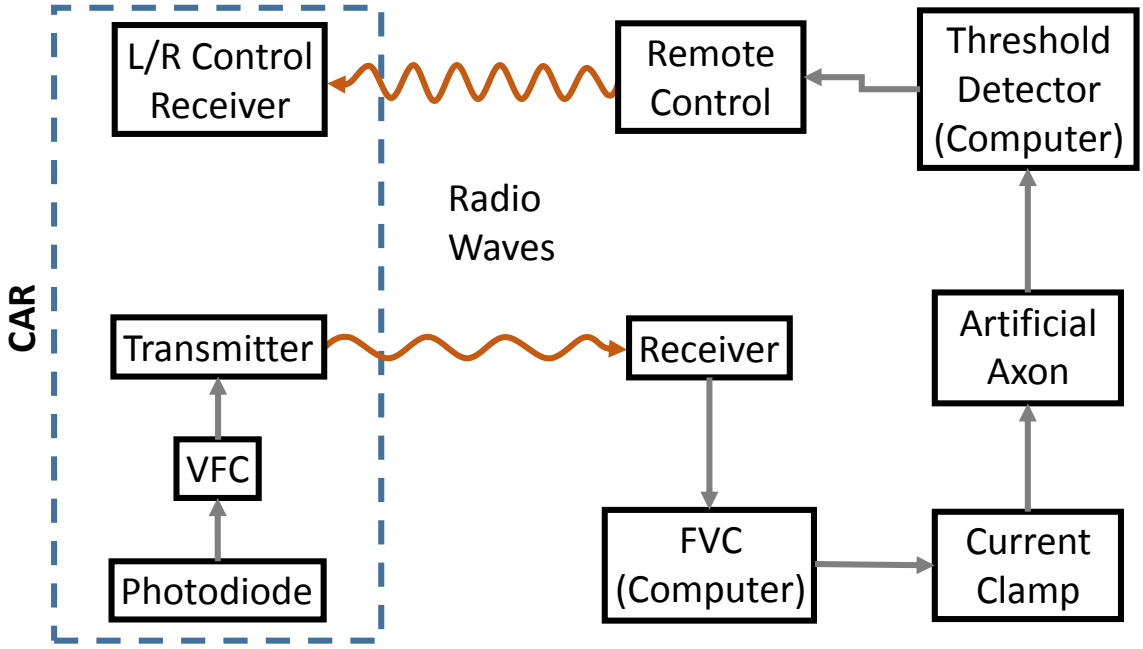

Figure 7.6: Connection diagram for the Burr-Brown VFC32. V_{in} is the photodiode output to be converted to frequency, and f_{out} is the output converted to frequency. An external resistor value $R_1 = 48\,k\Omega$ is chosen to make the VFC frequency linearly proportional to the photodiode output, and an external capacitor value $C_1 = 8\,nF$, is chosen to cap the frequency maximum at $4\,kHz$. The pull-up resistor $R_{pu} = 10k\Omega$, integrating capacitor $C_2 = 22\,nF$, and $\pm V_{CC} = \pm 12\,V$. The pin connection diagram is taken directly from the datasheet for the VFC32, and the external connections in the figure are added manually.

$V_{in} = 12\,V$ and $\pm V_{cc} = \pm 12\,V$, linearity is achieved in the VFC32 with resistor choice $R_1 = 12\,V/0.25\,mA = 48\,k\Omega$. Capacitor C_1 determines the maximum frequency output. The relationship between f_{out} and C_1 in the VFC32 is given by

$$f_{out} = \frac{V_{in}}{7.5\,R_1\,C_1} \tag{7.7}$$

Although the VFC32 is capable of frequency outputs up to $500\,kHz$, downstream components struggle with changes in f_out at frequencies above $4\,kHz$; input to the AA drops to zero when the photodiode output is changing. $C_1 = 8\,nF$ caps the frequency at $\sim 4\,kHz$, where changing photodiode output is transmitted to the AA without issue.

7.2.5 Transmitter and receiver

Two separate radio wave transmitters are used for left/right turning, 433 and 315 MHz, one transmitter for each direction. The transmitter takes in digital input from the VFC, and the receiver puts out a 3 V digital signal. Encoder/decoder components typically paired to transmitters/receivers are excluded here because there is no interference between transmitters, and there is no interference from other devices in the lab where the navigation demonstration is performed. Furthermore, these simple receivers struggle with transmitted data frequencies above 17 kHz, but encoder oscillator frequencies must be larger than this to transmit VFC input in the kHz range.

7.2.6 Frequency-to-voltage conversion

Unlike voltage-to-frequency, the frequency-to-voltage conversion is done by software. While the VFC32 can convert frequency to voltage, the wireless receiver outputs a frequency duty cycle that is different from the VFC. To correct for the mismatch by hardware is unnecessarily complicated. Therefore, the frequency to voltage conversion is instead done by computer using LabVIEW. The program converts frequency to voltage, which is then fed to the input of the current clamp which forms the "synapse" injecting into the AA. The command voltage to the clamp is thus $V_{CC} = \alpha f$, where f is the receiver frequency and α is a proportionality constant. There are two independent circuits for the right and left axons. The constant is chosen so that it matches the electrophysiology characteristics of the corresponding axon (mainly dependent on leak current, Nernst potential, number of channels) and is therefore different between axons. The receiver output becomes noisy at frequencies near zero, so an added filter is written into LabVIEW to filter out this frequency noise. LabVIEW interprets this noise as large frequencies as high as 15 kHz. The filter removes frequencies higher than 3900 Hz, before the voltage conversion.

7.2.7 The vehicle

The GPTOYS model S911 was selected for two reasons. First, for its power. The S911 can carry the photodiode electronics and its mounting components at controlled speeds. Second, the S911 was selected for its speed in turning. In one turn, the S911 makes a full swing from one direction to the other in $\sim 300\,ms$. This is sufficiently fast for navigation, given that one period between two AA spikes is on the order of $\sim 1\,s$.

From the manufacturer, left/right movement on the model S911 car's remote is controlled by a $5\,k\Omega$ potentiometer configured as a voltage divider. For computer software control of left/right turning, the potentiometer is physically removed, and the car remote is connected to a National Instruments NI USB-6008 data acquisition device (DAQ). Analog turn signals are given to the car remote by LabVIEW through the DAQ, in place of the potentiometer. The negative terminal of the remote's battery is connected to the DAQ's ground channel, and turn voltages are supplied by the DAQ to the remote's "signal" pin in the voltage divider circuit.

The smallest-radius left turn corresponds to a $0\,V$ signal with respect to ground. The smallest-radius right turn corresponds to $3\,V$, and forward directed wheel orientation corresponds to $1.5\,V$. Signal values between $0\,V$ and $3\,V$ correspond to larger turn radii that decrease linearly as the signal moves away from $1.5\,V$ in either direction. When an axon's membrane potential exceeds the set trigger voltage, LabVIEW sends an analog voltage signal to the car remote to make a smallest-radius turn in the direction of the axon that fired. The analog turn signal persists until LabVIEW detects a voltage signal (from the other axon) to turn in the opposite direction.

From the manufacturer, forward motion of the car is also controlled by a $5\,k\Omega$ potentiometer configured as a voltage divider in the car remote. The stop position corresponds to a $3\,V$ signal, and maximum speed corresponds to a $0\,V$ signal. In the remote's circuit protocols for forward motion, the applied signal must be at $3\,V$ when the remote is turned on. The car begins to move at $150\,mV$ below $3\,V$, i.e. $2.85\,V$. We slow down the car for compatibility with the slow ($\sim 1\,Hz$) firing rate of the axons. Two modifications are introduced.

First, a LabVIEW function generator supplies square pulses with amplitude $\sim 150\,mV$ and period $500\,ms$ for forward motion, with an offset chosen so that the maximum voltage is $3\,V$. Second, four $50\,W$ resistors are connected in parallel to the car's motor to reduce the motor's current. This is a high-current RC motor, so the power resistors are necessary. These modifications bring the car's speed down to $20 - 30\,cm/s$.

7.3 Navigation with two Artificial Axons

7.3.1 The electrophysiological parameters

For the navigation run, the axon parameters were set/measured as follows. Left axon: at maximum photodiode output, the current clamp injects ${I_{CC}}^{max} = 74\,pA$ into the axon; the number of open channels at peak voltage is approximately $N = 380$; the membrane capacitance is $C = 190\,pF$. Right axon: ${I_{CC}}^{max} = 64\,pA$, $N = 720$, and $C = 190\,pF$.

The CLVC protocol during firing (V_C, Fig. 7.7) is incidental to the particular inactivation dynamics of the KvAP. Channels will completely inactivate if the membrane potential is not pulled down to a large negative value after firing. The channel recovery rate from inactivation has a sigmoidal dependence on the membrane voltage, with the turning point at about $-100\,mV$. Pulling the membrane voltage down to $\sim -100\,mV$ is typically sufficient to maintain firing. For this navigation run, the following settings were used. For the left axon: when the membrane voltage reaches the trigger value $V_T = 4.5mV$, the command voltage to the CLVC changes from $V_C(1) = -127\,mV$ to $V_C(2) = -455\,mV$ for $t_T = 1.3\,s$, pulling the membrane voltage to a large negative value. For the right axon: $V_T = 0\,mV$, $V_C(1) = -145\,mV$, $V_C(2) = -364\,mV$, $t_T = 1.0\,s$.

The clamp value $V_C(2)$ is chosen with a big safety margin to address the fact that sometimes the leak conductance of the AA changes in the course of a run. For example, you can see in Figure 7.7(a), looking at the negative swings of the spikes, that the envelope of the spikes is roughly constant (at $\sim -280\,mV$) for $0 < t < 80\,s$, then increases for $80 < t < 100\,s$, then stabilizes again (at $\sim -120\,mV$) for $t > 100\,s$. This increase is caused by an increase in

leak conductance of the axon, from $\sim (83\,G\Omega)^{-1}$ to $\sim (2.4\,G\Omega)^{-1}$, approximately. However, even with the increased leak, the same CLVC protocol is able to pull the resting voltage down below $-100\,mV$, allowing the channels to recover from inactivation and so be able to fire repeatedly. Similarly, you see that in the right axon (Fig. 7.7(b) the leak conductance increases and then decreases again for $20 < t < 50\,s$. The origin of these slow fluctuations in leak conductance is presumably that the interface between lipid bilayer and solid support is not as stable as one would wish, in the present system. Similar fluctuations in leak conductance are observed even in the absence of channels, so this is a membrane phenomenon. In the present system, a membrane with channels lasts typically 10 min before it breaks; exceptionally we have lifetimes of 1 hour. Without channels, a membrane lasts typically 1 hr. Thus there is need to significantly improve the stability of the system if it is to be scaled up even modestly.

7.3.2 A Navigation result

The car moves in a (previously decluttered) laboratory room of about $5 \times 5\,m^2$; in the navigation run, the light source is in the SW corner of the screen, and the car starts at the NE corner, facing W. The other bright spots on the screen are reflections of the light source from objects at the periphery of the room. Figure 7.8 is a picture of the room seen from the ceiling.

The car's speed is slowed down to match it to the rather slow axons, so the car moves in adopted short, regular spurts of forward motion. The actual average speed of the car is however not constant because at times the tires slip on the polished floor. From an engineering standpoint, this circumstance is seen as simply one of many "defects" or sources of noise in the system. There are many such sources of randomness, from the microscopic scale of the individual ion channels in the AA to the macroscopic scale of the tires. As a result, the trajectory of the car, the "behavior", is not deterministic (starting from identical initial conditions, different realizations of the car's trajectory will be different); however, the car does find the light source in the end. Figure 7.9 shows the trajectory corresponding to

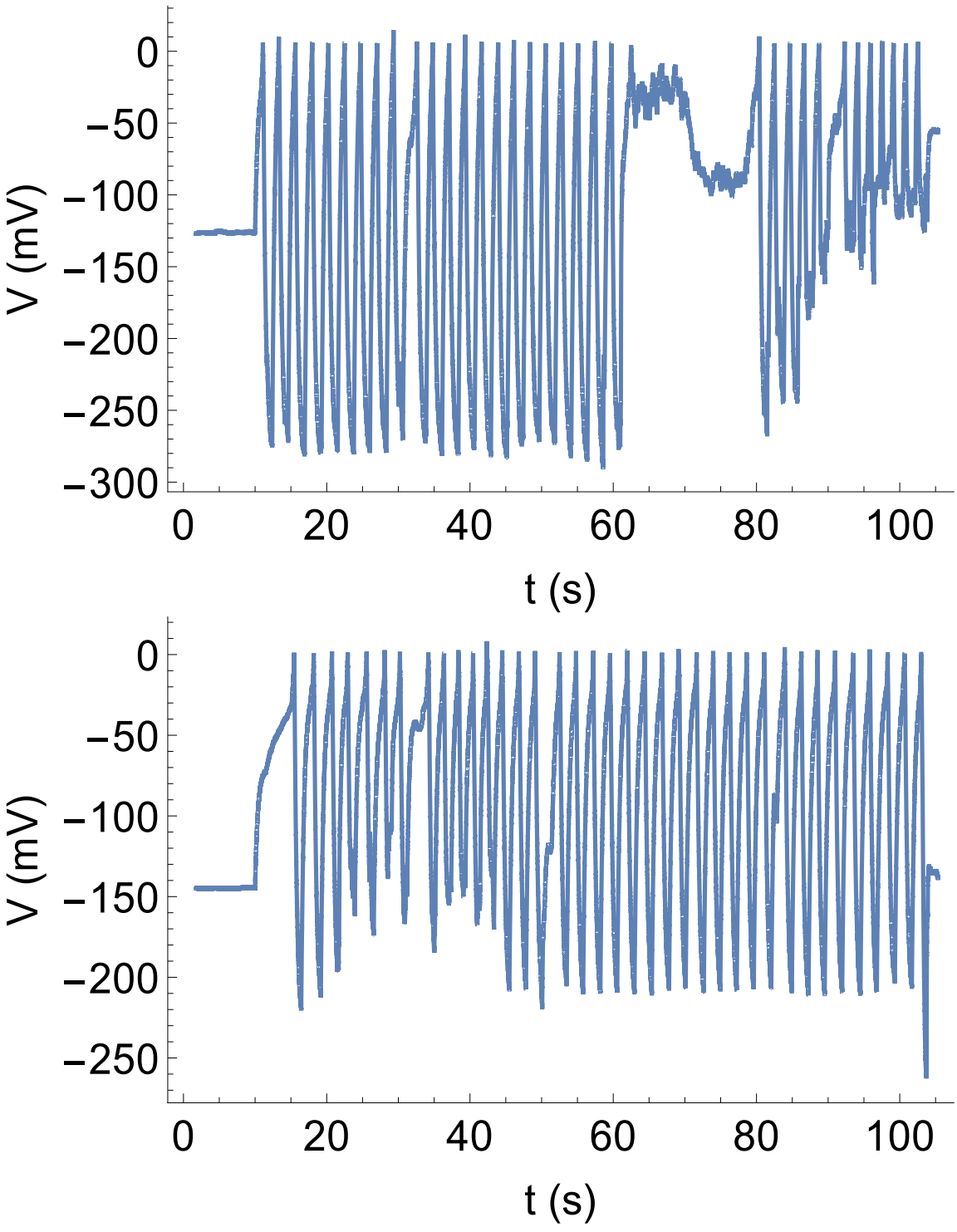

Figure 7.7: Whole time series of action potentials corresponding to the navigation run. Time $t = 0\,s$ corresponds to the start of the video. The data recording begins 1.75 seconds later. (a) Left axon; (b) right axon.

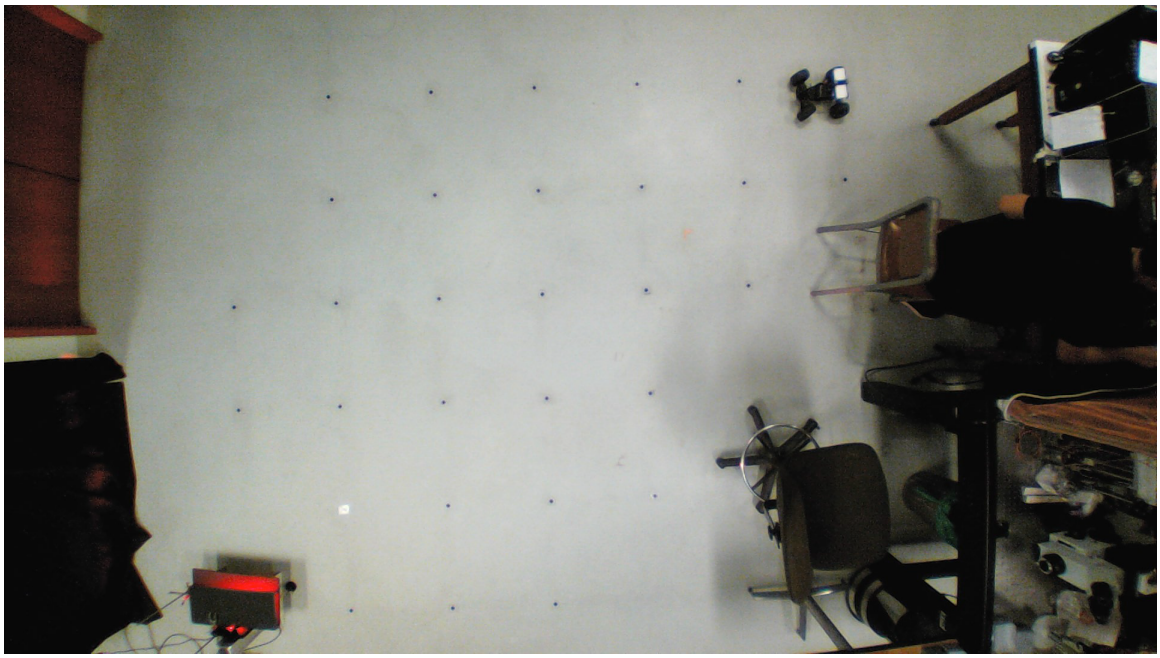

Figure 7.8: Still of the room of the room of the demo, seen from the ceiling. The car and light source are at diametrically opposite corners. Visible on the right is the optical table with the artificial axons and the electronics, as well as H.G.V.

the navigation run.

The very simple "machine language" with which the system operates is as follows. Figure 7.10(a) shows action potentials in the two AAs over a time of $10\,s$; the blue trace is the membrane potential of the left AA, the yellow trace is the right AA. The response of the car is that when the blue trace crosses $4.5\,mV$ from below, the wheels turn left and stay there until further notice; similarly, when the yellow trace crosses $0\,mV$, the wheels turn right and stay there. What decides, then, whether overall the car is turning L or R is the relative phase of the spikes in the two AAs. In the example shown, for $45 < t < 50.5\,s$ the car is, overall, turning R because the time interval between a yellow and the next blue zero crossing is larger than the time between a blue and the next yellow. On the other hand, for $50.6 < t < 56\,s$ the car is overall turning L; this is a consequence of the R photodiodes seeing less light for $50 < t < 52\,s$ Fig. 7.10, which causes a delay in the yellow spikes, changing the phase relation between blue and yellow spikes. Even with identical stimuli (input currents from the "synapses"), the firing rates of the two AAs are not the same (due to physical

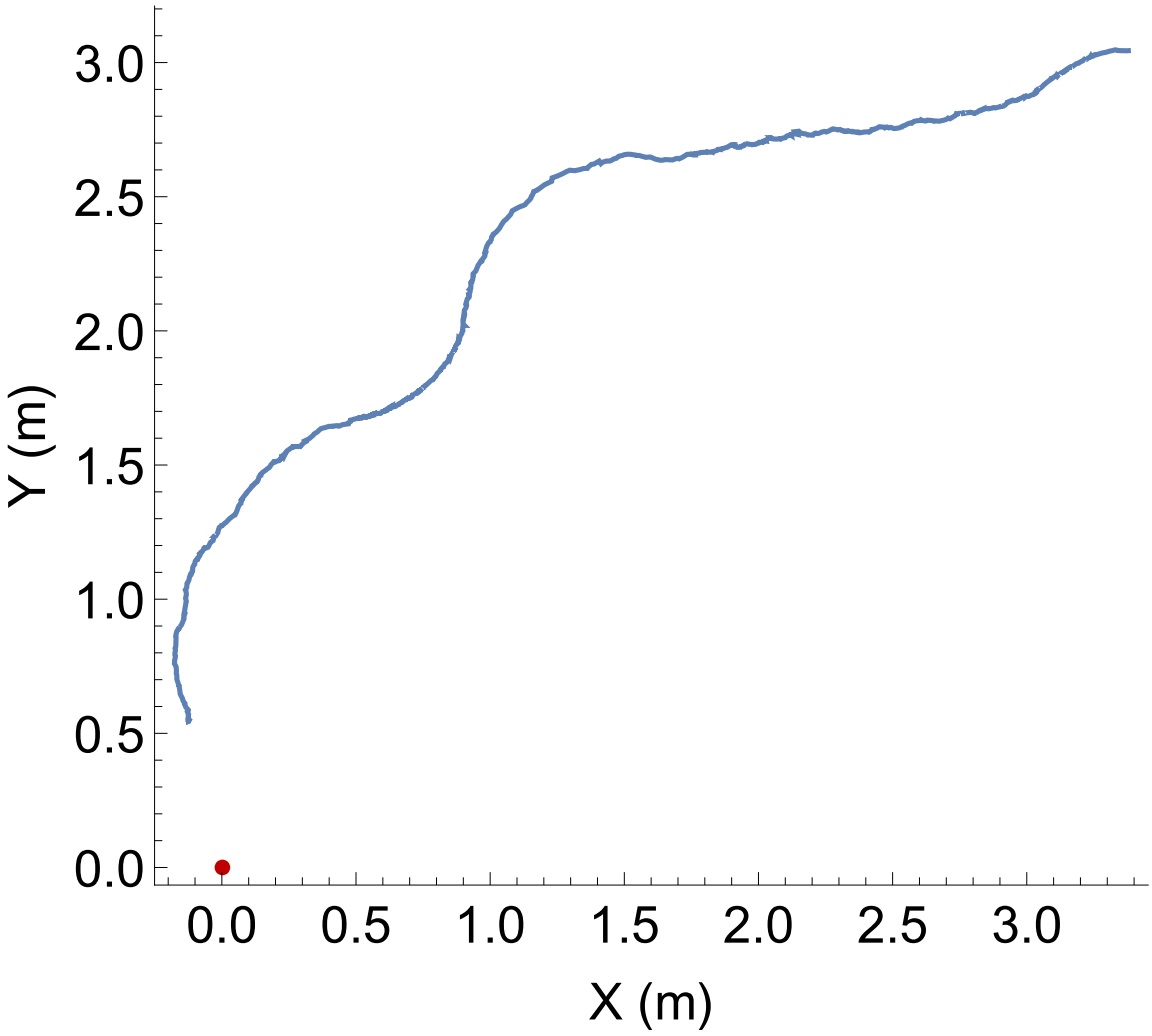

Figure 7.9: Car trajectory corresponding to the navigation run. The light source is at the origin; the scales on the axes are in m, and the car starts at $(x, y) = (3.4, 3.0)$.

differences between the AAs, for instance, different number of ion channels, different leak currents, etc.). This circumstance introduces "phase noise", yet another source of (non-thermal) stochasticity which however does not prevent the overall working of the system. That is, the two AAs do not need to be perfectly tuned as far as firing rates.

Figure 7.10 shows, for the same run as in part (a), the frequency coming out of the voltage to frequency converter, for the L (blue) and R (yellow) circuit. The current injected by the corresponding "synapse" into the L / R axon is proportional to this frequency. While the firing rates of the two AAs do not need to be perfectly tuned, if, for equal light, one firing rate is larger than the other, this introduces a bias in the approach to the light source. In the realization shown in Figure 7.9, the right AA had a faster firing rate, and a right turn bias is visible in the trajectory.

7.4 Discussion

7.4.1 Model

One axon receives input from a current clamp and a CLVC. The current clamp receives input from the photodiode "eyes," thus serving the function of the synapse in biological neurons. The membrane equation is as follows:

$$C\frac{dV}{dt} = N_0(p_O\,\chi + \chi_\ell)[V_N - V(t)] + \frac{1}{R_C}[V_{CLVC} - V(t)] + \frac{1}{R_{CC}}V_{CC}(t) \qquad (7.8)$$

The open probability p_O and CLVC trigger are modeled and described in previous chapters. The voltage V_{CC} provides the input for navigation, and thus its dependencies are described here. The V_{CC} term is expanded and expressed as a function of both the photodiode/light source distance and the angle of incidence for light on the photodiode surface. Some notation is needed to describe the contributions to V_{CC}: $i = \{R, L\}$, $j = \{1, 2, 3\}$ and $k = \{+1, -1\}$. j indetifies the photodiode. $k = +1$ is associated with left turns, and $k = -1$ is associated with right turns. Therfore, $k = +1$ when $i = R$, and $k = -1$ when $i = L$.

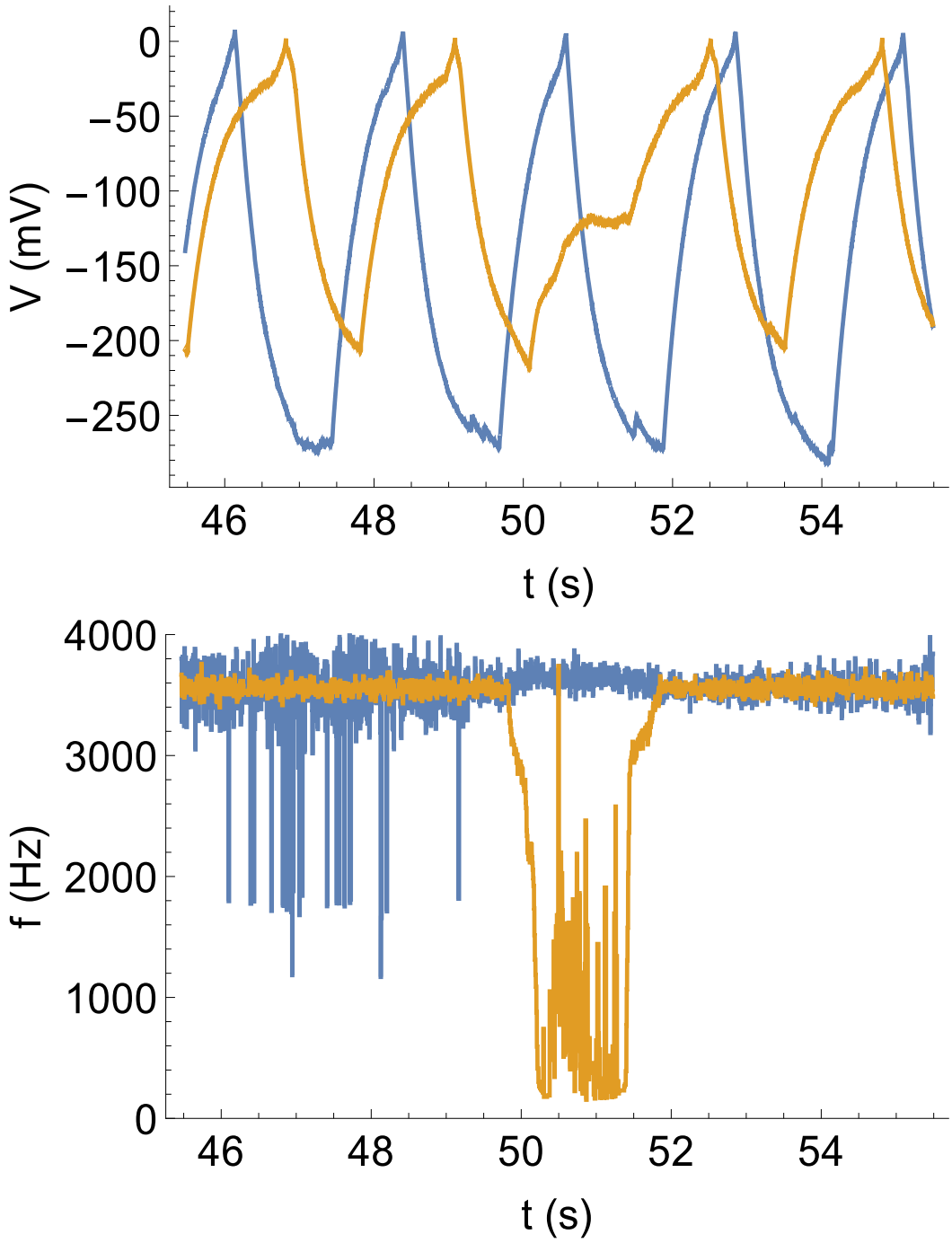

Figure 7.10: (a) Membrane potential in the Left artificial axon (blue trace) and the Right AA (yellow trace) for part of the navigation run. (b) The signal at the output of the voltage to frequency converter (VFC), for the R and L circuits, and the same time interval as in (a). The currents injected by the synapses into the respective AAs are proportional to these signals.

The current clamp injects current $I_{CC} = (R_{CC})^{-1} V_{CC}$ into the axon, where

$$V_{CC}{}^{(i)} \;=\; c \sum_{i=1}^{3} V_p{}^{(ij)} \tag{7.9}$$

The variable c is a scaling constant that moves the voltage to a range that will produce picoAmp current output by the current clamp. $V_p{}^{(ij)}$ is the photodiode output voltage described by eqn. 7.1 for the j^{th} photodiode on side i of the car. Equation 7.1 for $V_p{}^{(ij)}$ is rewritten with subscripts as:

$$V_p(r_i, \phi_{ij}) \;=\; (V_S - V_b) \left[\Theta[r_0(\phi_{ij}) - r_i] + \frac{r_0^2(\phi_{ij})}{r_i{}^2} \Theta[r_i - r_0(\phi_{ij})] \right] + V_b \tag{7.10}$$

r_i is the distance between the light source and the photodiodes on side i, and ϕ_{ij} is the angle of incidence for light on the j^{th} photodiode on side i. The light source is at the origin. In this model, all j photodiodes for turns in direction i are at the same position r_i. This is an acceptable approximation because the separation between the j photodiodes is $\sim 1\,cm$, negligible compared to the $\sim 5\,m$ distances traveled by the car.

The angle ϕ_{ij} depends on the car's position and orientation with respect to the light source; some vector work is required to express ϕ_{ij} in these terms. Figure 7.11 illustrates the components for finding individual incident angles. The vector $\mathbf{r} = (x, y)$ is measured from the origin to the bisecting point between the left and right photodiodes on the car; in the model, this is treated as the car's position vector. The velocity vector $v = (\dot{x}, \dot{y})$ is perpendicular to $\mathbf{r}$, and the speed is treated as constant. The vector $\mathbf{d}_i$ from the car center to a photodiode depends on the index k: $\mathbf{d}_i = d(k\hat{\mathbf{v}} \times \hat{\mathbf{z}})$. As mentioned above, $k = +1$ when $i = R$, and $k = -1$ when $i = L$. The vector that points directly from the origin to the photodiodes is the sum $\mathbf{r}_i = \mathbf{r} + \mathbf{d}_i$.

The vector $\hat{\mathbf{n}}_{ij}$ is normal to the photodiode surface. This normal vector uses a coordinate system with $\hat{\mathbf{v}}$ as its y-axis and $(\hat{\mathbf{v}} \times \hat{\mathbf{z}})$ as the x-axis for the right photodiodes, and $(\hat{\mathbf{z}} \times \hat{\mathbf{v}})$ as the x-axis for the left photodiode. The normal vector for any photodiode is:

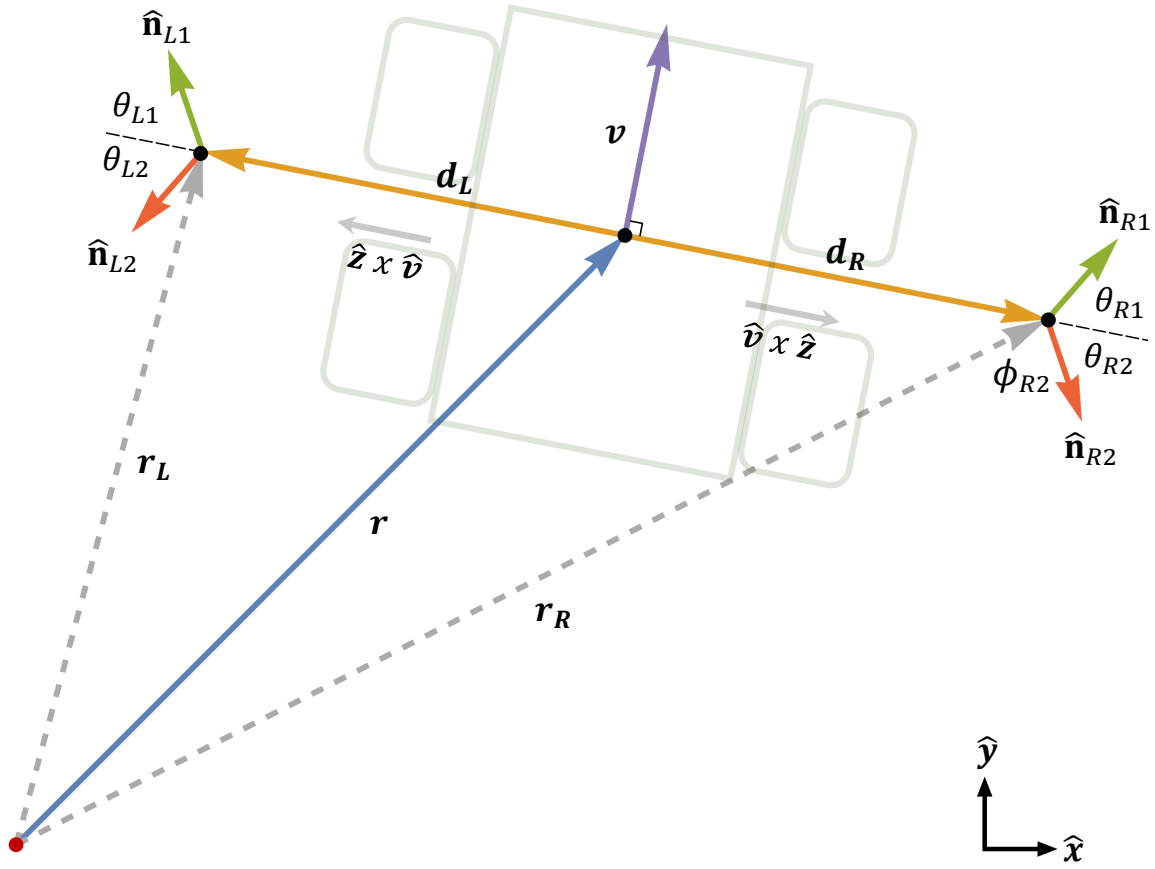

Figure 7.11: Illustration of the model vectors. There are two photodiodes for turns on each side of the car, represented by the normal vectors $\hat{\mathbf{n}}_{ij}$. The vectors r_L and r_R point form the light source at the origin to the left and right turn photodiodes, respectively. ϕ_{R2} is the incident angle for light on one photodiode.

$$\hat{\mathbf{n}}_{ij} \;=\; cos(\theta_{ij})\,(k\,\hat{\mathbf{v}} \times \hat{\mathbf{z}}) + sin(\theta_{ij})\hat{\mathbf{v}} \tag{7.11}$$

The angles θ_{ij} are photodiode positions measured from the $k\hat{\mathbf{v}} \times \hat{\mathbf{z}}$ axis. In the navigation experiments, there are $j = 3$ photodiodes on each side i at positions $\theta_{i1} = \pi/2$, $\theta_{i2} = 0$, and $\theta_{i3} = -\pi/2$. In the figure, there are two photodiodes on each side i at positions $\pm\pi/2$. Photodiode number and geometry are simple adjustments in the model.

Finally, the angle of incidence on any given photodiode is

$$\phi_{ij} \;=\; (-\mathbf{r}_i) \cdot \hat{\mathbf{n}}_{ij} \tag{7.12}$$

This angle changes in time and depends on the velocity vector.

In the model, the position of the car in time is represented by the vector r in Fig. 7.11.The motion of the car is treated as uniform circular motion, with $\mathbf{a} = \boldsymbol{\omega} \times \mathbf{v}$ and $\boldsymbol{\omega} = (k\hat{\mathbf{z}})v/R$, where R is the turn radius of the car. Left-Right turning is a change in the direction of the angular frequency by the index k. The protocol is as follows: when the right axon R spikes, k is set to +1; when L spikes, k switches to -1. The equations of motion for the car are:

$$\begin{cases} \ddot{x} \;=\; k(t)\frac{v}{R}\dot{y} \\ \ddot{y} \;=\; -k(t)\frac{v}{R}\dot{x} \end{cases} \tag{7.13}$$

The membrane equation 7.8, rate equations (see chapter 2 eqn 2.6), and equations 7.10, 7.12 and 7.13 constitute the model for navigation. We set initial conditions $x(0)$, $y(0)$, $\dot{x}(0)$, $\dot{y}(0)$, and $k(0)$, and solve numerically.

7.5 Concluding remarks

The goal with this demo is to instigate the development of "ionic networks" [VZ17]. A large network of artificial axons connected by tunable synapses would form an interesting neuroscience breadboard. One use would be to analyze principles of how the "microscopics" of action potentials may give rise to macroscopic behavior. Such a program is within

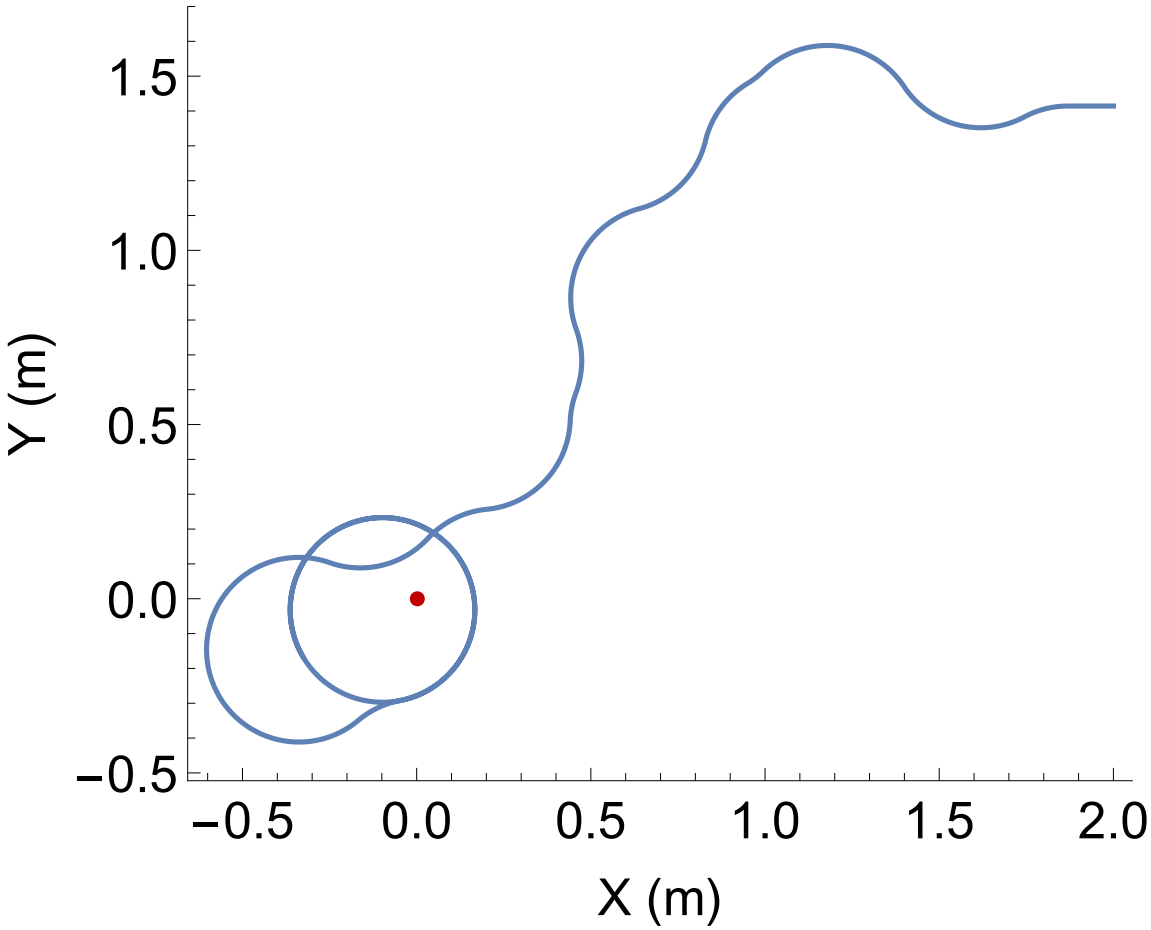

Figure 7.12: Car trajectory obtained from a simulation where the right AA has a firing rate 1.9 times higher than the left AA, for the same light seen. The car still "finds" the light source, which is at the origin.

the traditional focus of condensed matter physics, which seeks to understand "emergent" macroscopic properties starting from the microscopic components and interactions. At a higher level of description, the relation between information flow and behavior need not be based on complicated rules in order to produce complex behavior. In his delightful book "Vehicles", Valentino Braitenberg explains how simple control mechanisms can lead to surprisingly complex behavior [Bra84]. His very first example in the book is the car with left/right control. However, the specific microscopics of action potentials puts constraints on the flow of information and also provides specific mechanisms for the interaction of different bits of information. If we believe that the latter process is essential for "thought", we want our test network to be based on nodes which support action potentials. Even this simple, non-interacting system is not trivial to analyze, if one gets into a little detail, though it is easy enough to simulate. Let us come back to the issue of different firing rates for equal light intensity. Figure 7.12 shows the trajectory from a simulation with similar initial conditions as the navigation run in Fig. 7.9. In the simulation, the right AA had a firing rate 1.9 times higher than the left AA, for the same light received at the photodiode. The right turn bias is visible in the car's trajectory, but overall the car still finds the light source. The end state is a limit cycle which is a circle containing the light source. How much difference in the firing rates can be tolerated depends on the other parameters of the system. For example, with the firing rate ν, the car speed u, the turn radius of the car r, the initial distance to the light source L, we can form the two dimensionless numbers $\chi = u/(\nu r)$ and $\rho = r/L$. Then we can discuss, in this parameter space, the basin of attraction of the set of limit cycles which form the desirable end states. However, this is already a complicated question to explore analytically, for such a simple dynamical system!

Looking to the future, we are far from being able to construct a self-contained ionic network. Some of the difficulties seem surmountable with present day engineering, others would require new inventions. In the context of this demo, for example, we can see a path for substituting some of the electronic components with ionics. The CLVC could be dispensed with by adding a second ionic gradient, e.g. of Na^+, and corresponding voltage gated ion channels. Photodiodes could in principle be replaced by AAs with embedded channel

rhodopsin. On the other hand, ionics based "synapses" compatible with the $100\,mV$ scale of ionic action potentials require new inventions. Finally, 3D printing technology currently being developed to produce scaffolds for directed neuronal growth [al18] could probably form the basis for scaling up our AA network.

REFERENCES

[AB73] Clay M. Armstrong and Francisco Bezanilla. "Currents Related to Movement of the Gating Particles of the Sodium Channels." *Nature*, **242**:459–461, 1973.

[AES09] Rajagopal Ananthanarayanan, Steven K. Esser, Horst D. Simon, and Dharmendra S. Modha. "The Cat is Out of the Bag: Cortical Simulations with 10^9 Neurons, 10^{13} Synapses." *Proceedings of 2009 IEEE/ACM Conference on High Performance Computing Networking, Storage and Analysis*, 2009.

[al02] Claire Wyart et al. "Constrained synaptic connectivity in functional mammalian neuronal networks grown on patterned surfaces." *J. Neurosci. Methods*, **117**:123, 2002.

[al11] Giacomo Indiveri et al. "Neuromorphic silicon neuron circuits." *Frontiers in Neuroscience*, **5**:73, 2011.

[al12] Emanuele Marconi et al. "Emergent Functional Properties of Neuronal Networks with Controlled Topology." *PLoS ONE*, **7**:e34648, 2012.

[al13] Thomas Pfeil et al. "Six networks on a universal neuromorphic computing substrate." *Frontiers in Neuroscience*, **7**:11, 2013.

[al15] Anca M Pasca et al. "Functional cortical neurons and astrocytes from human pluripotent stem cells in 3D culture." *Nature Methods*, **12**:671, 2015.

[al17] Catherine D. Schuman et al. "Survey of Neuromorphic Computing and Neural Networks in Hardware." *arXiv:1705.06963*, 2017.

[al18] Daniela Espinosa-Hoyos et al. "Engineered 3D-printed artificial axons." *Scientific Reports*, **8**:478, 2018.

[AM96] Sanjay Kumar Aggarwal and Roderick MacKinnon. "Contribution of the S4 Segment to Gating Charge in the Shaker K+ Channel." *Neuron*, **16**(6):1169 – 1177, 1996.

[AZ13] Amila Ariyaratne and Giovanni Zocchi. "Nonlinearity of a voltage gated potassium channel revealed by the mechanical susceptibility." *Phys. Rev. X*, **3**:011010, 2013.

[AZ15] Amila Ariyaratne and Giovanni Zocchi. "Artificial phosphorylation sites modulate the activity of a voltage-gated potassium channel." *Phys. Rev. E*, **91**:032701, Mar 2015.

[AZ16] Amila Ariyaratne and Giovanni Zocchi. "Toward a minimal artificial axon." *J. Phys. Chem. B*, **120**:6255, 2016.

[BCP07] Mark F. Bear, Barry W. Connors, and Michael A. Paradiso. *Neuroscience: Exploring the Brain*. Lippincott Williams & Wilkins, 3rd edition, ISBN: 0-7817-6003-8, 2007.

[BCP16] Laura J. Batterink, Jessica D. Creery, and Ken A. Paller. "Phase of Spontaneous Slow Oscillations during Sleep Influences Memory-Related Processing of Auditory Cues." *Journal of Neuroscience*, **36**(4):1401–1409, 2016.

[BD04] György Buzsáki and Andreas Draguhn. "Neuronal Oscillations in Cortical Networks." *Science*, **304**(5679):1926–1929, 2004.

[Bez00] Francisco Bezanilla. "The Voltage Sensor in Voltage-Dependent Ion Channels." *Physiological Reviews*, **80**(2):555–592, 2000. PMID: 10747201.

[BH16] Richard W. Baker and Frederick M. Hughson. "Chaperoning SNARE assembly and disassembly." *Nature Reviews Molecular Cell Biology*, **17**:465–479, 2016.

[BHG15] Dirk Bucher, Gal Haspel, Jorge Golowasch, and Farzan Nadim. *Central Pattern Generators*, pp. 1–12. American Cancer Society, 2015.

[BMS11] Anil Bollimunta, Jue Mo, Charles E. Schroeder, and Mingzhou Ding. "Neuronal Mechanisms and Attentional Modulation of Corticothalamic Alpha Oscillations." *Journal of Neuroscience*, **31**(13):4935–4943, 2011.

[BPS92] N Brose, AG Petrenko, TC Sudhof, and R Jahn. "Synaptotagmin: a calcium sensor on the synaptic vesicle surface." *Science*, **256**(5059):1021–1025, 1992.

[BR01] Simon Bernèche and Benoît Roux. "Energetics of ion conduction through the K+ channel." *Nature*, **414**:73–77, 2001.

[Bra84] Valentino Braitenberg. *Vehicles*. MIT Press, Cambridge, MA, 1984.

[CBW06] John C. Chang, Gregory J. Brewer, and Bruce C. Wheeler. "Neuronal network structuring induces greater neuronal activity through enhanced astroglial development." *J. Neural Eng.*, **3**:217, 2006.

[CCM09] Jessica A. Cardin, Marie Carlén, Konstantinos Meletis, Ulf Knoblich, Feng Zhang, Karl Deisseroth, Li-Huei Tsai, and Christopher I. Moore. "Driving fast-spiking cells induces gamma rhythm and controls sensory responses." *Nature*, **459**:663–667, 2009.

[CJL07] Julio F. Cordero-Morales, Vishwanath Jogini, Anthony Lewis, Valeria Vásquez, Marien D. Cortes, Benoît Roux, and Eduardo Perozo. "Molecular driving forces determining potassium channel slow inactivation." *Nature Structural &Amp; Molecular Biology*, **14**:1062–1069, 2007.

[CK98] F Crick and C Koch. "Consciousness and neuroscience." *Cerebral Cortex*, **8**(2):97–107, 1998.

[DF03] Joseph G. Duman and John G. Forte. "What is the role of SNARE proteins in membrane fusion?" *American Journal of Physiology-Cell Physiology*, **285**(2):C237–C249, 2003. PMID: 12842832.

[DKC98] Stanislas Dehaene, Michel Kerszberg, and Jean-Pierre Changeux. "A neuronal model of a global workspace in effortful cognitive tasks." *Proceedings of the National Academy of Sciences*, **95**(24):14529–14534, 1998.

[DPB10] Emrah Dzel, Will D Penny, and Neil Burgess. "Brain oscillations and memory." *Current Opinion in Neurobiology*, **20**(2):143 – 149, 2010. Cognitive neuroscience.

[Fet97] Eberhard E. Fetz. "Temporal Coding in Neural Populations?" *Science*, **278**:1901–1902, 1997.

[FKG01] Rafael Fernández-Chacón, Andreas Königstorfer, Stefan H. Gerber, Jesús García, Maria F. Matos, Charles F. Stevens, Nils Brose, Josep Rizo, Christian Rosenmund, and Thomas C. Südhof. "Synaptotagmin I functions as a calcium regulator of release probability." *Nature*, **410**:41–49, 2001.

[FKN08] André A. Fenton, Hsin-Yi Kao, Samuel A. Neymotin, Andrey Olypher, Yevgeniy Vayntrub, William W. Lytton, and Nandor Ludvig. "Unmasking the CA1 Ensemble Place Code by Exposures to Small and Large Environments: More Place Cells and Multiple, Irregularly Arranged, and Expanded Place Fields in the Larger Space." *Journal of Neuroscience*, **28**(44):11250–11262, 2008.

[FM06] Ofer Feinerman and Elisha Moses. "Transport of information along unidimensional layered networks of dissociated hippocampal neurons and implications for rate coding." *J. Neurosci.*, **26**:4526, 2006.

[FRM08] Ofer Feinerman, Assaf Rotem, and Elisha Moses. "Reliable neuronal logic devices from patterned hippocampal cultures." *Nature Physics*, **4**:967–973, 2008.

[FSM05] Ofer Feinerman, Menahem Segal, and Elisha Moses. "Signal propagation along unidimensional neuronal networks." *J. Neurophysiol.*, **94**:3406, 2005.

[GKM97] Wulfram Gerstner, Andreas K. Kreiter, Henry Markram, and Andreas V. M. Herz. "Neural codes: Firing rates andbeyond." *PNAS*, **94**:12740–12741, 1997.

[HCD09] Christopher D. Harvey, Forrest Collman, Daniel A. Dombeck, and David W. Tank. "Intracellular dynamics of hippocampal place cells during virtual navigation." *Nature*, **461**:941–946, 2009.

[Hen95] Paul N Hengen. "Purification of His-Tag fusion proteins from Escherichia coli." *Trends in Biochemical Sciences*, **20**(7):285 – 286, 1995.

[HH52] A. L. Hodgkin and A. F. Huxley. "A quantitative description of membrane current and its application to conduction and excitation in nerve." *The Journal of Physiology*, **117**:500–544, 1952.

[HKM98] Lise Heginbotham, Ludmila Kolmakova-Partensky, and Christopher Miller. "Functional Reconstitution of a Prokaryotic K+ Channel." *The Journal of General Physiology*, **111**(6):741–749, 1998.

[HLA94] L. Heginbotham, Z. Lu, T. Abramson, and R. MacKinnon. "Mutations in the K+ channel signature sequence." *Biophysical Journal*, **66**(4):1061 – 1067, 1994.

[HLK99] Lise Heginbotham, Meredith LeMasurier, Ludmilla Kolmakova-Partensky, and Christopher Miller. "Single Streptomyces lividans K+ Channels." **114**(4):551–560, 1999.

[HS98] Sarah F. Hamm-Alvarez and Michael P. Sheetz. "Microtubule-Dependent Vesicle Transport: Modulation of Channel and Transporter Activity in Liver and Kidney." *Physiological Reviews*, **78**(4):1109–1129, 1998. PMID: 9790571.

[JLC03] Youxing Jiang, Alice Lee, Jiayun Chen, Vanessa Ruta, Martine Cadene, Brian T. Chait, and Roderick MacKinnon. "X-ray structure of a voltage-dependent K^+ channel." *Nature*, **423**:33–41, 2003.

[JRC03] Youxing Jiang, Vanessa Ruta, Jiayun Chen, Alice Lee, and Roderick MacKinnon. "The principle of gating charge movement in a voltage-dependent K+ channel." *Nature*, **423**:42–48, 2003.

[KK98] Laszlo Kiss and Stephen J. Korn. "Modulation of C-Type Inactivation by K+ at the Potassium Channel Selectivity Filter." *Biophysical Journal*, **74**(4):1840 – 1849, 1998.

[KKR11] Daniel Kümmel, Shyam S. Krishnakumar, Daniel T. Radoff, Feng Li, Claudio G. Giruado, Frederic Pincet, James E. Rothman, and Karin M. Reinisch. "Complexin cross-links prefusion SNAREs into a zigzag array." *Nature Structural & Amp; Molecular Biology*, **18**:927–933, 2011.

[KLK99] Laszlo Kiss, Joseph LoTurco, and Stephen J. Korn. "Contribution of the Selectivity Filter to Inactivation in Potassium Channels." *Biophysical Journal*, **76**(1):253 – 263, 1999.

[KLL11] Julie Koenig, Ashley N. Linder, Jill K. Leutgeb, and Stefan Leutgeb. "The Spatial Periodicity of Grid Cells Is Not Sustained During Reduced Theta Oscillations." *Science*, **332**(6029):592–595, 2011.

[Koc99] Christof Koch. *Biophysics of Computation: Information Processing in Single Neurons*. Oxford Univ. Press, 1999.

[Koc04] Christof Koch. *A Quest for Consciousness: A Neurobiological Approach*. Roberts & Co, 1st edition, ISBN-10: 0974707708, 2004.

[Koc18] Christof Koch. "What Is Consciousness?" *Scientific American*, **318**:30–64, 2018.

[Kot05] Boris Kotchoubey. "Event-related potential measures of consciousness: two equations with three unknowns." In Steven Laureys, editor, *The Boundaries of Consciousness: Neurobiology and Neuropathology*, volume 150 of *Progress in Brain Research*, pp. 427 – 444. Elsevier, 2005.

[Kuo02] Arthur D. Kuo. "The Relative Roles of Feedforward and Feedback in the Control of Rhythmic Movements." *Motor Control*, **6**(2):129–145, 2002.

[LHM01] Meredith LeMasurier, Lise Heginbotham, and Christopher Miller. "Kcsa." *The Journal of General Physiology*, **118**(3):303–314, 2001.

[LI95] JE Lisman and MA Idiart. "Storage of 7 +/- 2 short-term memories in oscillatory subcycles." *Science*, **267**(5203):1512–1515, 1995.

[LJY96] Yi Liu, Mark E Jurman, and Gary Yellen. "Dynamic Rearrangement of the Outer Mouth of a K+ Channel during Gating." *Neuron*, **16**(4):859 – 867, 1996.

[LTC07] Stephen B. Long, Xiao Tao, Ernest B. Campberll, and Roderick MacKinnon. "Atomic structure of a voltage-dependent K+ channel in a lipid membrane-like environment." *Nature*, **450**:376–382, 2007.

[Nel03] Philip Nelson. *Biological Physics*. W. H. Freeman and Company, 2003.

[ODB15] Marie Engelene J. Obien, Kosmas Deligkaris, Torsten Bullmann, Douglas J. Bakkum, and Urs Frey. "Revealing neuronal function through microelectrode array recordings." *Frontiers in Neuroscience*, **8**:423, 2015.

[PSM06] Zhiping P. Pang, Ok-Ho Shin, Alexander C. Meyer, Christian Rosenmund, and Thomas C. Südhof. "A Gain-of-Function Mutation in Synaptotagmin-1 Reveals a Critical Role of Ca2+-Dependent Soluble N-Ethylmaleimide-Sensitive Factor Attachment Protein Receptor Complex Binding in Synaptic Exocytosis." *Journal of Neuroscience*, **26**(48):12556–12565, 2006.

[PYA07] Medha M. Pathak, Vladimir Yarov-Yarovoy, Gautam Agarwal, Benoît Roux, Patrick Barth, Susy Kohout, Francesco Tombola, and Ehud Y. Isacoff. "Closing In on the Resting State of the Shaker K+ Channel." *Neuron*, **56**(1):124 – 140, 2007.

[QRK05] R. Quian Quiroga, L. Reddy, G. Kreiman, and C. Koch. "Invariant visual representation by single neurons in the human brain." *Nature*, **435**:1102–1107, 2005.

[RJL03] Vanessa Ruta, Youxing Jiang, Alice Lee, Jiayun Chen, and Roderick MacKinnon. "Functional analysis of an archaebacterial voltage-dependent K^+ channel." *Nature*, **422**:180–185, 2003.

[RLM98] Jean-Louis Rigaud, Daniel Levy, Gervaise Mosser, and Oliver Lambert. "Detergent removal by non-polar polystyrene beads." *European Biophysical Journal*, **27**(4):305–319, 1998.

[SCM09] Daniel Schmidt, Samuel R. Cross, and Roderick Mackinnon. "A Gating Model for the Archeal Voltage-Dependent K^+ Channel KvAP in DPhPC and POPE:POPG Decane Lipid Bilayers." *J. Mol. Biol.*, **390**, 2009.

[Sig94] F. J. Sigworth. "Voltage gating of ion channels." *Quarterly Reviews of Biophysics*, **27**(1):140, 1994.

[SKP01] Piotr Suffczynski, Stiliyan Kalitzin, Gert Pfurtscheller, and F.H Lopes da Silva. "Computational model of thalamo-cortical networks: dynamical control of alpha rhythms in relation to focal attention." *International Journal of Psychophysiology*, **43**(1):25 – 40, 2001. Thalamo-Cortical Relationships.

[SN09] Sakmann and Neher. *Single-Channel Recording*. Springer, 2nd edition, ISBN: 9781441912305, 2009.

[SNU96] Yoshihiko Sako, Norimichi Nomura, Aritsune Uchida, Yuzaburo Ishida, Hiroyuki Morii, Yosuke Koga, Toshihiro Hoaki, and Tadashi Maruyama. "Aeropyrum pernix gen. nov., sp. nov., a Novel Aerobic Hyperthermophilic Archaeon Growing at Temperatures up to 100°C." *International Journal of Systematic and Evolutionary Microbiology*, **46**(4):1070–1077, 1996.

[SSD99] Kelly J. Suter, Bret N. Smith, and F.Edward Dudek. "Electrophysiological Recording from Brain Slices." *Methods*, **18**(2):86 – 90, 1999.

[SSL12] Sepideh Sadaghiani, René Scheeringa, Katia Lehongre, Benjamin Morillon, Anne-Lise Giraud, Mark D'Esposito, and Andreas Kleinschmidt. "Alpha-Band Phase Synchrony Is Related to Activity in the Fronto-Parietal Adaptive Control Network." *Journal of Neuroscience*, **32**(41):14305–14310, 2012.

[SSP96] Sang-Ah Seoh, Daniel Sigg, Diane M Papazian, and Francisco Bezanilla. "Voltage-Sensing Residues in the S2 and S4 Segments of the Shaker K+ Channel." *Neuron*, **16**(6):1159 – 1167, 1996.

[SWC13] Surjo R. Soekadar, Matthias Witkowski, Eliana G. Cossio, Niels Birbaumer, Stephen E. Robinson, and Leonardo G. Cohen. "In vivo assessment of human brain oscillations during application of transcranial electric currents." *Nature Communications*, **4**, 2013.

[TBK16] Giulio Tononi, Melanie Boly, and Christof Koch. "Integrated information theory: from consciousness to its physical substrate." *Nature Reviews Neuroscience*, **17**:450–461, 2016.

[Tur08] Gina G. Turrigiano. "The Self-Tuning Neuron: Synaptic Scaling of Excitatory Synapses." *Cell*, **135**(3):422 – 435, 2008.

[UL05] Christian Ungermann and Dieter Langosch. "Functions of SNAREs in intracellular membrane fusion and lipid bilayer mixing." *Journal of Cell Science*, **118**(17):3819–3828, 2005.

[VZ17] H.G. Vasquez and G. Zocchi. "Coincidences with the artificial axon." *EPL*, **119**:48003, 2017.

[VZ18] Hector Garcia Vasquez and Giovanni Zocchi. "Analog control with two Artificial Axons." *arXiv:1806.08001*, 2018.

[Wan10] Xiao-Jing Wang. "Neurophysiological and Computational Principles of Cortical Rhythms in Cognition." *Physiological Reviews*, **90**(3):1195–1268, 2010. PMID: 20664082.

[WFF90] W.F. Wonderlin, A. Finkel, and R.J. French. "Optimizing planar lipid bilayer single-channel recordings for high resolution with rapid voltage steps." *Biophysical Journal*, **58**(2):289 – 297, 1990.

[WZ11] Andrew Wang and Giovanni Zocchi. "Artificial Modulation of the Gating Behavior of a K+ Channel in a KvAP-DNA Chimera." *PLOS ONE*, **6**(4):1–8, 04 2011.

[YBC06] Vladimir Yarov-Yarovoy, David Baker, and William A. Catterall. "Voltage sensor conformations in the open and closed states in rosetta structural models of K+ channels." *Proceedings of the National Academy of Sciences*, **103**(19):7292–7297, 2006.

[YSC94] G. Yellen, D. Sodickson, T.Y. Chen, and M.E. Jurman. "An engineered cysteine in the external mouth of a K+ channel allows inactivation to be modulated by metal binding." *Biophysical Journal*, **66**(4):1068 – 1075, 1994.

[ZAD18] Benedikt Zoefel, Alan Archer-Boyd, and Matthew H. Davis. "Phase Entrainment of Brain Oscillations Causally Modulates Neural Responses to Intelligible Speech." *Current Biology*, **28**(3):401 – 408.e5, 2018.

[ZMK01] Yufeng Zhou, Joao H. Morais-Cabral, Amelia Kaufman, and Roderick MacKinnon. "Chemistry of ion coordination and hydration revealed by a K+ channelFab complex at 2.0 resolution." *Nature*, **414**:43–48, 2001.